UNIVERSITÀ DEGLI STUDI DI TRIESTE

XXIX CICLO DEL DOTTORATO DI RICERCA IN

INGEGNERIA E ARCHITETTURA

STUDY OF A NEW SOLUTION TO REDUCE VIBRATION

TRANSMISSION THROUGH PILLARS ON BOARD SHIPS

Settore scientifico-disciplinare: ING-IND/02

PH. D. CANDIDATE
EMANUELE BROCCO

PH. D. PROGRAM COORDINATOR
PROF. DIEGO MICHELI

THESIS SUPERVISOR
PROF. MARCO BIOT

ACADEMIC YEAR 2015/2016

Abstract

In the last decades, the demand for higher comfort levels on board of ships has increased year by year. Comfort has always been a key factor in cruise ships and pleasure yachts, though recently, the attention to the condition of seafarers has also increased. Several studies in the last years focused on how to improve comfort on board, suggesting methods and analytical instruments for the prediction of vibration and noise levels during the ship design process. Other studies investigated how to reduce the vibration transmitted from the machinery to the ship or how to reduce the vibration of radiating surfaces with the aim of reducing the noise levels on board.

Some early studies, addressed pillars as a key factor in vibration transmission, this viewpoint was shared also by shipbuilding companies. Aim of this work is to study a device for the reduction of vibration transmission through the pillars. This research is a first step in the development of such device. The main element of the isolator is a resilient element. In order to guarantee the structural capability of the device, the design loads acting on the pillars have been evaluated on a reference yacht and on a cruise ship using both scantling rules and direct FE calculation. Prototypes with different designs have been built and their dynamic characteristics have been studied in a laboratory experimental facility basing on the ISO 10846 standard for the laboratory measurement of the vibro-acoustic properties of isolators. The prototype design showing the lowest transmissibility has been tested on a real scale mock-up representing a portion of two decks with the typical structure of a cruise ship. The real scale test shows the effectiveness of the isolator in the reduction of the vibration transmitted through the pillar.

In addition, a simplified finite element model of the isolator has been set up using the data measured on the mock-up structure and the simplified model has been used to study the isolator effectiveness on a superyacht finite element model. The comparative numerical study and most of all the experimental tests led to very positive results which could pave the way to promising developments in the future.

Sommario

Negli ultimi decenni si è registrato un costante aumento nella domanda di comfort a bordo delle navi. Il comfort è sempre stato un elemento chiave per il settore crocieristico e per la diportistica dove il benessere dei passeggeri è un fattore fondamentale. Tuttavia, oggi anche le condizioni del personale di bordo hanno assunto una maggiore importanza. Diverse ricerche negli ultimi anni si sono concentrate sul miglioramento del comfort a bordo, proponendo metodi e strumenti analitici per la previsione dei livelli di vibrazione e rumore durante le fasi di progettazione della nave. Altri studi hanno invece mostrato come ridurre le vibrazioni trasmesse dai macchinari alla nave o come ridurre le vibrazioni delle superfici radianti con l'obiettivo di ridurre i livelli di rumore a bordo.

In passato alcuni studi hanno identificato il puntello come principale elemento nella trasmissione delle vibrazioni da un ponte all'altro; opinione condivisa anche dall'industria navale. L'obiettivo di questa ricerca è lo studio di un dispositivo per la riduzione delle vibrazioni trasmesse attraverso i puntelli. L'isolatore è composto da un elemento resiliente e al fine di garantire la capacità strutturale del dispositivo, i carichi di progetto utilizzati per il dimensionamento dei puntelli sono stati valutati su una nave da crociera e su uno yacht di riferimento, applicando sia i regolamenti di classifica sia mediante calcolo diretto utilizzando un modello ad elementi finiti. Sono stati costruiti alcuni prototipi con diverse configurazioni le cui caratteristiche dinamiche sono state valutate secondo lo standard internazionale ISO 10846 che fornisce le linee guida per la misura in laboratorio delle proprietà vibro-acustiche degli isolatori. Inoltre il prototipo con la configurazione con minor trasmissibilità è stato testato su un simulacro di interponte in scala reale avente struttura tipica di una nave da crociera. I risultati della prova al vero hanno dimostrato l'efficacia dell'isolatore nel ridurre le vibrazioni trasmesse attraverso il puntello.

Le misure al vero sul simulacro di interponte navale sono state utilizzate per definire e validare un elemento semplificato in grado di rappresentare il comportamento dinamico dell'isolatore da utilizzare per previsioni numeriche di

livelli di vibrazione a bordo di imbarcazioni. L'elemento così definito è stato utilizzato all'interno di un modello ad elementi finiti di uno yacht di grandi dimensioni e i benefici derivanti dall'uso di un puntello isolato sono stati confrontati con la previsione dei livelli di comfort ottenuti con un puntello standard. L'analisi numerica comparativa e soprattutto i test sperimentali hanno mostrato risultati molto positivi che gettano le basi per un futuro sviluppo dell'isolatore.

Table of contents

List of Tables

List of Figures

Introduction

Early studies in the field of comfort on ships start investigating the effects of high noise levels on seafarers showing how a steady sound level of 65 dB(A) generated by a ship diesel engine can affect their nocturnal sleep [1]. Researchers also stress that the continuous exposition of sailors to high noise levels, due to ship operation, may reduce their capacity to recover from fatigue, leading to poorer daytime performance and, possibly, disaster at sea. Finally, they suggest that reducing noise and vibration can improve the life quality of those living on board a ship. Also international organizations are warning on the effects of fatigue and its detrimental effect on performance and alertness and once more, exposure to excessive levels of noise and vibrations is included among the main causes of fatigue. [2].

More recently, a study in the field of perceived comfort on board ships shows that, for cruise ships, acoustic comfort is the prominent factor of comfort aboard a ship and also its weakest point [3]. Among the noises causing discomfort, the noise of engine, stabilizer fins and bow thruster were addressed as some of the major causes of disturbance. Furthermore, the influence of acoustic discomfort on persons produces sleep disturbance and irritation.

Classification societies suggest additional class notation for comfort assessment on board both for passengers and for crew members [4, 5, 6, 7] based mainly on noise and vibration limits. Limits for passengers are stricter than those for crew members stressing the fact that comfort on board passenger ship and in particular on cruise ship is a factor of paramount importance [8, 9]. While class notation is optional, from 2014 IMO resolution 337(91), [10], has entered in force. The resolution sets new limits for noise levels in the inhabited areas of ships, aiming at providing standards for an acceptable environment for seafarers beyond the protection against noise.

This shows that the interest for comfort is growing and that the main contributors to the overall comfort level are noise and vibration perceived on board of ships.

On board ships, vibration and noise are generated by various sources. Propellers and cavitation, propeller shaft rotation, main mover engine, gearboxes, gen-set, pumps, air compressors and, in general, all the reciprocating machinery installed on board are sources of noise and vibration [11, 12, 13].

Main propulsion engine, for example, generates airborne noise in the surrounding air and, through pressure oscillation, in the exhaust gas system. This noise is generated in the audible frequency range from 15 Hz to 16 kHz. Resilient mount, pipes and other devices that connect the diesel engine to the auxiliary plant and to the ship structure constitute the transmission path of the engine's vibration energy, from these points the vibration is transmitted to all the other spaces of the ship [14]

Vibration generated by on-board sources propagates through ship structures and reach the receiving space where interaction between the structure and the surrounding air generates noise; this mechanism of propagation is called structure born noise [15]. Moreover, most of the noise is generated by vibrations of the solid structure propagating the vibrational energy of remote acoustical and mechanical sources [16]. These considerations lead to the conclusion that the first thing to do in order to avoid noise disturbances is reducing structure-borne noise transmission from the source to the receiver.

During the years, many researchers have studied ways to reduce the vibration and noise at the receiving space on board ships. The use of passive methods, as isolator or surface treatment, is a common practice, nevertheless, in recent years a number of studies concentrated on hybrid solutions [17, 18] or on full active vibration reduction systems [19, 20, 21, 22]. These solutions are particularly suited for low vibration reduction but, nowadays, these relate to mainly experimental prototypes.

During the years, passive solution for noise and vibration reduction demonstrated to be the more flexible and effective for the shipbuilding industry. Reducing noise and vibration could be tackled mainly in three ways. The first is acting on the source of vibration. At this stage, the more frequent solution is the decoupling of the vibration source from the ship structure using resiliently mounted machinery. Studies concentrate both on the characterization of the resilient mounts [23, 24, 25, 26] and on their interaction with ships structures [14, 27, 28, 29, 30].

Another way is to act on the radiating surface instead of the source. Recent studies focus on the development of solutions to decouple the floor from the ship deck in order to reduce both the vibrational energy transmitted to the floor and the disturbances generated by human activities and transmitted to the decks and to the whole ship structure [31]. This frame also includes surface treatments as the application of viscoelastic layer on deck or on the side plating or bulkhead [32, 33, 34, 35, 36], these treatments add damping to the plating so to reduce their vibration amplitude, thus the sound radiated.

The third way to face the problem of vibration transmission is to act on the vibration transmission path to reduce the vibrational energy flow to the receiving spaces. In case of excessive noise and vibration levels, some studies suggest suspending the complete deckhouses [10], however, this solution is only suitable for smaller vessels.

This thesis focuses on the study and the development of a device to lower vibration transmission through deck supports connecting adjacent decks. The device was conceived by a company active in the field of noise and vibration control on ships. The work is a first insight in the design of such an isolator and a first attempt to validate the effectiveness of this type of solution. The study also aims at clarifying the effectiveness of such solutions which were used in the past on pleasure vessels and whose effectiveness had never been proved by systematic studies. Some attempts had been made, indeed, to reduce vibration transmission by simply inserting resilient elements at the end of pillars though they were not specifically designed to this purpose.

A first layout of the isolator has been studied and the resilient element materials have been selected after having assessed maximum working loads acting on pillars. Prototypes of different design alternatives have been built in order to evaluate their dynamic characteristics. Experimental dynamic characterization, both in low and high frequency range, lead to the identification of the best alternative that have been studied on a real scale mock-up. The real scale tests, even though on an incomplete structure and with simplified excitation source, show positive results and assess the effectiveness of the solution in lowering the vibration transmission through the pillars.

After this introduction, the study presents the problem of vibration transmission through pillars and suggests a sketch of the device along with a simplified analytical model to show its working principle.

The second part of the work concentrates on the methods used in the development of the pillar isolator. Initially, it deals with experimental tests in order to characterize the dynamic behaviour of isolators both in low and high frequency range. Afterwards it proposes a real scale test procedure and finally it shows how to develop a simplified numerical model of the pillar isolator.

The last part shows the relevant results of the complete experimental campaign. It starts from the evaluation of the main loads acting on the pillars and the definition and buildings of the prototypes. It goes through the results of the high and low frequency characterization to the real scale test. Finally, the simplified model of the isolator is used to compare the predicted vibration levels of a standard pillar with an isolated pillar on a yacht.

1 Vibration transmission reduction through pillars

Pillars, or stanchions, are vertical beams or column elements supporting a deck girder [37]. They are widely used in cruise ships where public spaces need to be wide and open for aesthetic and appealing reasons, but they are widely used also in merchant ships and smaller vessels especially in way of engine rooms where large and continuous spaces are need to house engines and related auxiliaries and a continuous bulkhead cannot be fitted.

Pillars, as part of the ship structure, are to be considered as one of the possible structure-borne noise transmission path [38]. Pillars are a critical point for vibration transmission because they readily spread vibrational energy to the ship structure especially if installed near main propulsion diesel engine or other machinery producing remarkable vibration levels [39]. In these cases pillars are the primary path for structure-borne noise transmission [40]. As reported in [11], the use of pillars is not recommended because they provide only low transmission loss between source and receiver spaces.

1.1 Device outline and description

The tested and developed device is intended to decouple the pillar from the deck where it is placed. Referring to the sketch reported in Figure 1.1, the pillar (1), when the device is fitted, is disconnected from the deck plating (7). The free end, at the bottom side of the pillar, is closed with a plate and is positioned on a resilient element (5). An external shell (2) contains the resilient element placed under the pillar and is filled by a viscoelastic material (6) to increase the damping to the solution. A vertical restraint system (3), along with another decoupling element (4), prevent excessive vertical motion when the pillar is subject to traction load instead of compression.

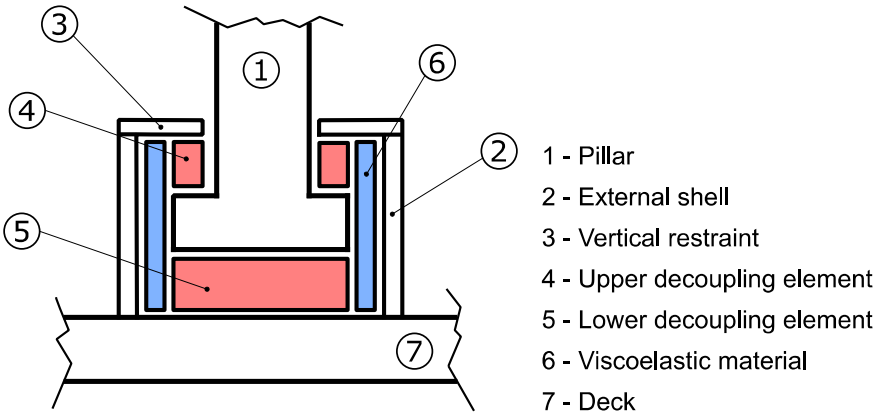

Figure 1.1 - Pillar isolator sketch

1.2 Working principle

A former study show that longitudinal waves govern the structure borne noise transmission in pillars [11]. The same report states: "At most frequencies of interest, the structure-borne noise transmission through stanchions is governed by wave effects in the stanchion. At the natural frequencies of the longitudinal waves in the stanchion, the stanchion acts as a rigid coupling between decks. Thus, in the absence of damping in the stanchion, the transmission loss between decks connected by a stanchion is zero at the longitudinal wave natural frequencies." The former consideration leads to consider the problem of vibration transmission through the deck supports as mainly drive by axial vibration disregarding the effect of other vibration types. Thus, in a first approximation, it is possible to simplify the problem disregarding the other deck's supporting structure as side plate and bulkhead and consider the system composed by the deck and the pillar as a single degree of freedom (SDOF) system. The lower deck on which the pillar is placed supports also the machinery representing the vibration source, in the SDOF system this mechanism will be approximated to a base excitation applied to the pillar. The SDOF system is shown in Figure 1.2.

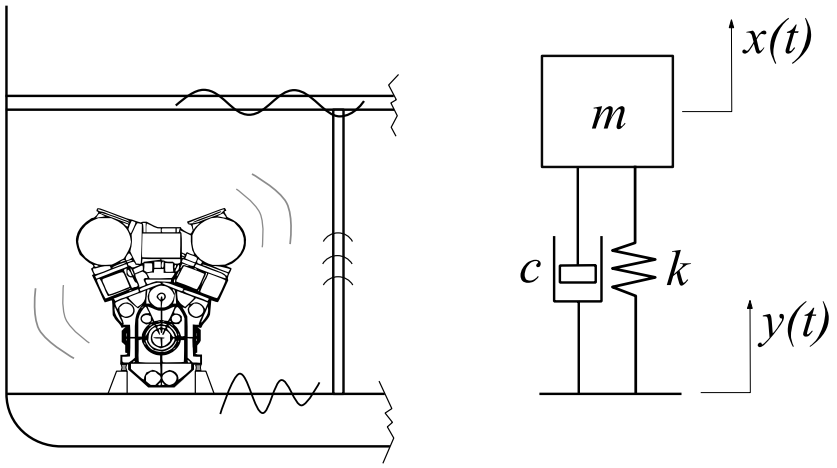

Figure 1.2 - SDOF system definition

The suspended mass, m, represent the deck while the pillar is the spring, with stiffness k, with an associated damper, with damping c. Assuming a sinusoidal base excitation, $y(t) = Y\cos(\omega t)$, the SDOF motion equation can be written as follows:

$$m\ddot{x} + c(\dot{x} - \dot{y}) + k(x - y) = 0 \tag{1.1}$$

The solution of the nonhomogeneous differential equation is given by the sum of the solution of the homogenous equation and the particular solution. The homogenous equation is the motion equation of the unforced system, its solution is an oscillation decaying with time and depending on the initial condition, i.e.: initial displacement and initial velocity. After sufficient time has passed, the motion reaches a steady state and the system oscillates at the frequency of the external forcing [41]. Focusing only on the steady state response and then considering only the particular solution, the ratio between the mass motion, the upper deck, and the base motion, the lower deck, is called motion transmissibility and results as follows:

$$\left|\frac{X}{Y}\right| = \frac{\sqrt{1+(2\zeta r)^2}}{\sqrt{(1-r^2)^2+(2\zeta r)^2}} \tag{1.2}$$

Where $\zeta = c/2\sqrt{km}$ is the damping ratio and $r = \omega/\omega_n$ is the ratio between the circular frequency of the base motion and natural circular frequency of the SDOF system given by $\omega_n = \sqrt{k/m}$.

Figure 1.3 shows the motion transmissibility curve for a SDOF system with damping coefficient $\zeta = 0.02$. At lower frequency ratio, when the base motion frequency is smaller than the natural frequency of the system, the base motion is completely transmitted to the suspended element. When the base motion frequency approaches the natural frequency of the system, the motion of the base is amplified until the resonance is reached. After the resonance, $r = 1$, the motion decreases and, increasing the frequency of excitation, the response of the system becomes much lower than the base motion.

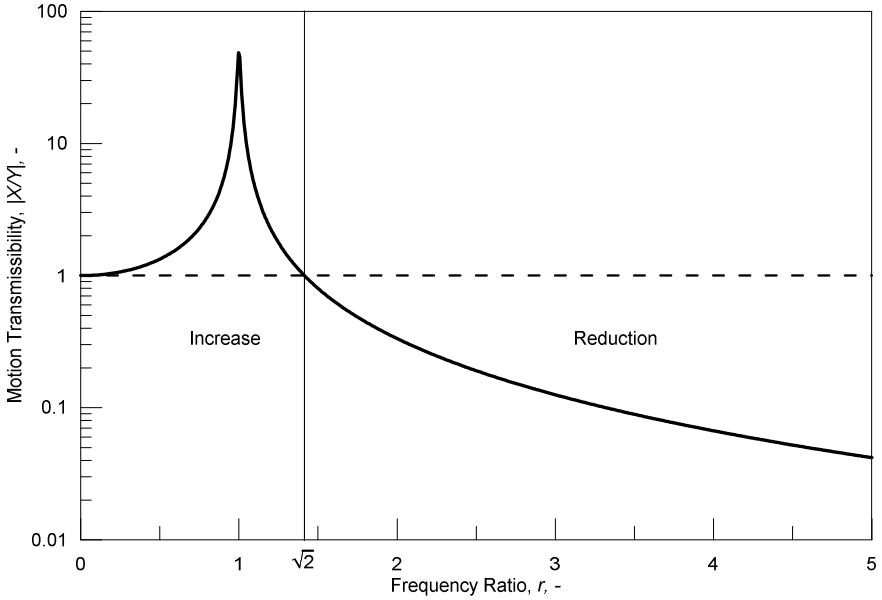

Figure 1.3 - Motion transmissibility curve for a SDOF system

In Figure 1.4 the transmissibility curves of two SDOF systems are now plotted against the frequency of the base motion. The two SDOF systems differ only for the stiffness value while the mass and the damping factor are the same. Reducing the stiffness of the system will lower its natural frequency and, comparing with the stiffer system, the reduction of the transmissibility will be reached on a wider range

of frequency. Taking in consideration a frequency after the “reduction point”, the stiffer system will have larger motion than the more flexible system.

The pillar isolator takes advantage from this mechanism to reduce the vibration transmitted to the deck in the audio frequency range. The isolated pillar will have a lower stiffness than the standard pillar and the reduction of its stiffness will be the aim of its development process.

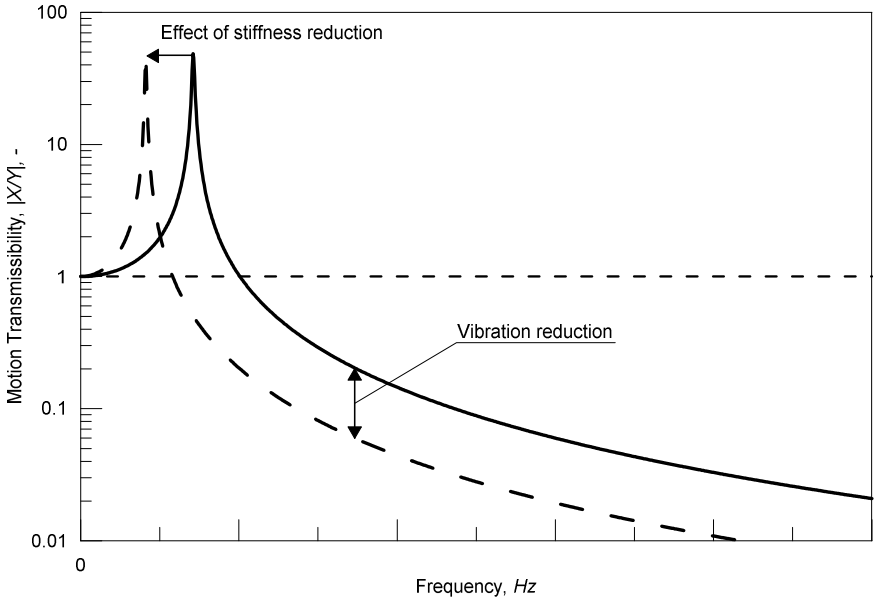

Figure 1.4 - Effect of stiffness reduction on motion transmissibility curve

Methods

2 Experimental evaluation of the dynamic stiffness

In the first step of the work, dynamic properties of the different prototypes have to be evaluated in order to identify the best available solution. In the SDOF system approximation introduced in Section 1.2, the influence of the stiffness in the transmissibility level is clear and stiffness is the parameter chosen to rank the different solutions to be tested.

Isolators made of elastomeric components show dynamic stiffness values that are usually much higher than their static stiffness [42]. Moreover, typical vibration isolators show internal resonance phenomenon that can increase the stiffness at frequencies corresponding to the internal standing waves frequencies [43, 44] leading to a strong frequency dependent behaviour. For these reasons it is important to measure the dynamic stiffness on the whole frequency range of use of the device.

The common standard for the experimental evaluation of the dynamic characteristics of resilient elements is the international standard *ISO 10846 - Laboratory measurement of vibro-acoustic transfer properties of resilient elements* [45]. The standard gives some guidelines and suggests several methods for the evaluation of the dynamic stiffness of passive resilient elements [46, 47, 48, 49].

The dynamic characterization of an isolator can be tackled with reference to a vibration source suspended on a receiving structure [50, 14, 27, 23]. This approximation is valid also in the case of a pillar isolator, considering only the two decks and the pillars connecting them.

A simplified approach dealing with complex structures subject to vibration is the four-pole parameter theory where a combination of linear lumped mechanical elements such as masses, springs and dampers describes the elastic system [51, 52, 53, 54, 55]. Such representation is possible also with linear distributed parameter systems as beams, plates and vibration isolators [56]. In addition, the elements must have two identifiable connection points, one corresponding to the input side and

one to the output side [57]. Following this representation, the system, composed by the source, the isolator and the receiving structure, can be represented as a three block system as in Figure 2.1.

Figure 2.1 - Four-pole parameters for the characterization of a lumped mechanical system

According to the four-pole theory, the isolator is subject to a force F_1 and moving with a displacement u_1 at the input side, while the output side moves of a quantity u_2 and transmits a force F_2. For each frequency, the equilibrium equation of the isolator can be written as follows:

$$\begin{cases} F_1 = k_{11}u_1 + k_{12}u_2 \\ F_2 = k_{21}u_1 + k_{22}u_2 \end{cases} \tag{2.1}$$

Where k_{11} and k_{22} represent the driving point stiffness when the vibration isolator is blocked at the opposite side, with $u_2 = 0$ and $u_1 = 0$ respectively. k_{12} and k_{21} are the blocked transfer stiffness and represent the ratio between the force on the blocked side and the displacement on the driven side. The definition of the stiffness elements, k_{ij}, is summarised as follows:

$$\begin{aligned} k_{11} &= \left.\frac{F_1}{u_1}\right|_{u_2=0} & k_{12} &= \left.\frac{F_1}{u_2}\right|_{u_1=0} \\ k_{21} &= \left.\frac{F_2}{u_1}\right|_{u_2=0} & k_{22} &= \left.\frac{F_2}{u_2}\right|_{u_1=0} \end{aligned} \tag{2.2}$$

Equation (2.1) is referred to a simplified system with only one degree of freedom. In a general case, F_i are vectors composed of three translation forces and three moments. The same applies also for u_i, that is composed by three translations and three rotations. In both equations (2.1) and (2.2), F_i and u_i are phasors while k_{ij} are complex quantities.

The stiffness of the receiving structure, excited through the isolators output force F_2, is defined as:

$$k_r = -\frac{F_2}{u_2} \tag{2.3}$$

where k_r is the driving point stiffness of the receiver and the sign is due to the reference system.

Combining (2.3) with (2.1) follows

$$F_2 = \frac{k_{21}}{1+\frac{k_{22}}{k_r}} u_1 \tag{2.4}$$

The force F_2, for a given input displacement u_1, depends on the isolator dynamic driving point stiffness and also on the receiver driving point stiffness. If $|k_{22}| \ll |k_r|$ then the output force F_2 approximates the blocking force (obtained with blocked displacement on the output side) and the relation (2.4) can be written as follows:

$$F_2 \approx F_{2,b} = k_{21} u_1 \tag{2.5}$$

Vibration isolators are effective only when receiver structure driving point stiffness are high if compared with the isolator driving point stiffness and in practical cases the inequality $|k_{22}| \leq 0.1|k_r|$ is satisfied. Under these circumstances, the approximation in (2.5) is valid and leads to a maximum approximation of 10%. Moreover, the relation shows that the dynamic transfer stiffness of the vibration isolator is the quantity that, for a given displacement u_1 on the input side, represents the vibration isolator.

3 High-frequency dynamic characterization

The ISO 10846-3:2002 [47] is the reference standard for the measurement of the dynamic characteristics of an isolator in the high frequency range. The standard suggests a method, the so-called indirect method, that applies to passive vibration isolators with linear dynamic behaviour and whose contact interfaces with source and receiver can be approximated as point contacts. The standard applies also to vibration isolators presenting non-linear static behaviour but showing, for a given static preload, an approximately linear response to dynamic input.

An example of test rig layout for the dynamic characterization of vibration isolator is reported in Figure 3.1.

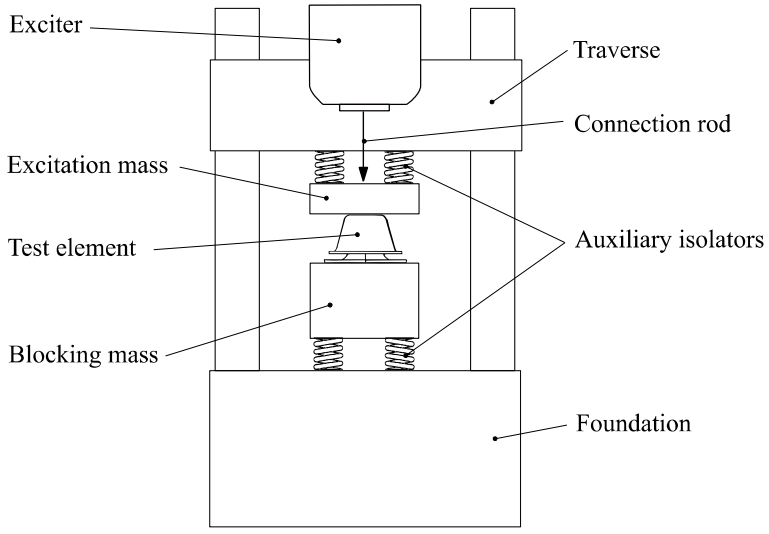

Figure 3.1 - Indirect method test rig arrangement

The method is particularly suited for high frequency measurements where problems related to the test facility structure resonance might occur. In the suggested method, the blocking force on the output side of the vibration isolator under test is derived from the acceleration of a compact mass, the blocking

mass m_2, placed at the output side of the isolator. The blocking mass needs to be dynamically decoupled from the rest of the structure both to allow its motion under the test element output force and to avoid flanking transmission during the test. Newton's law is used to derive the value of dynamic transfer stiffness starting from the acceleration of the blocking mass, relation (2.5) gives:

$$k_{21} \approx \frac{F_{2,b}}{u_1} = -(2\pi f)^2 (m_2 + m_f) T \tag{3.1}$$

Where T is the transmissibility, m_2 is the mass of the blocking mass, m_f is the mass of the output flange of the test element and f the frequency. Transmissibility is the ratio between displacement on input and output side of the test element, $T = u_1 / u_2$; the same values of transmissibility can be obtained if complex velocities or acceleration are used instead of displacement [41].

In (3.1) the blocking force value, $F_{2,b}$, is approximated because the contribution of the auxiliary elastic elements used to allow the blocking mass motion is neglected. Indeed, the dynamic equilibrium of the blocking mass could be written as:

$$F_2 = m_2 a_2 + k_{ae} u_2 \tag{3.2}$$

where the forces acting are the isolator output force F_2, the inertial force $m_2 a_2$ and the reaction given by the auxiliary isolator $F_{k,ae} = k_{ae} u_2$ being k_{ae} the dynamic stiffness of the auxiliary isolators. In practice, in the indirect method $\left|F_{k,ae}\right| \ll \left|m_2 a_2\right|$, because to lower the frequency of the blocking mass resonance, soft isolators or a significant mass are used. In addition, increasing the frequency, the contribution of the inertia increases consistently. It follows that the driving point stiffness of the receiving structure herein represented by the blocking mass is:

$$k_t = m_2 (2\pi f)^2 + k_{ae} \approx m_2 (2\pi f)^2 \tag{3.3}$$

The relation (3.1) is valid only if transmissibility is much lower than unity, $|T| \ll 1$, and if the frequency range, f, of investigation is higher than the greater frequency of rigid body motion, f_0, associated to the system composed by the blocking mass, the vibration isolator under test and the soft isolators bed, $f \gg f_0$. The first condition on the transmissibility implies that driving point

stiffness on the output side of the vibration isolator is much lower than the driving point stiffness of the receiver, i.e.: the blocking mass, so to consider valid the approximation reported in (2.5). The second condition is to avoid the influence of the blocking mass motion at its resonant frequencies on the acceleration measured on the output side of the test element.

At the lower side, the frequency range is determined by the frequency of the blocking mass suspension system while on the higher side it is determined by the stiffness of the blocking mass.

For rubber like isolators, the lowest internal frequency, along with the stiffer direction, is approximated by:

$$f_e \approx \frac{1}{2}\sqrt{\frac{k_0}{m_{el}}} \tag{3.4}$$

where f_e is the estimated lower internal frequency in *Hz*, k_0 is the low frequency stiffness and m_{el} is the mass of the elastic part of the isolator. Most isolators have a spring-like behaviour, with a constant stiffness, up to a frequency equal to $f_e / 3$. A value of the blocking mass, m_2, such that $f_0 \le 0.1 f_e$ allows reliable dynamic transfer stiffness measure from frequency range $f > f_e / 3$. For frequency lower than $f_e / 3$, dynamic transfer stiffness of the isolator can be approximated to the value measured for $f = f_e / 3$. This consideration applies if the expected working range of the isolator is higher than $f_e / 3$.

3.1 Test accuracy prescription

The approximation in (3.1) is valid only if the input vibration level is much higher than the output vibration level in order to avoid the influence of blocking mass modes on the outcomes of the test. ISO 10846-3 quantifies this difference lower limit as follows:

$$\Delta L_{1,2} = L_{a1} - L_{a2} \ge 20 \; dB \tag{3.5}$$

Where L_{a1} is the acceleration level on the input side and L_{a2} is the acceleration level on the output side. The acceleration level, both for the input and the output side is defined as

$$L_a = 10 \cdot \log_{10} \frac{a^2}{a_0^2} \tag{3.6}$$

where $a_0 = 10^{-6}\ m/s^2$ is the acceleration reference value.

The level difference, $\Delta L_{1,2}$, needs to be guaranteed at the lower limit of the analysis range while at the upper frequency, internal resonance phenomenon may occur in the resilient element [58, 44], increasing the transmissibility of the test element, so reducing consistently such value. The results, in this case, are still valid.

$\Delta L_{1,2}$ gives the lower limit for test range f_2. The upper limit, f_3, is given by the frequency at which the blocking mass stops to behave as a rigid body. The expression (3.1) is valid in the range $f_2 < f < f_3$ while, at frequency higher than f_3, the dynamic transfer stiffness is calculated as:

$$k_{21} = \frac{F_{2,b}}{u_1} \approx -(2\pi f)^2 (m_{2,eff} + m_f) T \tag{3.7}$$

$m_{2,eff}$ is the effective mass of the blocking mass. The effective mass is frequency dependent and it is defined as the ratio between the excitation force on the blocking mass, due to vibration isolator, and its acceleration. ISO 10846-3:2002 is valid only for frequency $f \le f_3$. The frequency limit f_3 is the frequency at which blocking mass starts behave as a deformable body and it is defined as the frequency at which the following inequality is valid:

$$|\Delta L| = \left| 10 \cdot \log_{10} \frac{m_{2,eff}^2}{m_2^2} \right| \ dB \le 1 \ dB \tag{3.8}$$

$m_{2,eff}$ needs to be measured and depends on the excitation direction. In order to measure the effective mass, the blocking mass needs to be suspended on an elastic support to guarantee a natural frequency of the SDOF system lower than 10 Hz.

The test layout for the measure of the effective mass is shown in Figure 3.2. Named S the contact area of the isolator output flange, the blocking mass is excited by a

force F_2 along the test direction in the centre of the contact area. Two accelerometers placed inside the contact area, symmetrically to the centre, and with a distance $D = \sqrt{S}$ measure the acceleration, a'_1 and a''_1, along the same direction. Both the acceleration and the force are phasors. The effective mass is defined as:

$$m_{2,eff} = \frac{2F}{(a'_1 + a''_1)} \tag{3.9}$$

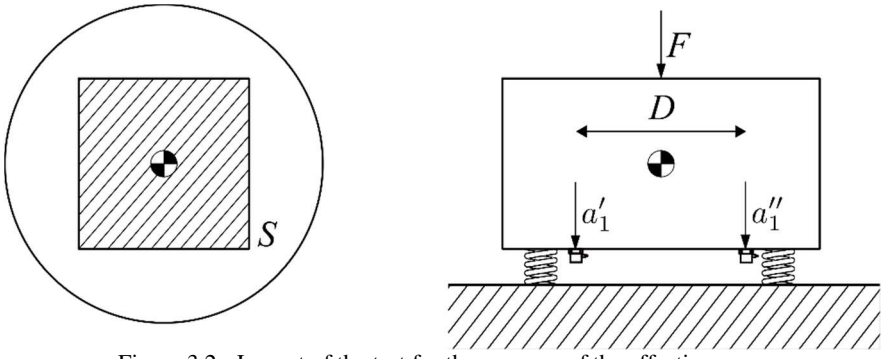

Figure 3.2 - Layout of the test for the measure of the effective mass

ISO 10846 defines the standard to dynamic transfer stiffness of vibration isolators excited by unidirectional force. The measurements along the three orthogonal directions are considered separately and an improper excitation could lead to high or unwanted response level along other directions. To guarantee the accuracy of the test, the accelerations along the other two orthogonal directions needs to be limited. With reference to a normal excitation, vertical excitation $a_{1,z}$, accelerations along the two perpendicular directions, $a_{1,x}$ and $a_{1,y}$, have to be measured at the side of the excitation mass. A possible layout for the accelerometer is showed in Figure 3.3. With reference to the standard, measurements are valid if the acceleration levels $a_{1,x}$ and $a_{1,y}$ are 15 dB lower than $a_{1,z}$ with $a_{1,z}$ measured on the centre of the excitation mass, or by the average of two accelerometers mounted symmetrically with respect to the centre of excitation mass.

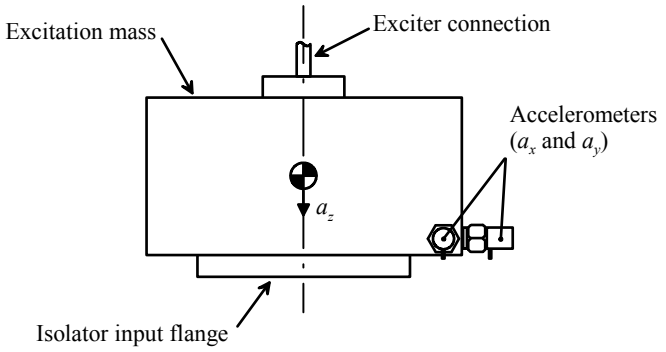

Figure 3.3 - Layout to measure perpendicular accelerations on the effective mass

To guarantee measurement accuracy it is fundamental to avoid flanking noise transmission that can be caused by the connection of the vibration source to the test rig structure but also from airborne noise. International standard does not report a minimum difference between the vibration level of the blocking mass and the vibration level measured on the foundation but the operator is addressed to demonstrate that the acceleration level measured on the foundation is low enough to guarantee the accuracy of the results. At Ship Noise and Vibration Laboratory, a difference in the acceleration level of 30 dB is considered acceptable. A 30 dB level difference means that the acceleration measured on the foundation is approximately 3% of the acceleration measured on the blocking mass.

The excitation could be provided with a step sine, a sine sweep or a bandlimited white noise. In case of step sine, at least 5 points per third octave band must be guaranteed. The excitation system needs to guarantee a vibration level, $L_{a,2}$, on the blocking mass of at least 15 dB above the background noise level measured on the same. In such cases, where minimum excitation level is reached, the aforementioned limitations on flanking noise are too strict, in fact, background noise level on the blocking mass and on the foundation are generally comparable. It is clear that in such cases, a 30 dB level difference is impossible to achieve and lower differences could be accepted.

3.2 High-frequency test rig description

At the Department of Engineering and Architecture of the University of Trieste, the Ship Noise and Vibration Laboratory (NVL) provides an experimental rig for high frequency dynamic characterization of vibration isolator in accordance with the ISO 10846-3 standard. The test rig was designed for dynamic characterization of resilient mount for marine medium speed diesel engine. Its peculiarity is the flexibility in test element dimension ranging from the small to the biggest resilient element available on the market nowadays for marine application. This characteristic allows also the test of vibration isolators different from resilient mounts, as in this case, where a pillar isolator with a pillar portion associated has been tested [26, 25].

Figure 3.4 shows the NVL high frequency test rig. A main supporting frame (B) rigidly connected on a concrete base supports the mobile traverse (E). The mobile traverse can move along the vertical axis allowing the test of elements with

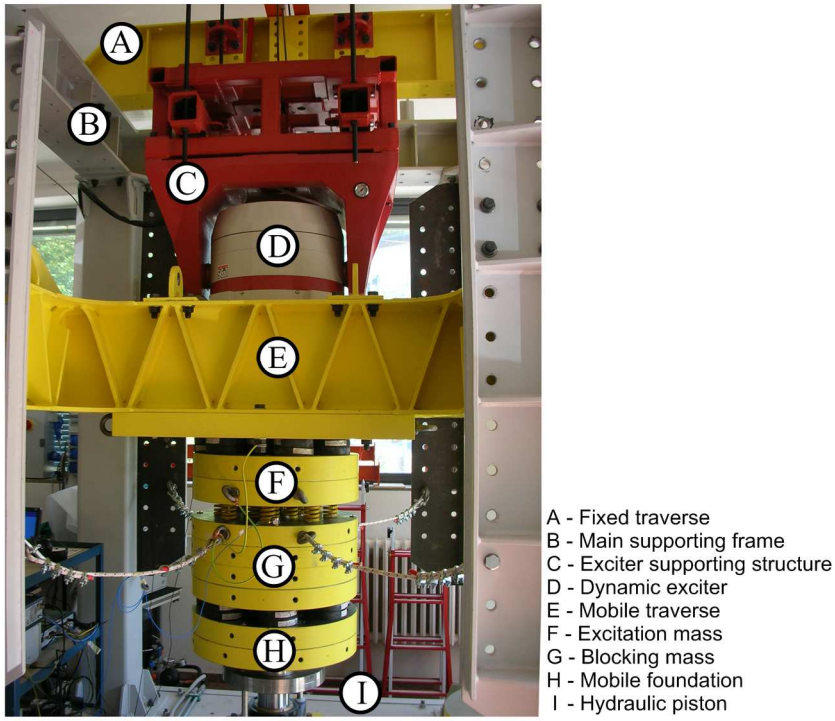

Figure 3.4 - High frequency test rig at NVL laboratories at University of Trieste

different heights. A fixed traverse (A) supports the dynamic exciter (D). The exciter is hinged to the fixed traverse by its supporting structure (C) and the insertion of elastic elements allows the dynamic decoupling of the exciter from the test rig frame. Below the mobile traverse there is the system composed by the moving masses, the excitation mass (F) and the blocking mass (G). The blocking mass is suspended above the mobile foundation (H) by auxiliary elastic elements. The foundation is rigidly connected on a hydraulic piston (I) that compresses the blocking mass, the test element and the excitation mass to the mobile traverse generating the static preload required for the test. Figure 3.5 shows a particular of the mobile system composed by the mobile foundation, the blocking mass and by the excitation mass. Between the hydraulic piston for static load and the mobile foundation a set of static load cells measure the preload applied to the element under test. The upper static load support plate, both in Figure 3.5 and in Figure 3.6, is connected to the mobile traverse and has a hole in its centre to allow the connection of the exciter to the excitation mass by a steel stinger rod. The whole system is sketched in Figure 3.7. The hydraulic preload system along with the supporting frame and mobile transverse are able to reach a static compression force of 150 kN. The excitation source is an electro dynamic shaker with a rated output force of 4 kN for a fixed sine excitation and a maximum frequency range up to 4 kHz. The limitations listed in Section 3.1 limit the effective analysis range of the test rig, the NVL experience on resilient mounts used on marine diesel engine shows a typical measurement range from 100 to 1000 Hz.

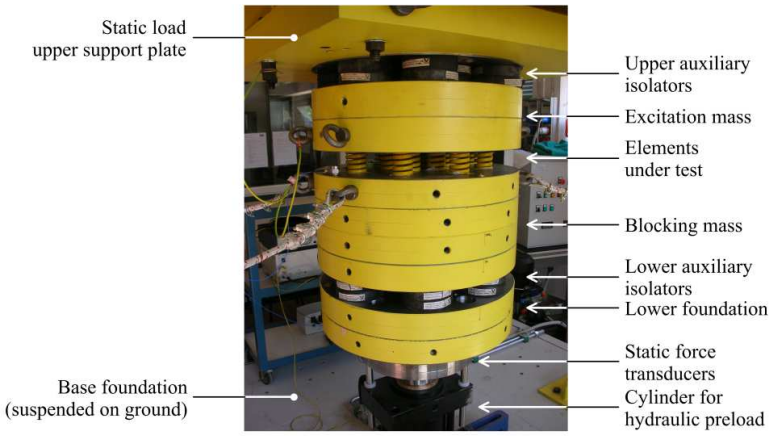

Figure 3.5 - Moving system [25]

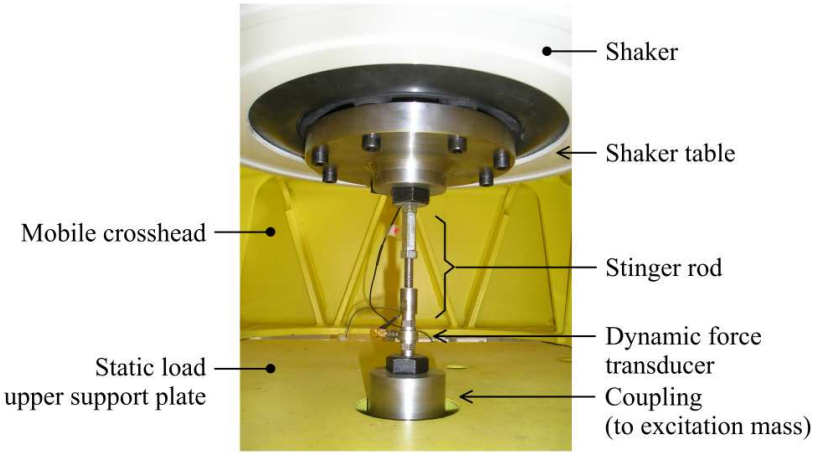

Figure 3.6 - Connection between the exciter and the excitation mass [25]

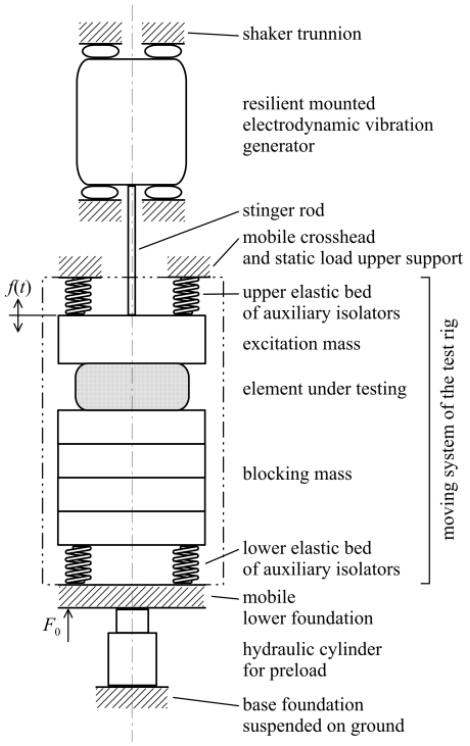

Figure 3.7 - Test rig layout [81]

4 Low-frequency dynamic characterization

The ISO 10846-2:2008 [46], is the reference standard for the measure of the mechanical dynamic properties of an isolator in the low frequency range. The standard presents the method for the direct measure of the dynamic transfer stifness of the isolator. As for the indirect method, the direct method applies to linear passive isolator or to those vibration isolators presenting non-linear static behaviour but showing, for a given static preload, an approximately linear response to dynamic input.

The direct method requires the measure of displacement, or velocity or acceleration, at the input side of the isolator and the measure of the blocking force at its output side. Figure 4.1 shows the basic test arrangement for the direct measure of the dynamic transfer stiffness. The element under test is placed between an actuator, on the input side, and a rigid foundation where the blocking force is measured by dynamic force transducer. The same actuator or a dedicated system applies the nominal static load to test element.

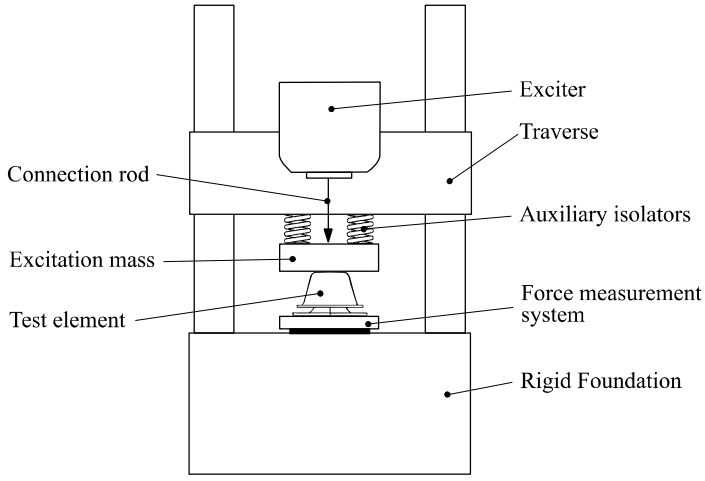

Figure 4.1 - Test rig layout for the direct measure of the dynamic properties of a vibration isolator

The dynamic transfer stiffness, $k_{2,1}$, is derived as:

$$k_{2,1} = \frac{F_2}{u_1} \text{ for } u_2 \ll u_1 \tag{4.1}$$

The condition reported in (4.1) is necessary to guarantee that the output side of the resilient element is effectively blocked. At higher frequency, flanking noise transmission problem may occur resulting in excessive motion of the blocked side, upper frequency limits for the validity of the direct method are generally reported between 300 *Hz* and 500 *Hz*, these limits depend mainly on the mechanical characteristic of the test rig structure.

4.1 Prescription for test accuracy

During direct measurement of dynamic transfer stiffness of vibration isolators, the following conditions have to be verified to guarantee the accuracy of the measurement:

- stiffness mismatch between the element under test and the rigid foundation of the test rig;
- blocking force measurement accuracy;
- unwanted input vibrations.

The first condition is the one reported in the definition of dynamic transfer stiffness as in (4.1). In most cases, accelerations are measured instead of displacement and as lower limit to guarantee a good approximation of the blocking force a difference of at least 20 dB between the accelerations measured on the excitation mass and on the foundations is required as follows:

$$\Delta L_{1,2} = L_{a_1} - L_{a_2} \geq 20 \; dB \tag{4.2}$$

L_{a_1} is the vertical acceleration measured on the excitation mass and L_{a_2} is the acceleration measured on the foundation or on the force distribution plate if more than a force sensor is necessary. The same limit is valid also if velocity or displacement are used instead of accelerations.

The second condition is on the accuracy of the output force measurement when a force distribution plate is used to distribute the force among more force transducer or to give sufficient stability to the output flange of the isolator. In such cases, recalling the symbol used in Figure 4.2, the approximated blocking force F_2' differs from the measured blocking force F_2 of a quantity $m_2 a_2$, corresponding to the inertial force associated to the motion of the force distribution plate. It has to be verified that the force used to move the distribution plate is small if compared with the output force measured by the transducer, thus reducing the systematic error in the measurement. A required limit on the mass of the distribution plate is the following:

$$m_2 \le 0.06 \cdot \frac{10^{L_{F_2}/20}}{10^{L_{a_2}/20}} \tag{4.3}$$

where m_2 is the mass of the force distribution plate, L_{F_2} is the output force level (refer to 10^{-6} N) measured by the force transducer and L_{a_2} the acceleration level measured on the force distribution plate. The inequality (4.3) is the same as accepting a maximum discrepancy between the values of F_2' and F_2 of 0.5 dB. If the condition is not verified the standard suggests to reduce the mass of the force distribution plate or to increase the stiffness of the force transducers. A method to correct the measure from the inertial effect of the force distribution plate is proposed in [59].

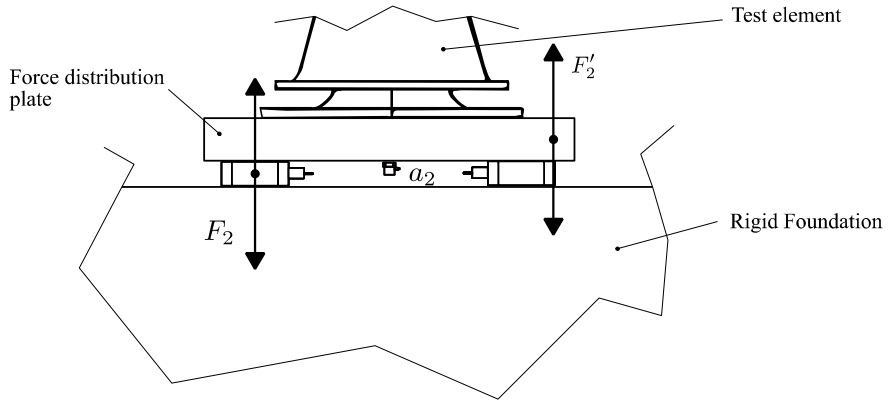

Figure 4.2 - Particular of the forces acting on the force distribution plate

The third limitation is on the input vibration quality. As the indirect method for high frequency range, also the direct method evaluate the dynamic transfer stiffness

of a vibration isolator subject to a unidirectional input vibration. In order to assess the accuracy of the measurement, the acceleration levels measured along the excitation direction and the acceleration levels measured along the two orthogonal direction must differ of at least 15 dB.

4.2 Description of the low-frequency test rig

An experimental-rig has been specifically designed to perform the dynamic characterization of the pillar isolator in the low frequency range according to direct method proposed in the standard [60].

The low frequency test rig designed and installed at NVL laboratories is shown in Figure 4.3. Two columns rigidly connected to a rigid foundation compose the frame of the test rig (A). The mobile traverse (B) is connected to the columns by four separate brackets allowing the test of element of different heights. A set of dynamic

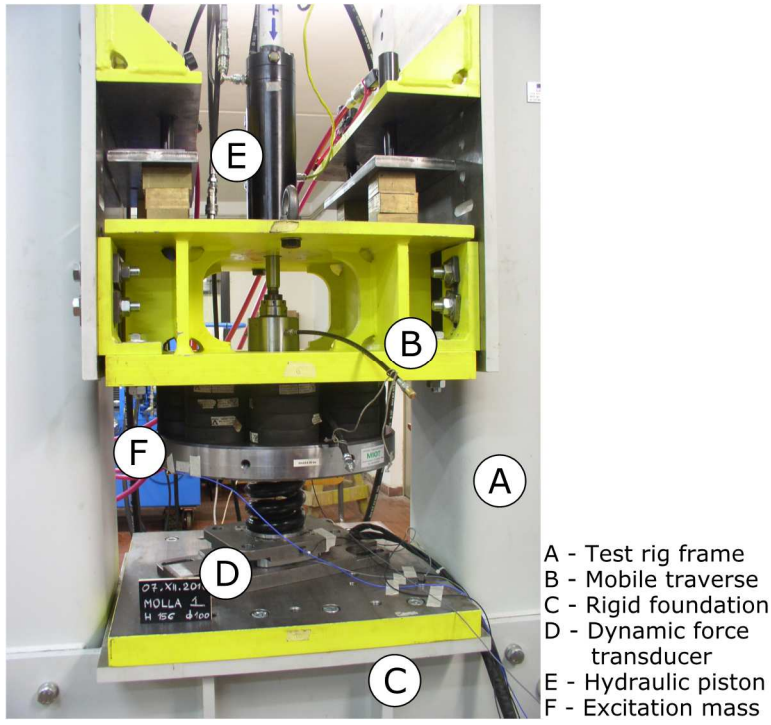

Figure 4.3 - Low frequency test rig at NVL laboratories at University of Trieste

force transducer (D), placed on the rigid foundation (C), measures the blocking force at the output side of the isolator. The vibration source (E) is rigidly connected to the top of the mobile traverse and it is connected to the excitation mass (F) by a sleeve passing through a linear bearing. The excitation mass, applying the input vibration to the test element, is decoupled from the mobile traverse by auxiliary isolators. Four pistons for the static preload compress the moving system composed by the mobile traverse, the excitation mass and the element under test.

Figure 4.4 shows a sketch of the low frequency test rig working principle. The preload system can achieve a compression force of 200 kN. The vibration source is a hydraulic actuator with a maximum rated force of 40 kN while the frequency range that can be covered using the low-frequency test rig goes from 0 Hz up to 180 Hz. The upper limit is governed by the resonance of the test rig frame that reduces the accuracy of the measure.

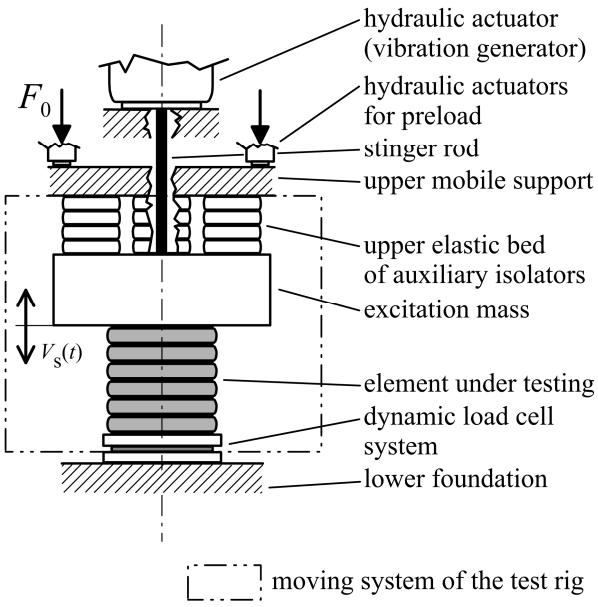

Figure 4.4 - Low frequency test rig sketch [79]

5 Real scale test

Real scale test of a pillar isolator is an important step because, during the years, vibration transmission and its paths have never been fully clarified. For on board vibration sources, like diesel engines, to lower the vibration transmitted to the ship structure it is enough to decouple the source using isolators, thus interrupting the main vibration transmission path. The case of the pillar is quite different, because the lower deck, namely the vibration source, is connected to the upper deck not only by the pillar but also through the side plates and through the bulkhead. Using the pillar isolator only one of the connections is interrupted while the other paths still transmit vibrations. The possibility that the vibrational energy not reaching the upper deck through the pillars could reach it through other paths still open could lead to null vibration reduction or to too poor benefits to justify the cost and the complexity introduced by the isolated pillar. Therefore, the assessment of the pillar isolator effectiveness on a real scale structure, which closely approximates those of a real ship, is a fundamental step in its development.

CSNI (Consorzio per Servizi Navali e Industriali) Scarl laboratories in Genoa, a company specialized in the development and testing of noise and thermal insulation solutions for marine application, provides a mock-up reproducing a between deck portion with typical structure of a cruise ship. Figure 5.1 shows a sketch of the mock-up. It consists of two reinforced decks, a side plating and a transversal bulkhead portion on two adjacent sides while the other two sides are open, in the corner, between the two open sides, a pillar supports the upper deck. The mock-up has a length of 6.68 m, a width of 6.28 m and a height of 2.72 m. The mock-up structure is suspended by four leaf springs placed at half-length of each side under the primary beams.

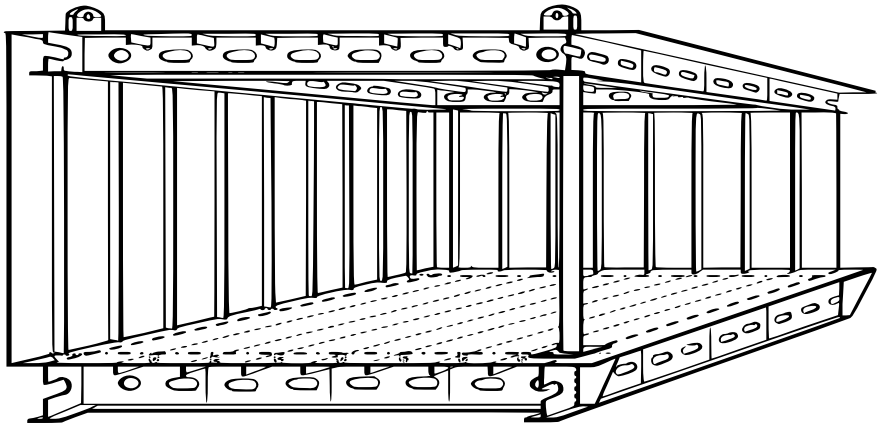

Figure 5.1 - Real scale mock-up sketch

5.1 Structure-borne noise sound insulation evaluation

Data about measurement of vibration transmission through pillars on board of a real ship is not available in literature. Only some evidence is to be found in the work of Borrough et al. (1979) [61] (only the abstract of the research presentation is available). In that case, authors used a measure of sound pressure levels to evaluate the influence of a pillar in structure-borne sound transmission. As result of their research, they suggest avoiding as far as possible the use of pillars.

In order to tackle the effectiveness of a pillar isolator, literature on the effectiveness assessment of isolator has been investigated. For resilient element under vibration source, the effectiveness, E, of the isolator ([57, 27, 62]) is defined by:

$$E = \frac{V_f\big|_{rigid}}{V_f\big|_{isolator}} \tag{5.1}$$

Where $V_f\big|_{rigid}$ is the vibration velocity of the foundation when the vibration source is rigidly connected to it and $V_f\big|_{isolator}$ is the vibration velocity on the foundation when the isolator is mounted. The insertion loss is defined as:

$$L = 20 \cdot \log_{10} |E| \tag{5.2}$$

Insertion loss, as defined above, evaluates the local effect of resilient element on machinery foundation.

Some index to evaluate the effect of distributed parameters isolation systems has been proposed in recent research on the characterization of ship's cabin floor insulation. In [34] insertion loss of a ship's cabin floating floor has been measured using accelerometers and exciting the floor with a tapping machine. The tapping machine has been moved to excite the structure in different points, while the accelerations measured on the bare deck, A, and on the floating floor placed on the deck, A_f, have been averaged. The insertion loss index has been calculated as follows:

$$IL_A = 20 \cdot \log_{10} \frac{A}{A_f} \tag{5.3}$$

In [63], basing on the results reported in [64] and [65], three different indexes are defined to evaluate the effectiveness of a new floating floor arrangement. The tests have been performed on real scale application of the floating floor solution under test on a ship's deck structure with dimensions of about $3\ \text{m} \times 3\ \text{m}$. The structure was excited with a hammer and the resulting acceleration was measured on a grid of points. Transmission loss index, TL, characterizes the difference of vibration velocity level between the lower side of the deck's portion (bare side) and the upper surface of the floating floor, as follows:

$$TL = L_{v,deck} - L_{v,floor} \tag{5.4}$$

$L_{v,deck}$ is the averaged velocity level measured on the lower face of the deck's plating and $L_{v,floor}$ is the averaged velocity level measured above the floor. The velocity level for each measure point is calculated as

$$L = 20 \cdot \log_{10} \frac{v}{v_{ref}} \tag{5.5}$$

with $v_{ref} = 10^{-9} m/s$ and the average values are calculated following the next formula:

$$L_v = 10 \cdot \log_{10} \left(\frac{1}{n} \sum_{1}^{i=n} 10^{L_i/10} \right) \tag{5.6}$$

Insertion Loss index, IL , represents the difference between the vibration velocities measured on the upper face of the deck's structure without the floating floor installed and the vibration velocities measured on the floor surface. Similarly to (5.3), insertion loss is defined by:

$$IL = L_{v,0} - L_{v,floor} \tag{5.7}$$

$L_{v,0}$ is the averaged velocity level measured on deck plating when the floating floor is not yet installed. The last index defined is the Insertion Loss of the base structure, IL_{bs} , and defines how the supporting structure is affected by the treatment, the application of the floating floor. Insertion loss base structure is defined by:

$$IL_{bs} = L_{v,0} - L_{v,deck} \tag{5.8}$$

The former indexes are given in third-octave band instead of narrow band with respect to the frequency range of analysis. The representation of the results as difference of average velocity levels in third-octave frequency band is a number of practical use in the design process although these indexes are used mainly to compare different solutions giving a quick and comprehensive rating of their overall performance.

Real scale effectiveness measurement of the vibration isolator installed to the pillar can be faced in a local way, taking into account, for example, only the transmissibility of the pillar installed on the mock-up, or in a global way trying to evaluate the mock-up's upper deck global response. Evaluating the global response of the upper deck is important because the vibration transmission path is defined not only from the pillar but also from the side plating and bulkhead connecting the lower and the upper deck. Since, for adjacent decks vibration transmission, the transmission path is defined not only by the pillar but also from the side plating and bulkhead connecting the lower and the upper deck, a global approach is better suited for the effectiveness assessment of such an isolator. Thus, in the real-scale test the global effectiveness of the isolator will be measured using the insertion loss index as defined in (5.7) where, instead of the vibration velocity of the floor surface, the vibration velocity of the upper deck when the pillar isolator is installed will be used.

5.2 Test description

Two different sets of measurements, one with the standard pillar and one with the isolated pillar, have to be carried out to investigate the effect of the vibration isolator on the structure-borne noise transmission. An electro dynamic shaker excites the structure in vertical direction near the base of the pillar while accelerometers measure acceleration of the mock-up structure in different points.

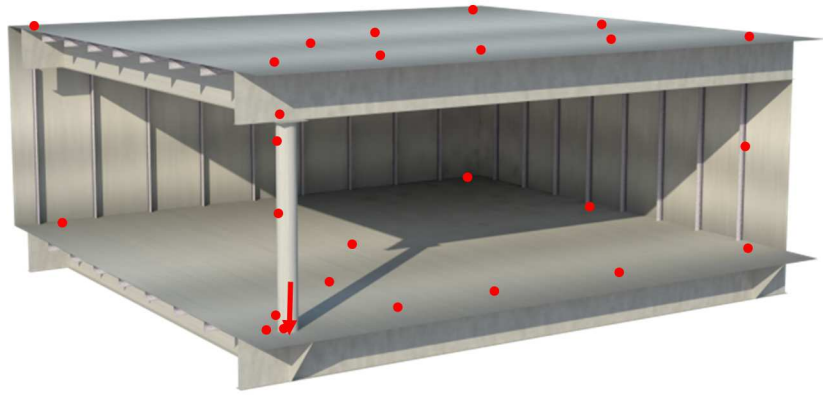

Figure 5.2 - Excitation and measure points position on the mock-up

In Figure 5.2, the arrow shows the position of excitation source while the points show the position of the accelerometers. Accelerometers positioned on the two decks and on the main beam supported by the pillar measure along the vertical direction. One triaxial accelerometer has been moved in three different positions along the pillar measuring the acceleration in the lower part, at its middle span and in the upper part.

Figure 5.4 shows a picture of the real scale mock-up. Since the main purposes of the mock-up are airborne sound insulation test and impact sound insulation test on insulation materials for marine applications, three cabins are reproduced, two cabins take place in between deck while one is placed on the upper deck. Figure 5.3 shows a particular of the shaker connection. The shaker has been elastically suspended using a floor crane and it has been connected to the supporting plate under the pillar using a stinger rod. Accelerometers have been connected to the structure using magnetic bases.

Figure 5.4 - Real scale mock-up

Figure 5.3 - Shaker connection near the base of the pillar

In addition to the global insertion loss of the upper deck, to have a better insight on the effect of the isolated pillars, also a pillar transmission loss and several local insertion loss have been calculated. The transmission loss indexes have been calculated between the base and the top of the pillar both for the standard pillar and for the isolated pillar. The local insertion loss indexes have been calculated grouping the measure points to evaluate the changes in structure-borne noise transmission in the main areas of the upper deck. Insertion loss have been calculated on the top of the pillar, on the upper deck's main supporting beam, along the side connection with the side plating and the bulkhead and near the centre of the upper deck self.

6 Simplified finite element model of the isolator

Data acquired during the dynamic characterisation of the pillar isolator prototypes can be used to define a simplified element for FE analysis. Such representation of the pillar vibration isolator can be useful for vibration level prediction in a design stage, where local finite element models of the ship structures are built to investigate its dynamic behaviour [66, 67, 68].

The simplified model has been developed using MSC Patran/Nastran environment. A BUSH element, a spring-damper structural element with nonlinear and frequency dependent capabilities [69], is the representation which better suits the purpose of a simplified model as depicted above. A BUSH element is defined by two nodes and its reference system is completely defined by an orientation vector. Mechanical and dynamic characteristics of the BUSH element are defined by stiffness and damping values, which can be nonlinear or frequency dependent, for all the 6 degrees of freedom. In the specific case, as shown in Section 12, only frequency dependent stiffness capability has been considered. The frequency response analysis has been carried out using the direct method in which the stiffness matrix of the model is updated and the motion equation are solved for each frequency step of the analysis.

To validate the definition of the simplified FE representation of the pillar vibration isolator, a finite element model of the mock-up has been created. The validation process went through a first phase in which the FE model of the mock-up with the standard pillar has been verified on the measurements taken on the ship's deck mock-up with standard pillar. The second phase was the set-up of the simplified pillar isolator model by successive update of the simplified element characteristics.

Figure 6.1 shows the mock-up FE model. Low order shell elements have been used to model the structure, flat bulb stiffener has been approximated to flat stiffeners and modelled with shell elements. Since the BUSH element representing the pillar isolator is a 1D element (element connecting two grid points) the pillar has been modelled in the same way to avoid the introduction of connecting elements

between the pillar isolator (BUSH) and an even explicit model of the pillar (using shell elements). The average size of the elements was the outcome of a sensitivity study where two different FE models of the mock-up structure have been compared. The reference model has been built following the considerations reported in [70]. The authors suggest the use of at least ten elements per bending wavelength where the bending wavelength is evaluated basing on the maximum frequency of analysis for an infinite plate. This consideration leads to an average edge element length of about 30 mm for a frequency range up to 500 Hz. The second model has elements length fixed to an average value of 100 mm. The result of the sensitivity analysis, based on the frequency response function evaluated on some relevant points, shows that the approximation introduced using larger elements is below a threshold of 3 dB on the most of the analysis range. Considering the computational effort and the iterative process planned for the simplified isolator model set-up, the model with average element edge of 100 mm has been chosen for the set-up and validation of the simplified isolator model.

As shown in Figure 5.4, three cabins are housed in the mock-up. The cabins wall are made of sandwich panel composed by a 2 mm steel plate and 50 mm mineral wool layer. Since the aim of the cabins is to reproduce a cruise ship environment

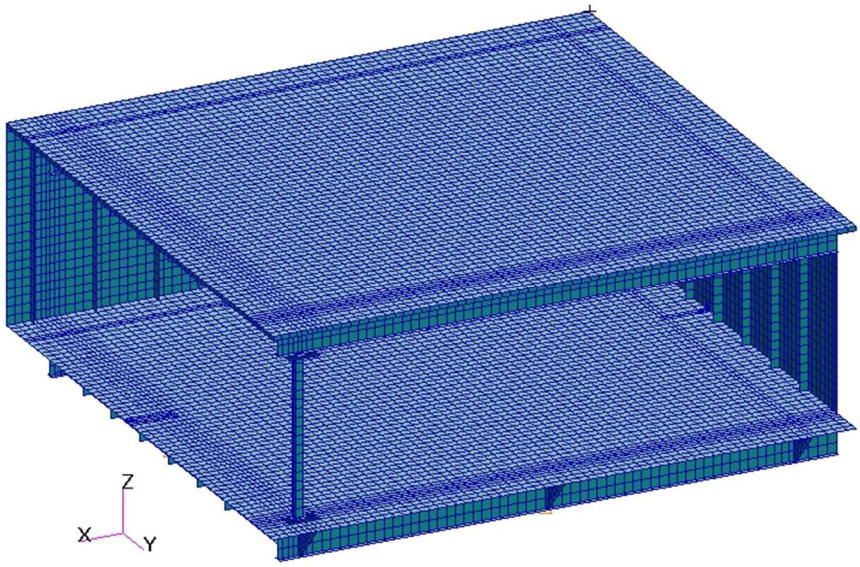

Figure 6.1 - Mock-up finite element model

from the point of view of noise insulation, their sidewall are only spot welded to the mock-up structure every 30 to 40 cm and a silicone sealing fills the remaining gaps. To simplify the problem, considering the fact that the connection of the cabins side walls is very limited with respect to the total perimeter of the cabins, the cabins have been neglected and their contribution to the global dynamic behaviour of the mock-up structure has been considered only in terms of locally distributed weight and damping. The stiffness of the spring leafs used to suspend the mock-up structure has been derived from impact test measurements. From the test, the vertical rigid body frequency has been identified while the mass has been evaluated using the FE model, so drawing the stiffness of the suspensions.

6.1 Use of correlation indexes

The definition of the pillar isolator simplified model involves both the analysis of the original mock-up structure, with the non-isolated pillar, and the modified structure. To verify the effectiveness of the representation of the pillar isolator simplified model it is important to verify that also the starting numerical models closely approximate the dynamic behaviour of the real structure, this check can be assessed making use of different correlation criteria.

The use of several types of correlation criteria is a common practice in model updating techniques, where a numerical model is subject to successive modifications until it reaches a certain degree of approximation of the physical model basing on such criteria. Model update techniques are often used in design process to increase the quality of numerical simulation results. These techniques are used mostly to investigate the dynamic behaviour of the structures when physical experiments might be very difficult or to solve vibration problems and reduce the time and the cost of testing of different design alternatives.

Model updating techniques use modal experimental data to refine the numerical model. The correlation between numerical and physical eigenvectors and the correlation between frequency response function of the degrees of freedom of the numerical model and of the physical structure are the key points of the update process [71, 72].

Model updating, depending on the dimension of the test structure and on the maximum frequency range of analysis, requires a big amount of measured points. In this study, only a limited number of points along the structure has been measured, those shown in Figure 5.2. With this amount of data, an update process could be carried out only on a very small frequency range with an upper limit not significant to the aim of the definition of a simplified model in a medium-high frequency range, however a local criterion can be used to validate the numerical model on some specific control points.

Local Amplitude Criterion, LAC, [73, 74] is a frequency function quantifying, for each degree of freedom the correlation between numerical results and experimental data. The Local Amplitude Criterion is defined as follows:

$$LAC_{ij}(\omega) = \frac{2\left|H^{*}_{Xij}(\omega)H_{Aij}(\omega)\right|}{\left|\left(H^{*}_{Xij}(\omega)H_{Xij}(\omega)\right)+\left(H^{*}_{Aij}(\omega)H_{Aij}(\omega)\right)\right|} \tag{6.1}$$

where the couple ij is defined by the i^{th} response and by the j^{th} excitation coordinates. H_{Aij} and H_{Xij} are the predicted and the measured FRF values at ω frequency, the $*$ denote the FRF complex conjugate.

Results

7 Maximum working load evaluation

The aim of the isolator is to reduce vibration transmission through the pillar, improving the comfort perceived on board. Cruise ships and superyachts have been identified as the first possible field of application of such a device and an analysis of two vessels of this kind has been carried out to find out the dimensions of the pillars in use and their compressive loads. One of the key factors in the selection of a proper resilient element is indeed the maximum compression load that it can withstand without damaging. Given the wide use of pillars and the high number of decks, the cruise ship represents a heavy working load condition for the pillar, while in case of a yacht the working condition is lighter. Loads acting on the pillars have been assessed using the formulations suggested by Lloyd's Register [4]. Due to the complexity of the cruise ship structure, the loads have been evaluated also using direct FE analysis carried out on an existing model of a typical large cruise ship, based on the guidelines reported in [75, 76]. Figure 7.1 shows the FE model of the cruise ship used in the analysis [77]. The model is a coarse mesh model, recommended for global response analysis of primary structure. Shell elements are used to model plates, girders' web and solid floors; flanges, longitudinals and pillars are modelled using beam element.

The loading conditions corresponding to maximum hogging and maximum sagging have been investigated. The results on some representative decks and for some of the most common pillars in use are presented in Table 7.1. Compression load and traction load for the corresponding pillar types have been taken as the maximum of

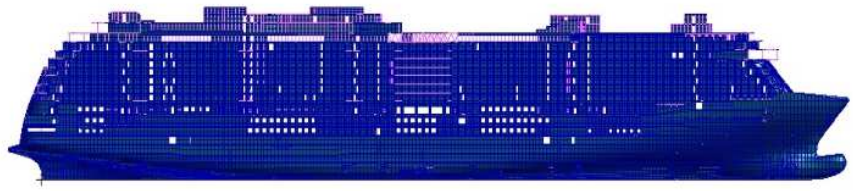

Figure 7.1 - FE model of the cruise ship used for load evaluation

the two load cases tested. The loads evaluated with the simplified formulations proposed by Lloyd's Register are considerably lower than those found by direct analysis. The reason of such difference is that in direct calculation also the effect of the design wave is taken into account.

Table 7.1 - Maximum pillar working load on a cruise ship [75]

Deck number	Pillar size	Maximum compresion load from FE model	Compression load from rules [4]	Maximum traction load from FE model
	mm	kN	(kN)	(kN)
7	300 × 300 × 14	956.331	688.896	401.826
10	200 × 200 × 14	456.231	482.227	440.895
16	110 × 100 × 12	224.257	137.779	-

The yacht on which the study was carried out has an overall length of 54 m, a maximum breadth of 9.6 m and 2.7 m draft with a full load displacement of 615 tons. It is composed by four decks with the last one not presenting pillars; Table 7.2 reports the results of the analysis.

Table 7.2 - Maximum pillar working load on a superyacht

Deck	Pillar section size	Compression load from rules [4]
	mm	kN
Main deck	Ø114.3 × 8	79.9
Lower deck	80 × 80 × 8	58.3

8 Prototypes construction

The evaluation of static load acting on pillars allowed the selection of the resilient element of the isolator. In order to minimize the impact of the device on the design process of the ship, the isolator dimension has to match the pillar section dimensions. It should also provide limited displacement under static loads. The whole load acting on a pillar needs to be supported by one single device, therefore, given the heavy load condition, materials such as rubber resilient elements should be avoided. As starting point to evaluate the specific load acting on the resilient element, the same pillar section dimensions has been considered as contact area between the pillar and the resilient element. The loads found out in the former section lead to the specific loads reported in Table 8.1.

Table 8.1 - Load per unit area of the pillars

Section type	Ship type	Section area	Maximum expected load	Specific load
mm	-	mm^2	kN	N/mm^2
300 × 300 × 14	Cruise	90000.0	956.3	10.6
200 × 200 × 14	Cruise	40000.0	482.2	12.1
110 × 100 × 12	Cruise	10000.0	224.3	22.4
Ø114.3 × 8	Yacht	10260.8	79.9	7.8
80 × 80 × 8	Yacht	6400.0	58.3	9.1

The imposed constraints and the high static load acting on the pillars increase the importance of the specific working load value. Various materials were considered for this use, though only a specific type of closed cellular polyurethane could best match the specifications required. The resilient material selected have a working specific load up to 6 N/mm^2 and can withstand load peaks up to 9 N/mm^2. Adopting the basic configuration proposed, consisting in the device dimensions close to the pillar section dimension, at least the yacht application can be covered. Furthermore, the loads taken into account represent the maximum design load, therefore an extreme condition, and not the real working condition of the pillars thus the possibility to apply the device on other ship structures, even using larger isolators.

Shape and dimension of pillar prototypes used in the study were selected in compliance with those generally used on board of superyacht. Prototypes differ as for shape and dimensions but also in the thickness of the viscoelastic layer between the external shell and the inner pillar. Considering that aim of the experimental test on prototypes was the evaluation of the dynamic stiffness of the decoupling device, the length of the pillars was selected in order to be tested on the test facilities available at the Ship Noise and Vibration Laboratory (NVL), so only a portion of the pillar has been associated to the device.

Since the work is a first trial to develop such type of isolator, the analysis has been limited to the case of pure compression load. In order to make the design and the construction of the prototypes as simple as possible any system to restrain the pillar movement in case of traction load have been neglected.

All the prototypes consist of an external shell, of 150 mm height, welded on a square base with 500 mm side and 15 mm thickness. The prototypes have a large base so to increase the contact area with the blocking mass and the stability of the system during the fitting of the test rig. Four triangular brackets, placed on the diagonals of the base plate, stiffen the connection between the external shell and the base.

The resilient pad is placed on the base plate and housed inside the external shell. The dimension of the pad is such that it is laterally constrained inside the containing shell. Despite the stiffness increase of the resilient element due to its lateral deformation constrain, the solution has been chosen to try to increase its maximum allowable specific load. For all the prototypes the thickness of the resilient element is 12.5 mm because this thickness configuration is the only one withstanding the working specific load identified in Section 7.

The pillar portion associated to the isolator has a length of 300 mm and is housed inside the external shell. A plate of 10 mm thickness close the bottom of the pillar so to increase the contact area with the resilient pad. A square or circular plate, with a span of 150 mm and a thickness of 15 mm, is welded on the top of the pillar portion and constitute the input flange of the prototype. Once the pillar section dimension has been chosen, the external shell section is selected to have a proper gap that is filled with a viscoelastic compound.

The results of the experimental tests shows same disturbance associated to the normal modes of the base in the high frequency range, this lead to the reduction of the base plate dimensions in the last prototypes.

The prototypes built for the experimental tests are listed in Table 8.2 along with the dimension of the main components. Some of them are also shown in Figure 8.1.

Figure 8.1 - Pillar isolator prototypes

Table 8.2 - Isolated pillar prototype list

Pillar Number	Pillar section	Cup section	Top plate dimension	Bottom plate dimension	Resilient pad dimensions	Viscoelastic thickness
	mm	mm	mm	mm	mm	mm
1	80 × 80 × 10	120 × 120 × 8	150 × 150 × 15	500 × 500 × 15	104 × 104 × 12.5	12
2	80 × 80 × 10	120 × 120 × 8	150 × 150 × 15	500 × 500 × 15	104 × 104 × 12.5	12
3	Ø 70 × 8	Ø 114.3 × 8.8	Ø 150 × 15	500 × 500 × 15	Ø 96 × 12.5	13.35
4	Ø 70 × 8	Ø 114.3 × 8.8	Ø 150 × 15	500 × 500 × 15	Ø 96 × 12.5	13.35
5	Ø 114.3 × 8.8	Ø 167 × 11.6	Ø 150 × 15	500 × 500 × 15	Ø 143.8 × 12.5	14.75
6	Ø 114.3 × 8.8	Ø 167 × 11.6	Ø 150 × 15	500 × 500 × 15	Ø 143.8 × 12.5	14.75
7	Ø 70 × 8	Ø 101.3 × 9.25	150 × 150 × 15	500 × 500 × 15	Ø 82.8 × 12.5	6.4
8	Ø 114.3 × 8.8	Ø 139.6 × 8	150 × 150 × 15	500 × 500 × 15	Ø 123.6 × 12.5	4.65
9	Ø 114.3 × 8.8	Ø 139.6 × 8	150 × 150 × 15	150 × 150 × 15	Ø 123.6 × 12.5	4.65
10	Ø 70 × 8	Ø 101.3 × 9.25	150 × 150 × 15	150 × 150 × 15	Ø 82.8 × 12.5	-

9 High frequency tests results

At the beginning of the experimental campaign, some tests have been carried out to identify the frequency range in which the limits for the accuracy of the measurement imposed by the reference standard ISO 10846-3:2002 [47] could be satisfied. The first configuration tested has a 500 kg blocking mass suspended on rubber element resilient bed. In the second configuration, the mass has been increased to 625 kg and the rubber element have been substituted with steel spring to reduce the height of the system. Figure 9.1 shows both the configurations.

a b

Figure 9.1 - High frequency test rig initial configuration (a) and improved configuration (b)

First test carried out on the original configuration shows the vertical resonance frequency of the blocking mass near 100 Hz due to the high stiffness of the test element. As a rule of thumb, to avoid blocking mass motion influences on dynamic stiffness measure, the measure can be considered reliable starting from a frequency three times higher than the resonance. This consideration leads to a lower frequency of about 300 Hz. Therefore, aim of the set up phase was to increase the available frequency range trying to lower the resonance frequency of the blocking mass. The blocking mass used in the high frequency-test rig is composed of steel disks, each one weighting 125 kg, fixed together by bolts. Due to clearances, only another disk could be added to the blocking mass and, to allow this change, steel spring isolator has been used instead of the rubber isolator. Figure 9.2 shows the transmissibility curves for the blocking mass in the two configurations, the first peak of the curves shows the vertical blocking mass resonance. The two changes lead to a small reduction of the vertical resonance frequency of the blocking mass. Increasing mass reduces the resonance frequency but using many parallel springs to withstand the static compression leads to a suspension that is stiffer than the one obtained through the rubber resilient element. The result of this opposing effect is a frequency reduction of about 20 Hz.

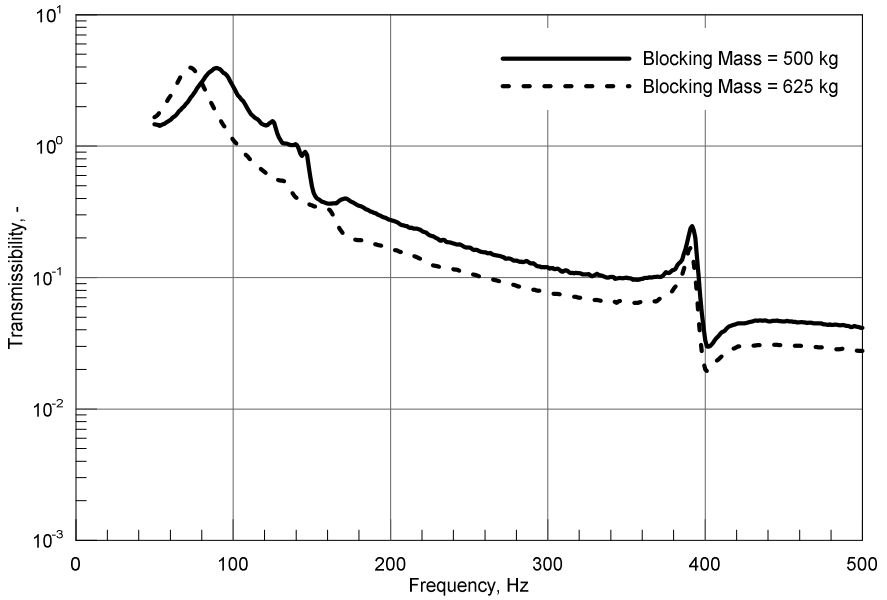

Figure 9.2 - Blocking mass transmissibility curves obtained with the initial configuration and the improved one

The arrangement of the blocking mass, composed by disks connected together instead of a unique block, has the pros that can be easily increased or reduced depending on the element to be tested while, on the other hand, it is a more flexible solution, if compared to a unique block of the same weight and dimensions. The blocking mass has been assessed to guarantee its stiffness. The effective mass has been evaluated according to the procedure reported in Section 3.1 and the result is reported in Figure 9.3. The difference between the effective mass and the real mass of the blocking mass is below the limit for a frequency range up to 1000 Hz.

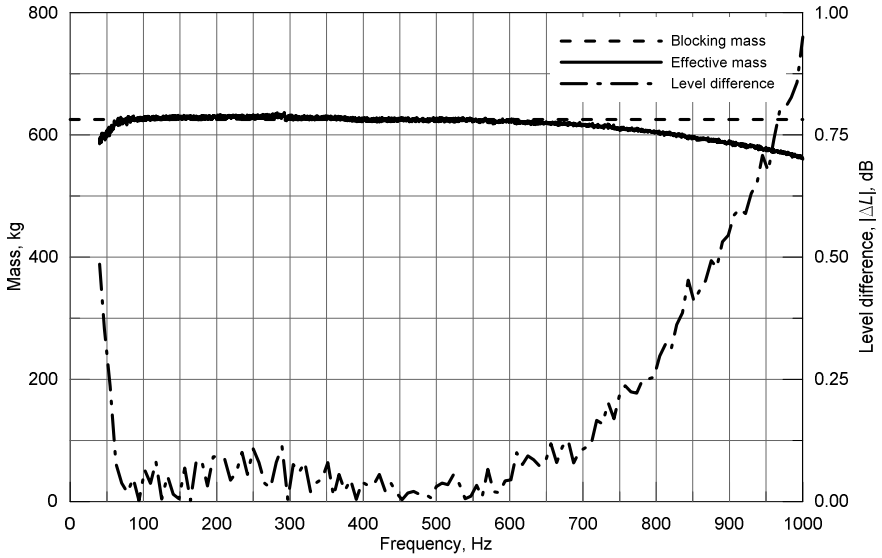

Figure 9.3 - Effective mass measure for the 625 kg blocking mass

Using Operating Deflection Shape, a simple analysis tool to show the mutual motion of different measurement points [78], the behaviour of the moving system has been investigated verifying the absence of unwanted motion and a prevalent vertical motion of the system in all the measurement ranges. The measure point definition is shown in Figure 9.4; the acceleration has been measured using a triaxial accelerometer that has been moved along the relevant points on the side of the masses composing the moving system. The system has been excited using an electrodynamic shaker controlled with a closed loop control chain using random spectrum with constant power spectral density between 50 and 1000 Hz.

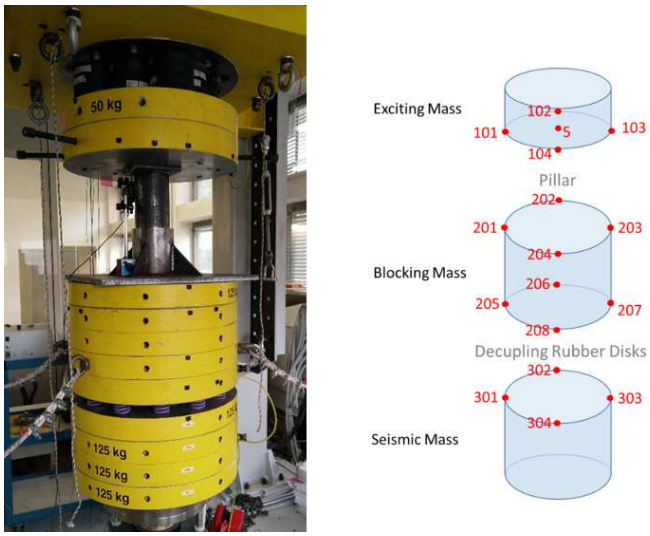

Figure 9.4 - ODS point definition

Figure 9.5 shows the transmissibility of the measure points; the reference point used in the analysis was the same used for the excitation input control and was located near the centre of the excitation mass at the interface with the isolated pillar prototype input flange (Point 5).

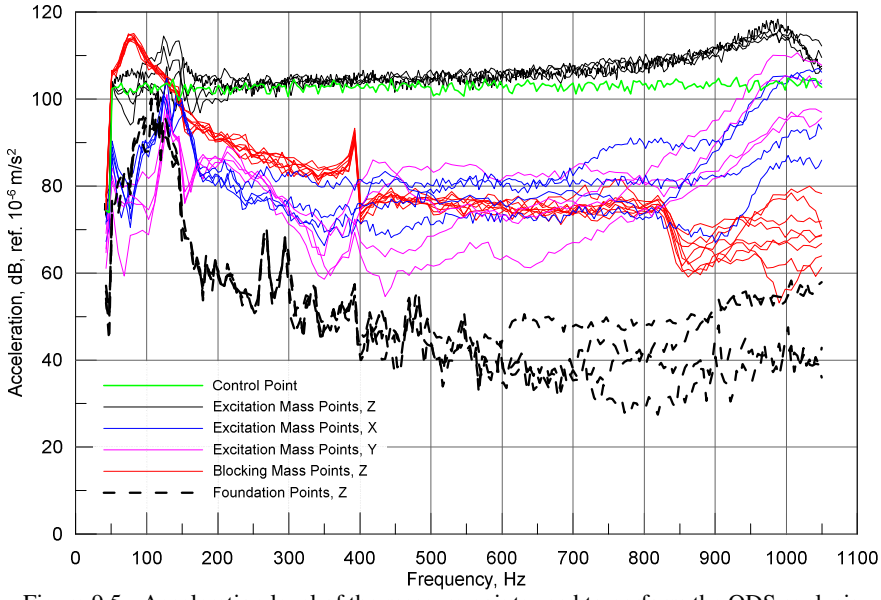

Figure 9.5 - Acceleration level of the measure points used to perform the ODS analysis

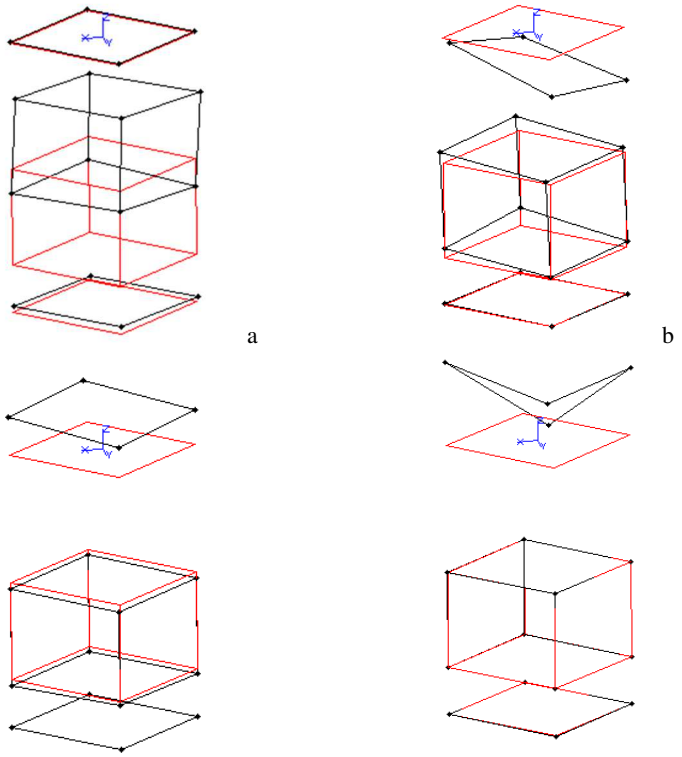

Figure 9.6 - Deflection shape evaluated at 77 Hz (a), 127 Hz (b), 380 Hz (c), 975 Hz (d)

Figure 9.6 shows some relevant deflection shapes carried out from the operating deflection shape (ODS) analysis. The red shape represents the undeformed system while the black shape represents the deformation of the system components at the corresponding frequency. Deflection shape at 77 Hz shows the vertical resonance frequency of the blocking mass. At 127 Hz a rotational motion of the excitation mass is clear; the disturbance is out of the expected frequency range of analysis and, moreover, the acceleration level along *x* and *y* direction are below the limit imposed by the reference standard. At 380 Hz, in way of a resonance peak, the system vertical motion is predominant, corresponding with the excitation direction along the *z* axis. Figure 9.6d shows a mode shape of the excitation mass thus, at higher frequency, the excitation mass starts to behave as a deformable body. The last point could lead to imprecision both on the control of the input excitation and on the uniform vibration at the input flange of the isolator. Since the prevailing

motion associated to the excitation mass bending mode is still vertical and the reference point for the controller is located near the contact point, the input vibration can be easily controlled. Moreover, taking into consideration the mode shape and the fact that the contact area is small, the input vibration can be approximately considered uniform on the contact area. Transversal motion of the excitation mass increases with the frequency and, at highest frequency, needs to be lowered improving the vertical alignment of the whole system.

9.1 Description of the experimental test

The maximum compressive load of the test rig is set by the springs used to suspend the blocking mass having a maximum load of 60 kN. This load is near to those evaluated for the pillars on the yacht. Moreover, it has to be kept in mind that the loads evaluated in Section 7 were extreme loads prescribed by the rules for the structural design of the pillars while the real load acting on a pillar is somehow unknown. Therefore, the prototypes have been tested using the maximum preload achievable from the test rig setting, 60 kN, and in a light load condition fixed at 30 kN preload. All prototypes have been tested at the same preload values, even though for the smaller prototypes the values exceeded the maximum allowable specific load.

All prototypes have been tested with a random vibration input excitation along the vertical direction with constant power spectral density in the frequency range from 100 to 1000 Hz. The excitation mass acceleration has been measured on the interface between the excitation mass and the input flange of the prototypes, as close as possible to the centre of the excitation mass. The acceleration on the blocking mass has been measured on two symmetrical points, with respect to the blocking mass centre, near its upper face and then the two signals have been averaged. To verify the input excitation level along the two orthogonal directions, a triaxial accelerometer has been placed on the side of the excitation mass. The last accelerometer has been placed on the foundation to verify the flanking noise level.

9.2 Prototype P6 with 30 kN static preload

Prototype P6, shown in Figure 9.7, has a pillar with circular section and an outer diameter corresponding to 114.6 mm. The external shell has an outer diameter of 167 mm and 11.6 mm thickness, is welded on the centre of a square base with 500 mm edge length and 15 mm thickness. The resilient pad is made of closed cell polyurethane with 143.8 mm diameter and 12.5 mm thickness and is housed on the bottom of the outer shell. The pillar portion has a length of 300 mm and its bottom is close with plate of the same dimension of the pillar section and a thickness of 10 mm. The viscoelastic filling the remaining gap between the containing shell and the pillar has an average thickness of 14.75 mm.

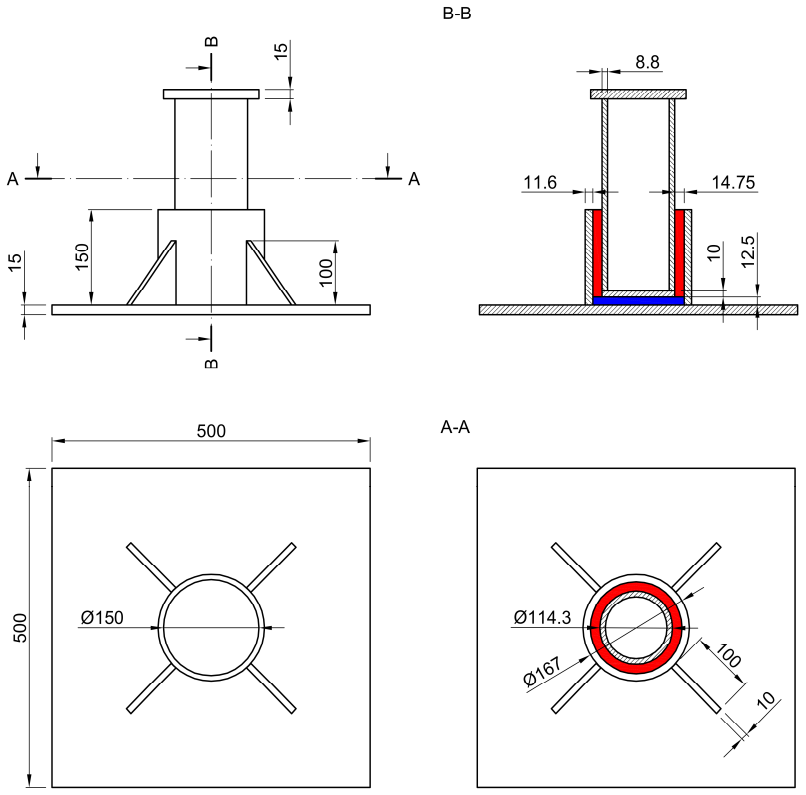

Figure 9.7 - Drawing of pillar isolator prototype P6

Figure 9.8 shows the acceleration levels measured on the excitation mass and on the blocking mass both in vertical direction. The continuous curve represents the acceleration level imposed on the excitation mass, the excitation applied is a white noise spectrum, constant in the range between 100 and 1000 Hz. Acceleration levels measured on the blocking mass decrease below the acceptable level at 300 Hz where the limit imposed by the international standard are satisfied (dash-dotted curve). After 300 Hz the measure is accurate in accordance with the simplification assumed in the indirect method [47]. The acceleration level on the blocking mass increases once more at 400 Hz, which shows a possible resonance of the prototype. A similar behaviour, but with lower amplitude, occurs at 800 Hz.

Figure 9.9 shows acceleration levels measured on excitation mass along two orthogonal directions on a plane perpendicular to the principal direction of excitation. In order to have a predominant direction of excitation, in accordance with international standard, the acceleration level measured on the side of the excitation mass along the orthogonal directions needs to stand at least 15 dB below the excitation level. At lower frequency, the acceleration level measured along *x* and *y* direction has levels exceeding the limit, however, their level is rapidly

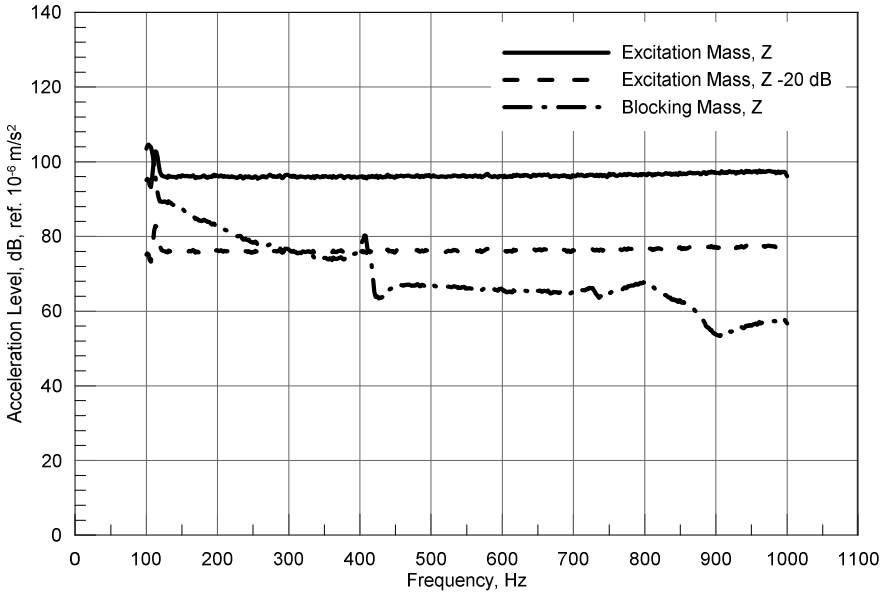

Figure 9.8 - Pillar P6 at 30 kN preload, results of acceleration level on excitation and blocking mass

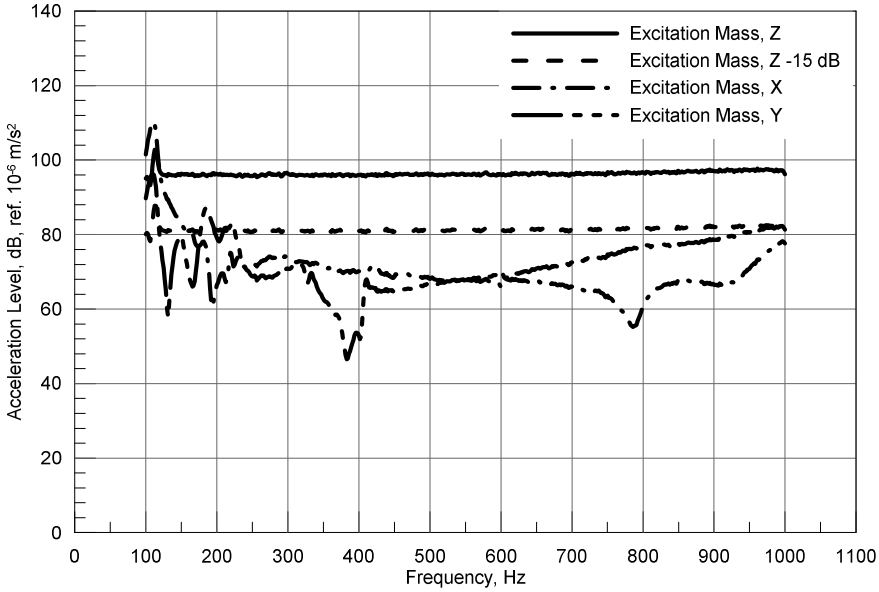

Figure 9.9 - Pillar P6 at 30 kN preload, results of acceleration level measured on excitation mass for unwanted direction excitation evaluation

decreasing and, after 250 Hz, it is largely below the limit. At higher frequency, the lateral acceleration level increases, though not exceeding the limit at 1000 Hz.

Figure 9.10 shows the acceleration level measured on foundation. In this case, it is important to verify that flanking noise levels are sufficiently low to avoid disturbances on the blocking mass motion, a difference of 30 dB between the vibration levels measured on the blocking mass and its foundation is enough to avoid unacceptable disturbance during the measurement. The limit is a rule of thumb, from Figure 9.10 it is clear that the limit is particularly strict indeed, the acceleration levels measured on the blocking mass seems not to be affected by the flanking noise even when its level exceed the imposed limit. Moreover, at higher frequency, the acceleration level measured on the foundation corresponds to the background noise measured when only the acquisition system and the electrodynamic shaker cooling system are active.

All the limitations imposed by the reference international standard lead to a validity range for the measurement that, for this prototype, is between 300 and 1000 Hz. In this range, the transmissibility curve, defined as the ratio between the acceleration measured on the input side of the element under test and the acceleration measured

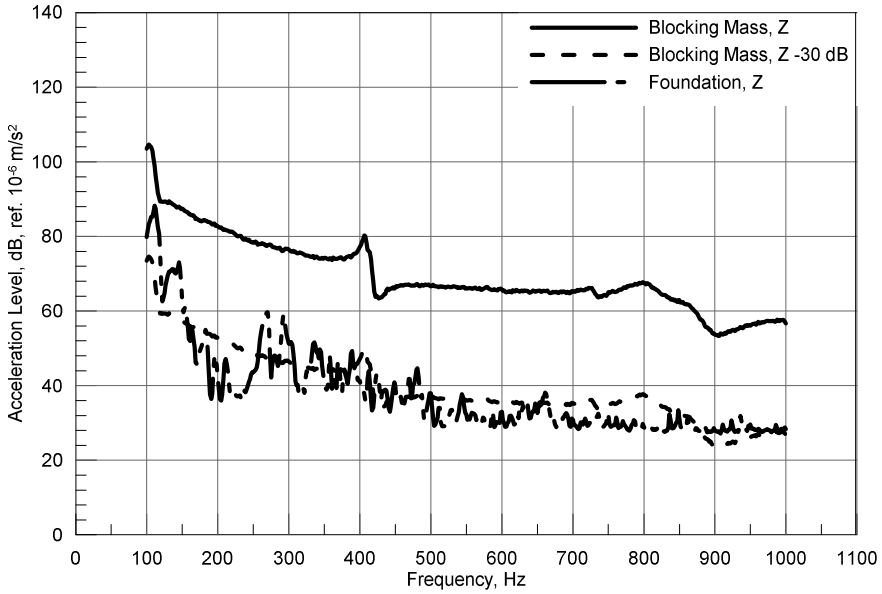

Figure 9.10 - Pillar P6 at 30 kN preload, results of acceleration level on blocking mass and rigid foundation for flanking noise influence evaluation

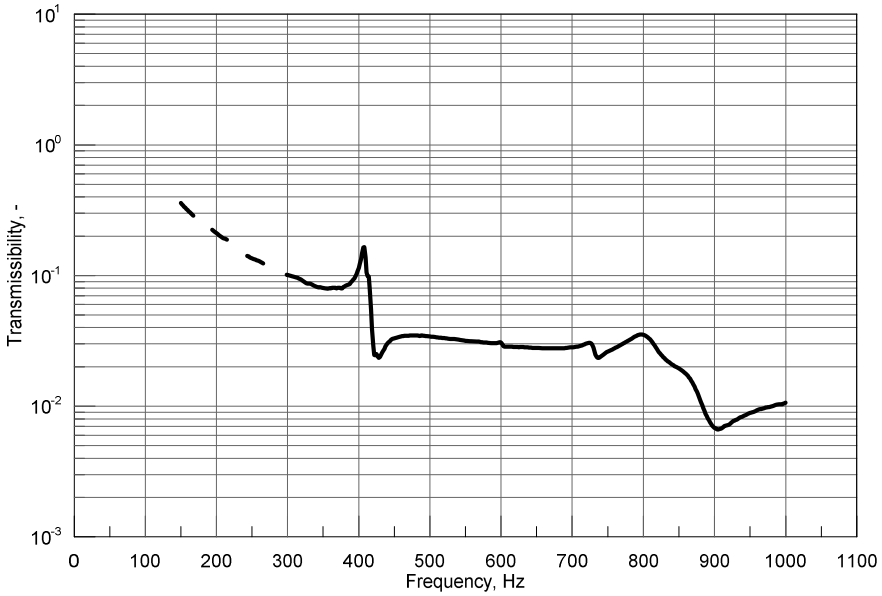

Figure 9.11 - Pillar P6 at 30 kN preload, transmissibility curve

on the blocking mass, of the prototype P6 is drawn in Figure 9.11. Even if inaccurate, the dashed line shows the transmissibility at frequency lower than 300 Hz.

Dynamic transfer stiffness is calculated starting from the value of transmissibility using Equation (3.7) and reported in Figure 9.12. The stiffness curve shows several peaks corresponding to internal resonances of the prototype.

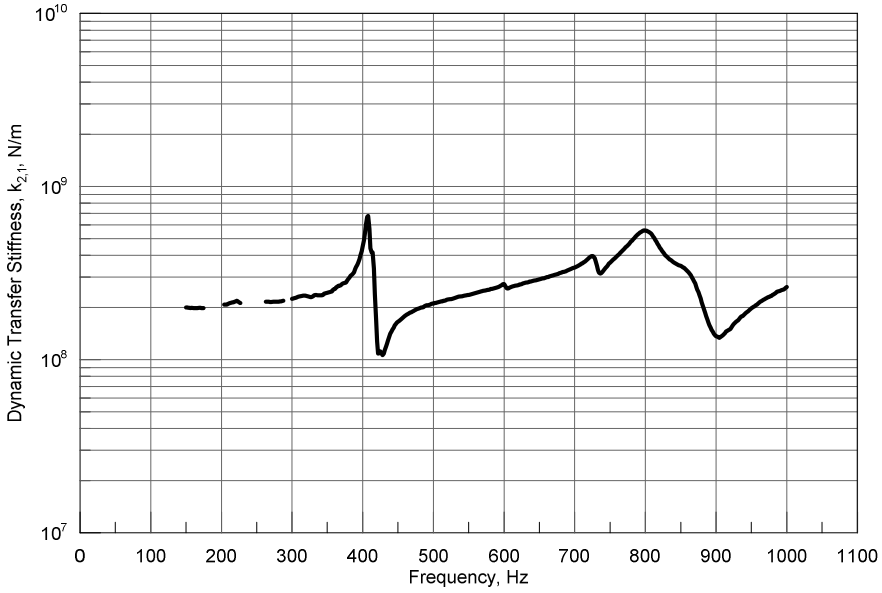

Figure 9.12 - Pillar P6 at 30 kN preload, dynamic transfer stiffness curve

9.3 Linearity test

The standard used is based upon the hypothesis of linearity between the excitation input and the force output. The standard suggests a simplified linearity test consisting in applying two input signals to the test element with a difference in level of at least 10 dB. Being the signal B 10 dB lower than the signal A, if the difference between the evaluated stiffness using A input signal and B input signal is comprised within 1.5 dB, the test element could be considered linear and the data carried out for the element are valid up the excitation level A. This simplification implies a maximum allowable variation of 19% of dynamic transfer stiffness when

considering an input signal variation of at least 3 times the original excitation signal.

The results of the test for the pillar isolator are showed in Figure 9.13 and Figure 9.14 where, respectively, the excitation levels and the resulting transfer stiffness are reported in third octave band frequency. Since for prototype P6 the validity range for the accuracy of the test starts from 300 Hz, the first third octave band to be considered in the linearity assessment has to be greater than this limit. Third octave band with 315 Hz centre band frequency has a lower band limit corresponding to 282 Hz thus, introducing a small error the 315 Hz band can be taken as first third octave band for the linearity assessment. The pillar isolator shows a perfect linearity except for the band corresponding to 315 Hz, however also in this band the difference in stiffness is acceptable.

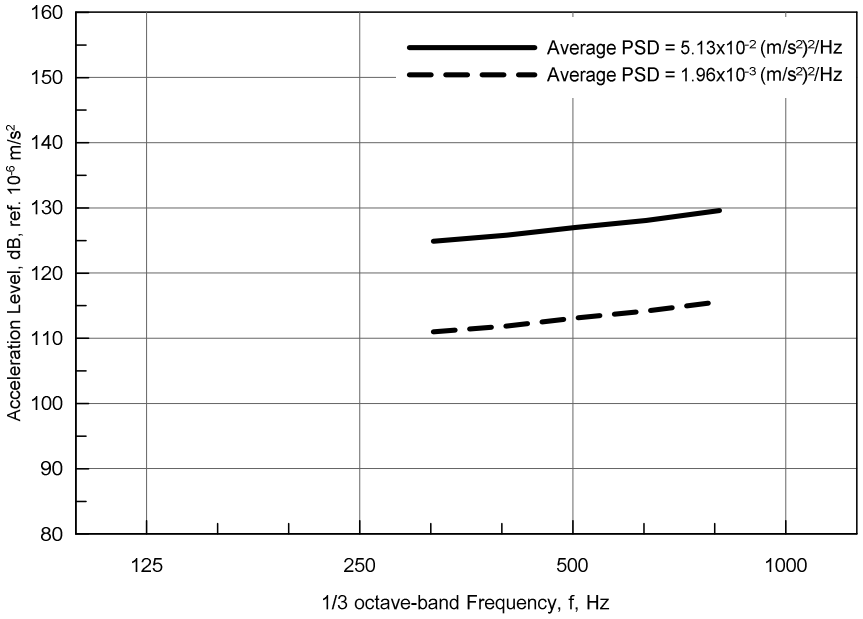

Figure 9.13 - Pillar P6 at 30 kN preload, comparison of excitation levels for linearity assessment

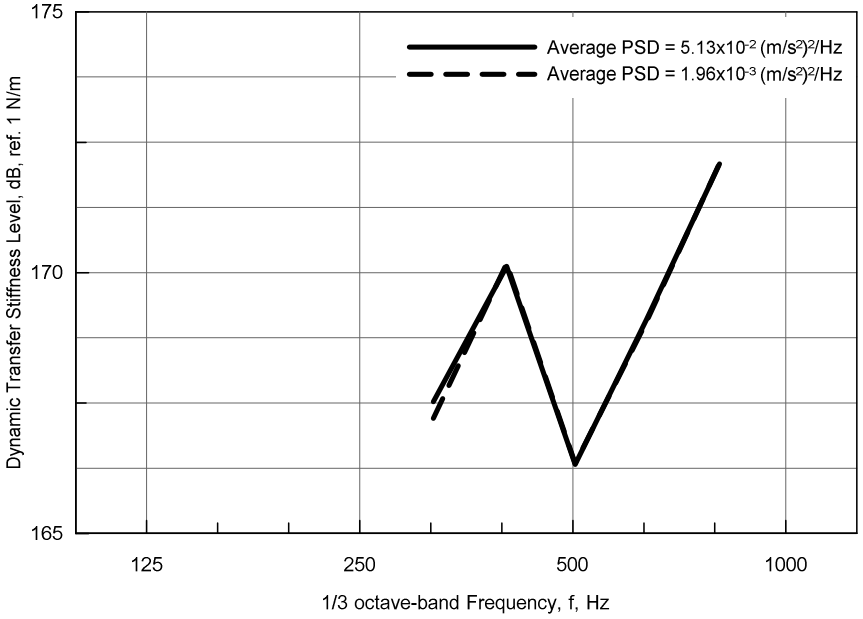

Figure 9.14 - Pillar P6 at 30 kN preload, comparison of dynamic transfer stiffness levels for linearity assessment

9.4 Dynamic transfer stiffness at 60 kN

Figure 9.15 and Figure 9.16 show, respectively, the transmissibility and dynamic transfer stiffness for pillar prototype P6 with a static preload of 60 kN. The stiffness curve measured under the two different preload shows the same dynamic behaviour except for a shift in the corresponding values of the stiffness. Considering the contact area between the pillars and the resilient element, the specific load acting on the resilient element were 2.90 N/mm^2 and 5.82 N/mm^2 for a static preload of 30 kN and 60 kN respectively. Thus, to an increase of the specific load applied on the resilient pad corresponds an increase of the stiffness of the prototype.

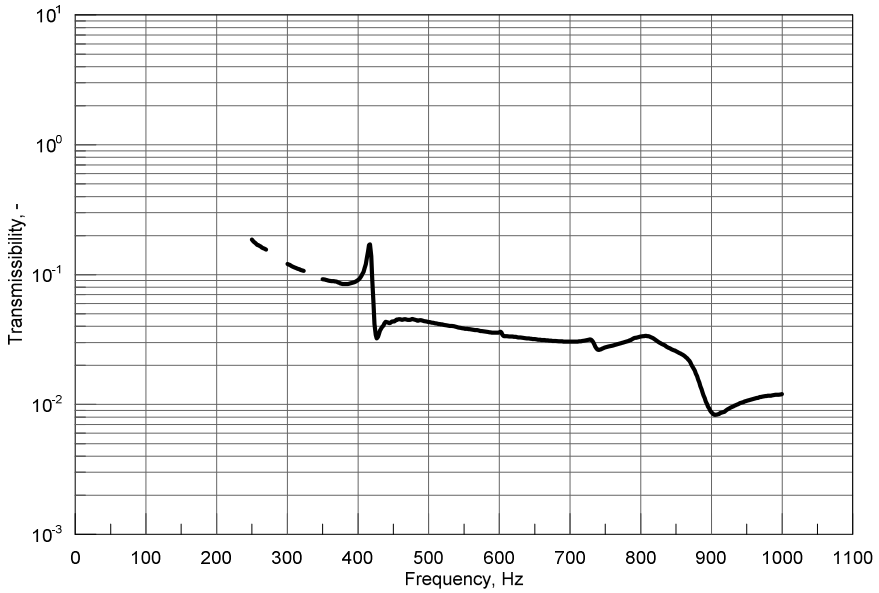

Figure 9.15 - Pillar P6 at 60 kN preload, transmissibility curve

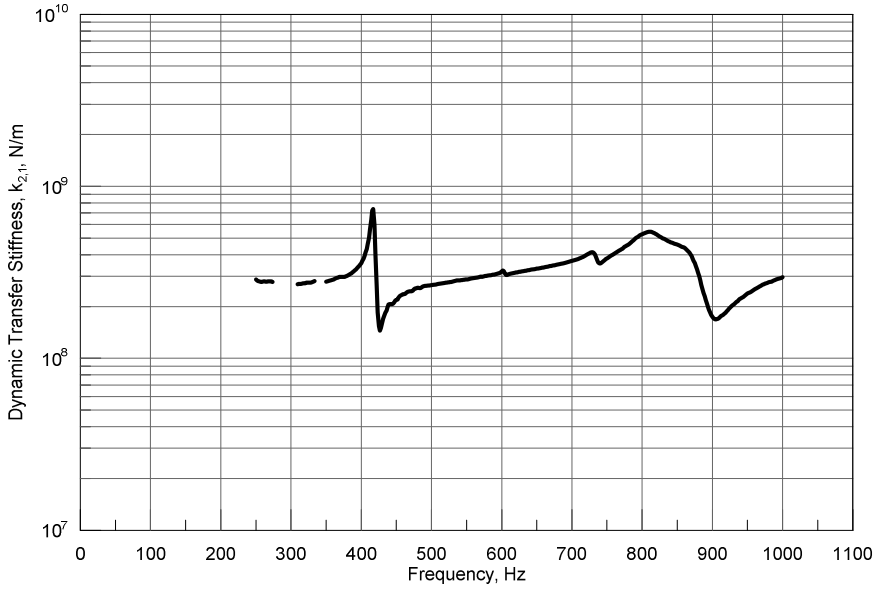

Figure 9.16 - Pillar P6 at 60 kN preload, dynamic transfer stiffness curve

9.5 Prototype P3

Prototype P3 is shown in Figure 9.17. It has a pillar portion with an external diameter of 70 mm and a thickness of 8 mm while the external shell, where the resilient element is housed, is a circular section with external diameter of 114.3 mm and a thickness of 8.8 mm. The pillar portion have a height of 300 mm, on the top side a flange of 150 mm diameter and 15 mm thickness is welded while on the other side, where the pillar lays on the resilient element, a plate of 10 mm thickness closes the pillar. The outer shell, as seen in prototype P6, is welded on a square plate with 500 mm side and 15 mm thickness and four stiffeners placed on the diagonal of the base plate are used to increase the stiffness of the connection with the base plate. The resilient element used is a circular layer of closed cell

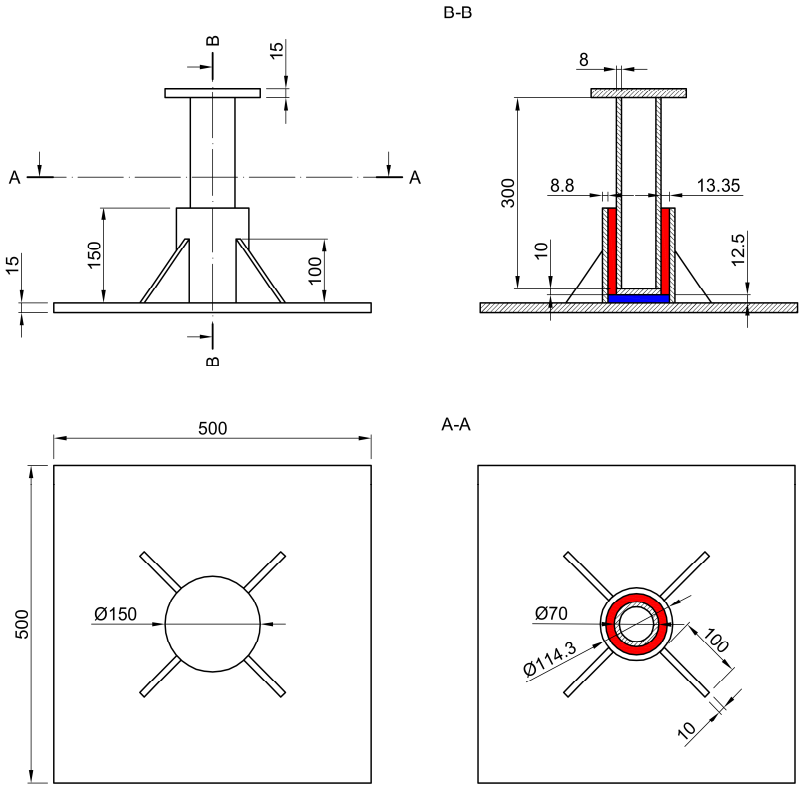

Figure 9.17 - Drawing of pillar isolator prototype P3

polyurethane with diameter of 96.1 mm and 12.5 mm thickness. The remaining space within the outer shell and the pillar portion is filled with viscoelastic compound, with a resulting thickness of 13.35 mm.

The tests, with respect to the P6 results, show an accuracy range improved with the lower frequency limit, due to blocking mass resonance, lowered at 220 Hz. This reduction is due the lower stiffness of the prototype P3 if compared with the prototype P6. Figure 9.18 and Figure 9.19 show respectively the transmissibility and the dynamic transfer stiffness. Both the transmissibility and the stiffness are consistently lower than those measured on the prototype P6. Comparing with the last, internal pillar resonances, at about 350 Hz and 800 Hz, move slightly to lower frequencies.

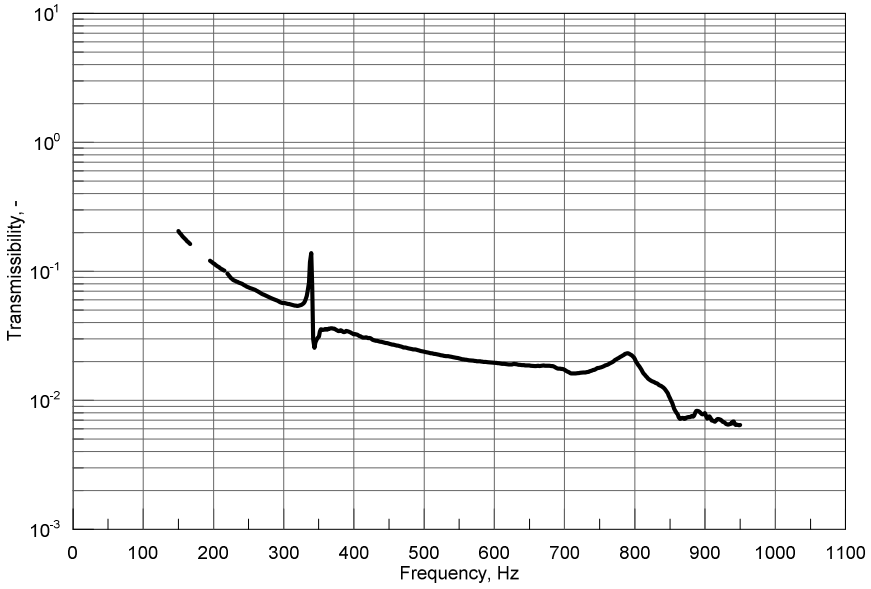

Figure 9.18 - Pillar P3 at 30 kN preload, transmissibility

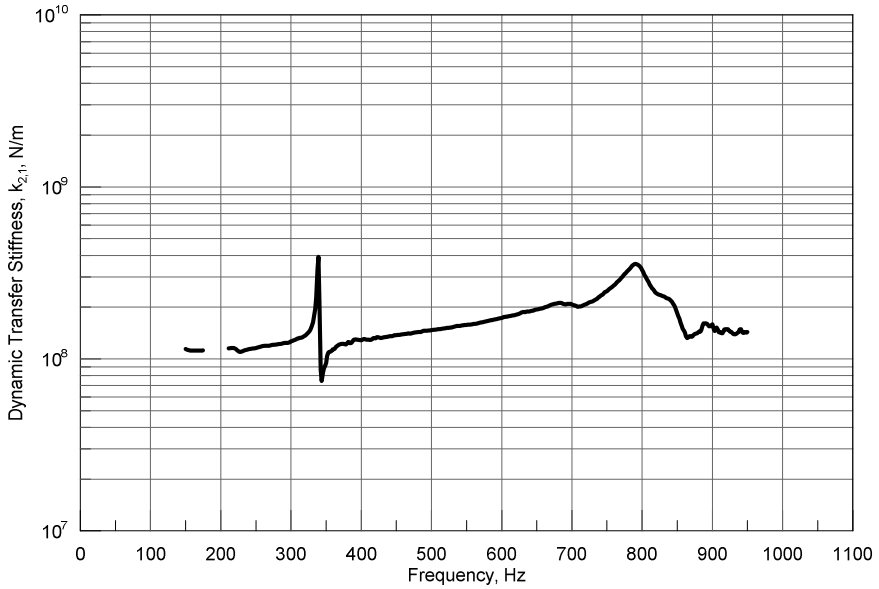

Figure 9.19 - Pillar P3 at 30 kN preload, dynamic transfer stiffness curve

9.6 Prototype P2

Prototype P2, shown in Figure 9.20, has a square section pillar with 80 mm edge while the containing shell is of the same shape with 120 mm edge. The pillar portion and the containing shell have thickness of 10 mm and 8 mm respectively. At the top of the pillar portion there is a welded square flange with 150 mm edge and 15 mm thickness; the bottom is closed with a square plate with 10 mm thickness. The containing shell, as seen in the former prototypes, is welded on a base plate with 500 mm edge and 15 mm thickness and stiffened with four stiffeners placed on the diagonals of the base plate and of the containing shell. Figure 9.21 and Figure 9.22 show the transmissibility and the dynamic transfer stiffness of P2 prototype with 30 kN static preload. The test validity range starts from 280 Hz up to 1000 Hz where the excitation spectrum ends. The transmissibility and stiffness values are similar to those obtained for the prototype P6 and the internal resonances that results in the peaks at about 400 Hz and 750 Hz.

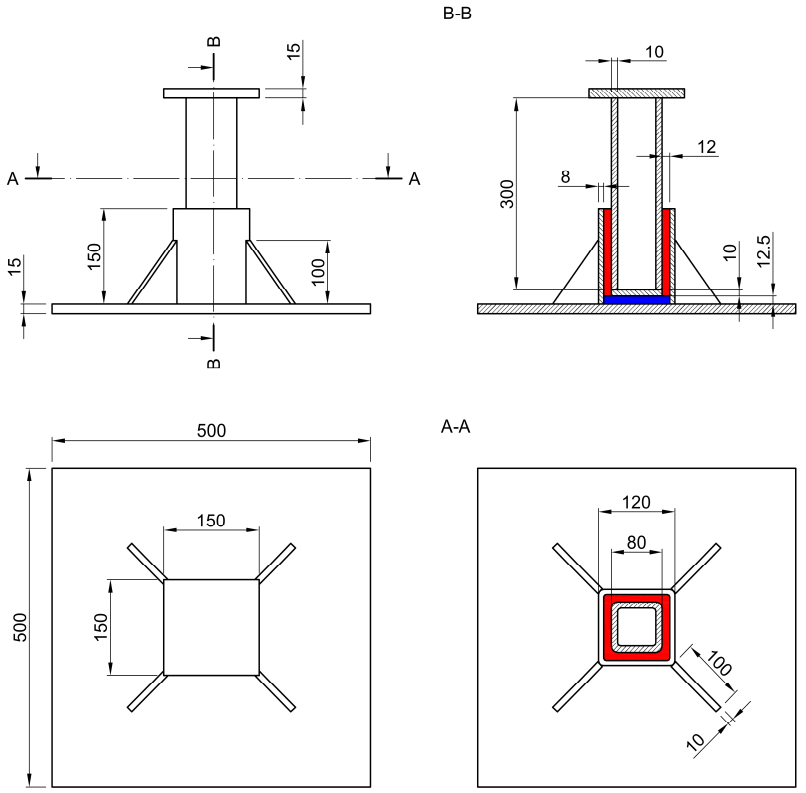

Figure 9.20 - Drawing of pillar isolator prototype P2

All the three prototypes tested show similar resonance peaks despite of the change of shape and specific load. During the last experimental test on prototype P2, accelerometers have been moved also on some points on the isolator putting in evidence that the acceleration measured on the base plate, i.e.: at half-length of one edge, was much higher than the acceleration measured on the blocking mass. This result led to a more accurate investigation of the dynamic behaviour of the base plate. First attempt to verify if the peaks are due to internal resonance of the vibration isolator itself or from the base plate motions has been done by rigidly connecting the base plate to the blocking mass. By drilling four holes in the prototype base plate its base plate has been constrained to the blocking mass using

four screws, the holes have been placed at half-length of the edge few centimetres inside the base plate borders.

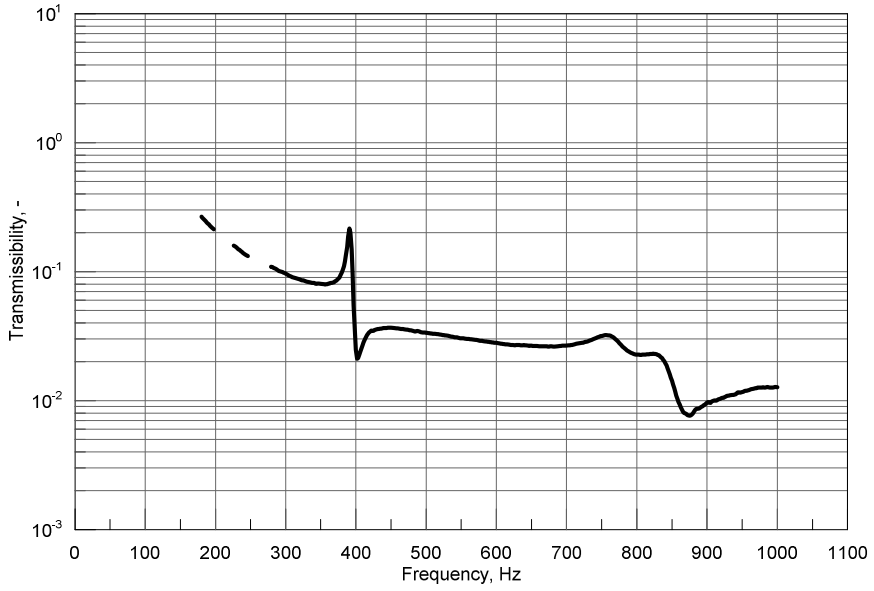

Figure 9.21 - Pillar P2 at 30 kN preload, transmissibility curve

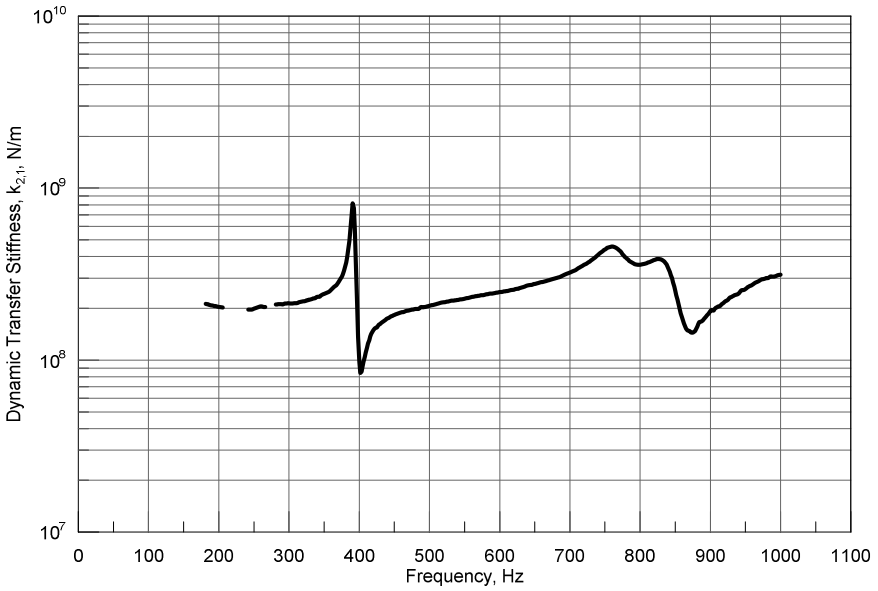

Figure 9.22 - Pillar P2 at 30 kN preload, dynamic transfer stiffness curve

The results for the prototype P2 connected to the blocking mass with a static preload of 30 kN, in terms of transmissibility and dynamic transfer stiffness, are shown in Figure 9.23 and Figure 9.24.

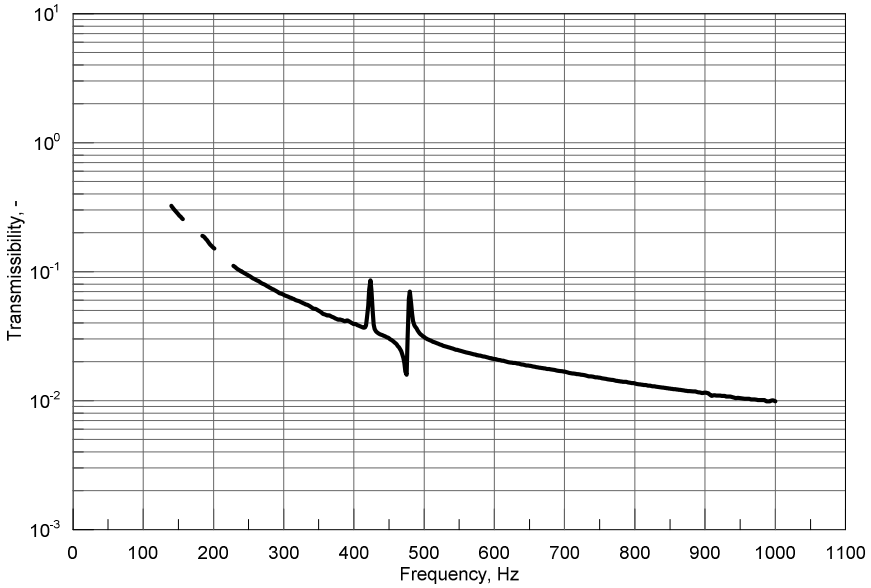

Figure 9.23 - Pillar P2, blocked on blocking mass, at 30 kN preload, transmissibility curve

The comparison of the resulting dynamic transfer stiffness for the free and the constrained base plate of prototype P2 is shown in Figure 9.25. Moving from the free to the constrained configuration, the first peak has moved at higher frequency while the peak at 750 Hz disappeared. The stiffness, in the constrained configuration, except for the peaks between 400 and 500 Hz, is constantly increasing with the frequency. Screw the base plate to the blocking mass increases the base plate stiffness but it is not enough to avoid high frequency resonance of the plate selves, moreover the introduction of the screws adds others degrees of freedom due to the stiffness of the screws, thus resulting in a second peak after the first one.

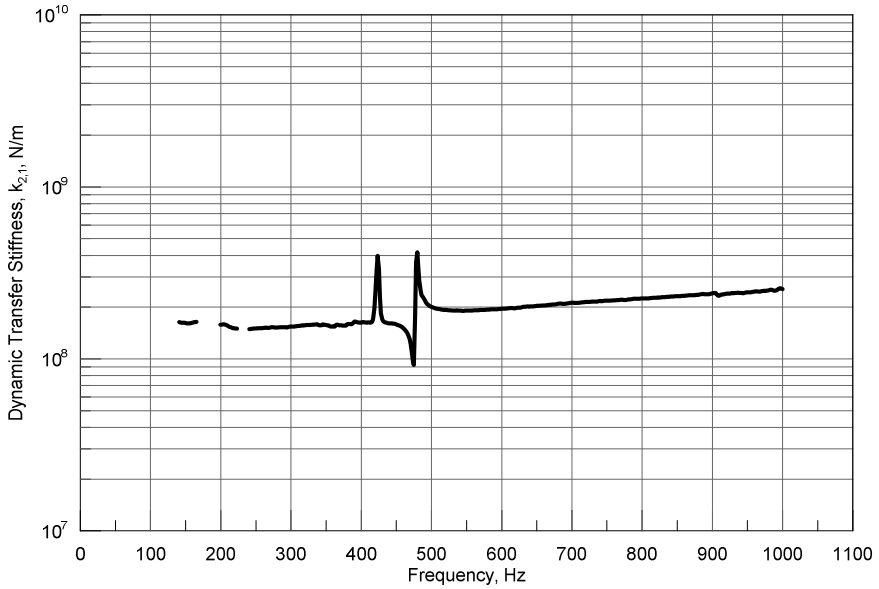

Figure 9.24 - Pillar P2, blocked on blocking mass, at 30 kN preload, dynamic transfer stiffness curve

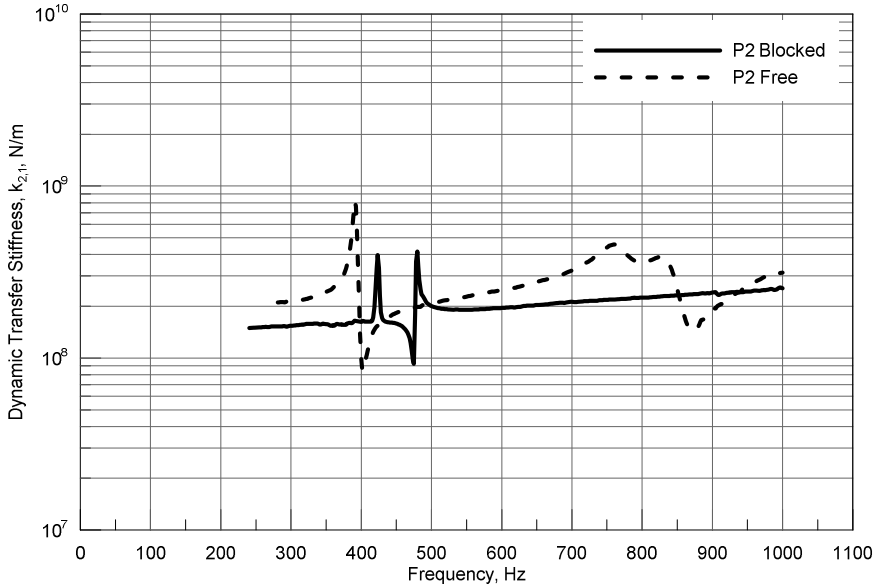

Figure 9.25 - Pillar P2 at 30 kN preload, dynamic transfer stiffness curve in free and blocked condition

Finally, a finite element model of the base plate associated to the prototype P2 has been created to verify the results of the latter findings. To simplify the problem, the pillar portion along with the resilient element and the viscoelastic layer have been neglected, modelling only the containing shell, the stiffeners and the base plate. Both the viscoelastic layer and the resilient pad are elastic element decoupling the motion of the system composed by the base plate and the containing shell from the motion of the pillar, therefore, in a first approximation, the two systems can be considered independently.

The model shown in Figure 9.26 is made of shell element with an average edge length of 10 mm and each part, i.e. the base plate, the stiffeners and the containing shell, has been modelled on its half thickness. The boundary condition has been described as a simple support along the junction between the containing shell and the base plate.

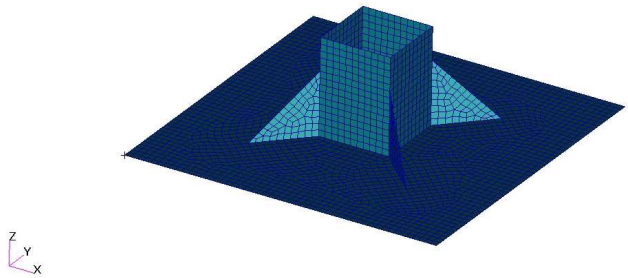

Figure 9.26 - Finite element model of prototype P2 base plate

The results of the modal analysis are shown from Figure 9.27 to Figure 9.29. The first mode at 364 Hz, taken in consideration for the simplification introduced in the model, match quite well with the first peak in the transmissibility curve obtained for the unconstrained prototype P2 (Figure 9.21). The modes found at higher frequency could explain the two peaks at 750 and 850 Hz but, in this case, the approximation has a higher influence on the results precision. However, aim of the analysis was simply to verify if the dynamic behaviour of the prototypes were compatible with the normal modes associate to the base plate.

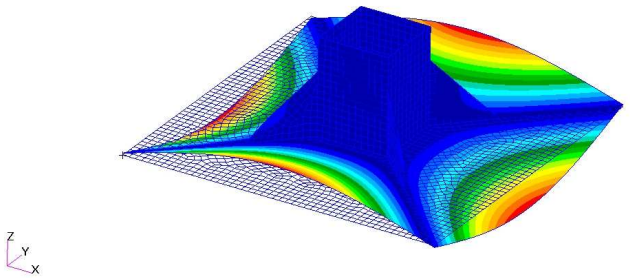

Figure 9.27 - Prototype P2 base plate, mode shape at 364 Hz

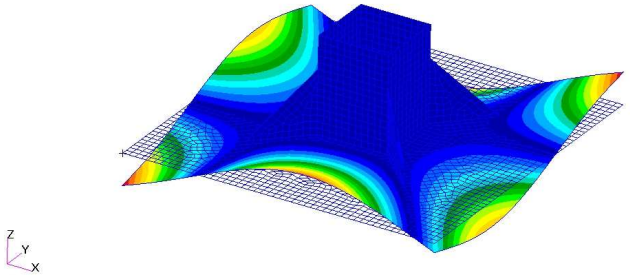

Figure 9.28 - Prototype P2 base plate, mode shape at 577 Hz

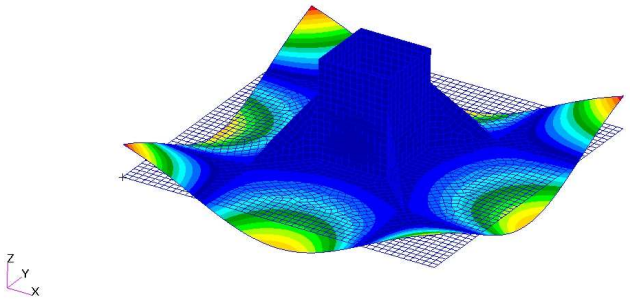

Figure 9.29 - Prototype P2 base plate, mode shape at 863 Hz

The analysis carried out shows how the dynamic of the output flange could affect the results of the experimental test leading to transmissibility and stiffness values influenced by base plate normal modes. The results obtained in this phase, even though not representing the real stiffness of the prototypes, can be used to compare the different solutions tested, since the base plate has a similar design in different prototypes tested and so a qualitative comparison of the prototypes behaviour can be done.

9.7 Effect of viscoelastic thickness reduction

The effects of viscoelastic layer thickness between the containing shell and the pillar have been investigated building two other prototypes. The prototypes, named P7 and P8, have been built on the layout of round shape pillars used in the former prototype.

Prototype P7, shown in Figure 9.30, has a pillar section of 70 mm diameter and the containing shell is 101.3 mm of outer diameter and 9.25 mm thickness leading to a viscoelastic layer of 6.4 mm thickness while prototype P3, with the same pillar dimensions, has a viscoelastic layer thickness of 13.35 mm. The prototype P8 is shown in Figure 9.31. Comparing with the prototype P6, it has the same pillar

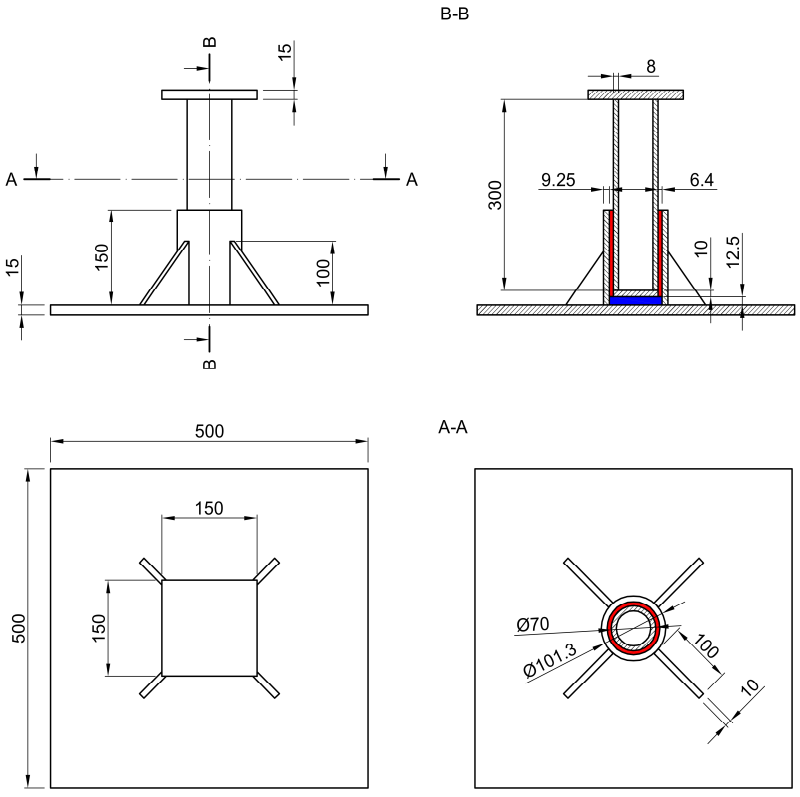

Figure 9.30 - Drawing of pillar isolator prototype P7

dimensions, 114.3 mm diameter, but a smaller containing shell with 139.3 mm outer diameter and 8 mm thickness. This leads to a viscoelastic layer of 4.65 mm thickness compared to 14.35 mm thickness of the prototype P6. Both the prototype P7 and P8, being built before the findings on base plate effect, have base plate with 500 mm edge and 15 mm thickness.

Figure 9.32 and Figure 9.33 show the comparisons of the dynamic transfer stiffness measured for the prototypes P3 and P7 and for the prototypes P6 and P8 respectively.

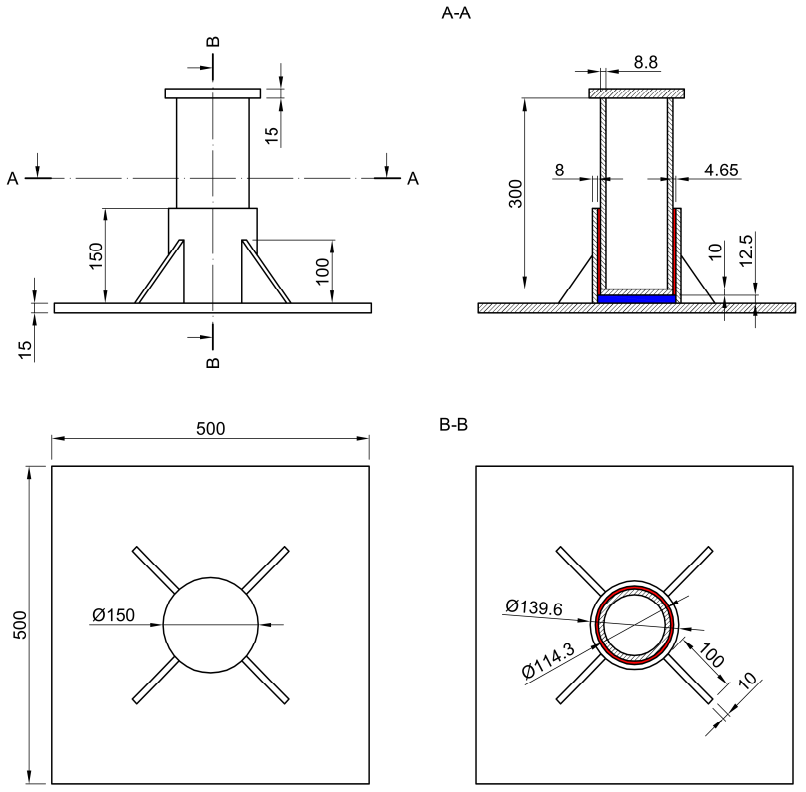

Figure 9.31 - Drawing of pillar isolator prototype P8

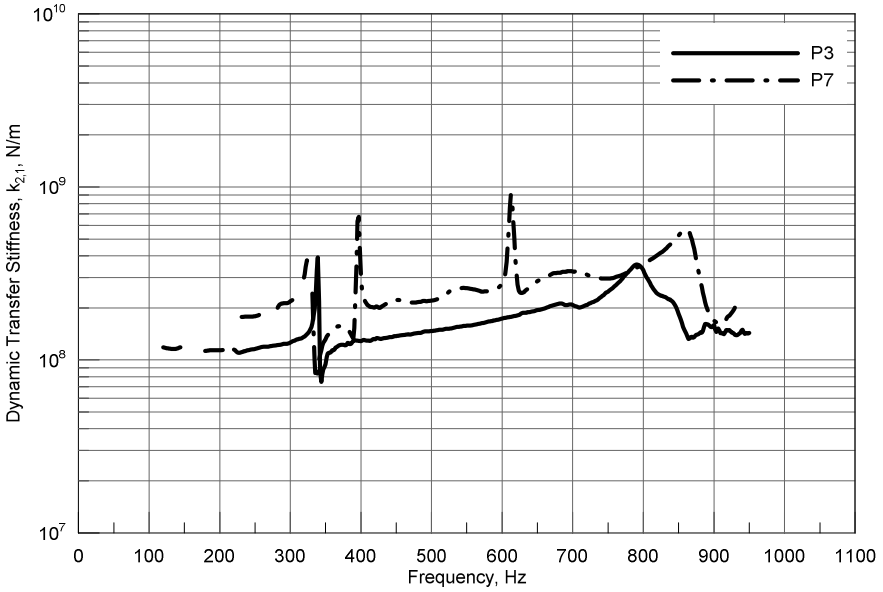

Figure 9.32 - Pillar P3 and P7 at 30 kN preload, dynamic transfer stiffness curves

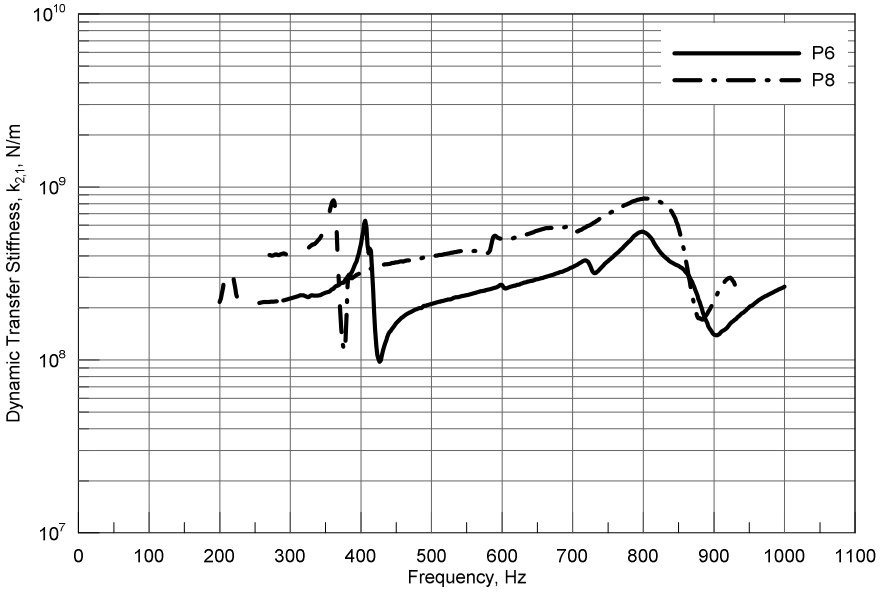

Figure 9.33 - Pillar P6 and P8 at 30 kN preload, dynamic transfer stiffness curves

For prototype P7, the measure is accurate starting from 330 Hz, the two peaks at 400 Hz and 620 Hz are due to misalignment of the moving system exciting rotation of the blocking mass. In correspondence of these values, the results shall not be considered accurate. Nonetheless, from the comparison with P3 transfer stiffness it is clear that a reduction of the viscoelastic layer thickness has an increasing effect on the stiffness of the vibration isolator. The same conclusion is valid for prototype P8, in this case the measure is accurate above 370 Hz without any incongruence due to misalignment of the system. For prototype P8 the dynamic transfer stiffness is nearly doubled if compared with the one measured for the prototype P6.

In both cases, the reduction of the viscoelastic thickness leads to the increase of the stiffness of the vibration isolator device, thus reducing the positive effect of the device.

9.8 Effect of base plate reduction

After the findings on the influence of the base plate modes on the response of the pillar isolator device, the effect of base plate has been analysed on a set of two prototypes, one with a wide base and one with a small one. Starting from prototype P8, another prototype with small base plate has been built. The prototype P9 is shown in Figure 9.34. As prototype P8, it has a 114.3 mm diameter pillar with a containing shell diameter of 139.6 mm and a viscoelastic layer thickness of 4.65 mm. The base is a square plate with 150 mm side and 15 mm thickness simply welded on the containing shell bottom while for the prototype P8, the base plate has 500 mm edge length. Figure 9.35 shows the dynamic transfer stiffness for the two prototypes at 30 kN static preload.

Prototype P8 measure is accurate after 370 Hz while prototype P9 after 400 Hz. Dynamic transfer stiffness of prototype P9 is not affected by motion of the base plate and it shows an approximately constant value for the dynamic transfer stiffness from 400 Hz up to 1000 Hz. The effect of base plate motion is clear when looking at prototype P8 stiffness, where the base plate resonance increases the transmissibility of the device, especially at higher frequencies.

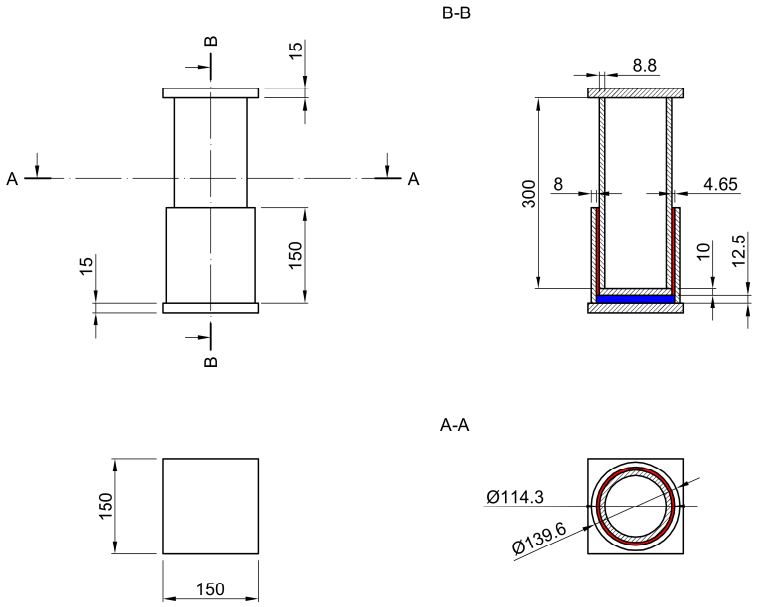

Figure 9.34 - Drawing of pillar isolator prototype P9

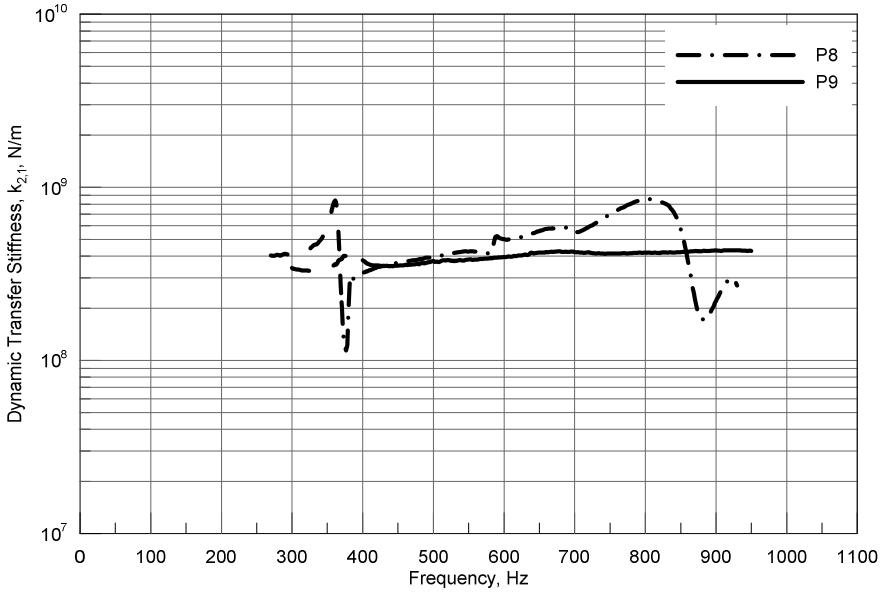

Figure 9.35 - Pillar P8 and P9 at 30 kN preload, dynamic transfer stiffness curves

9.9 Effect of preload

The effect of the static preload applied to the tests element has been evaluated on different prototypes and its effect is shown in Figure 9.36 on prototype P9 for two static preload condition, one with 30 kN and one with 60 kN preload.

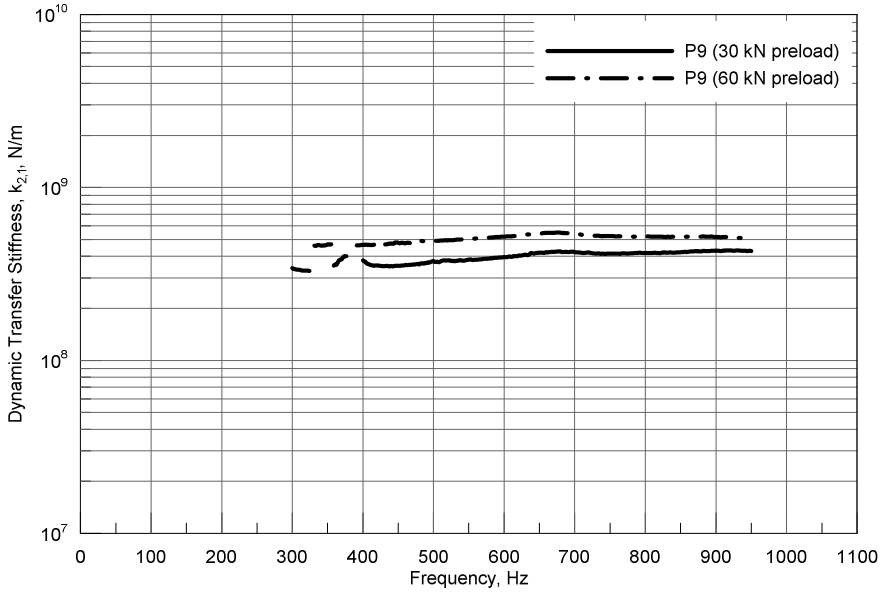

Figure 9.36 - Pillar P9 at 30 kN and 60 kN preload, dynamic transfer stiffness curves

The accuracy range for P9 prototype at 60 kN preload starts from 430 Hz, while for the measure at 30 kN starts at 400 Hz. The increase of preload applied to the prototype results in an increase of its dynamic stiffness, as shown in the former prototype. Being the pillar diameter 114.3 mm, the specific load on the resilient element are 2.91 N/mm^2 and 5.82 N/mm^2 for an applied preload of 30 kN and 60 kN respectively. There are slightly more differences between the stiffness measured with the two different preloads at lower frequencies, while at higher frequencies, near to the upper limit of the measurement range, differences tend to decrease.

9.10 Effect of viscoelastic filling suppression and base reduction

The reduction of viscoelastic layer thickness leads the development of the pillar isolator in the wrong direction. On the other hand, the initial viscoelastic thickness was already high if compared with other typical application as the dampening of ship decks where the increase of the viscoelastic layer over a specific value did not translate into an effective increase of damping [79, 80]. Moreover, an increase in the viscoelastic thickness layer will translate into a bigger device, which needs to be avoided. Starting from these considerations, another prototype without filling between the containing shell and the pillar has been built. Prototype P10, shown in Figure 9.37, has same pillar dimension as prototype P3 while it has a containing shell with 101.3 mm diameter and 9.25 mm thickness, in addition, the new prototype has a small base welded on the bottom of the containing shell. The comparison of the dynamic transfer stiffness for the two prototypes, both with static preload of 30 kN, is shown in Figure 9.38.

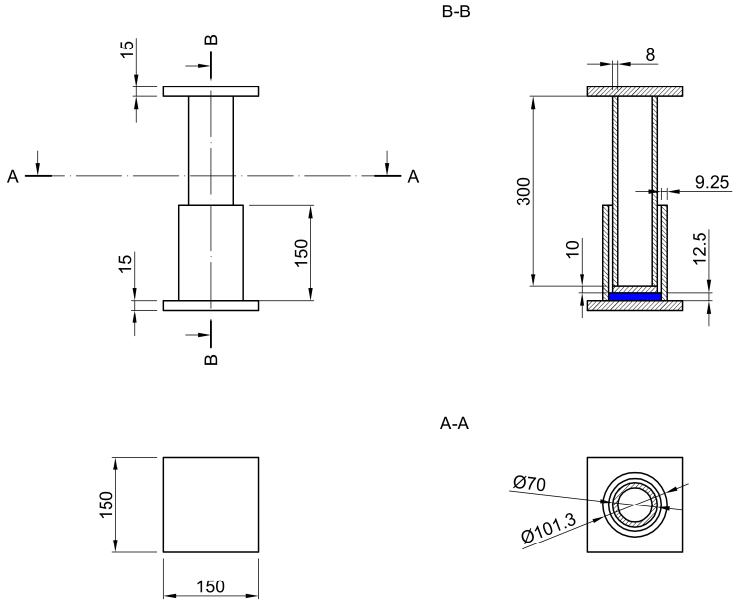

Figure 9.37 - Drawing of pillar isolator prototype P10

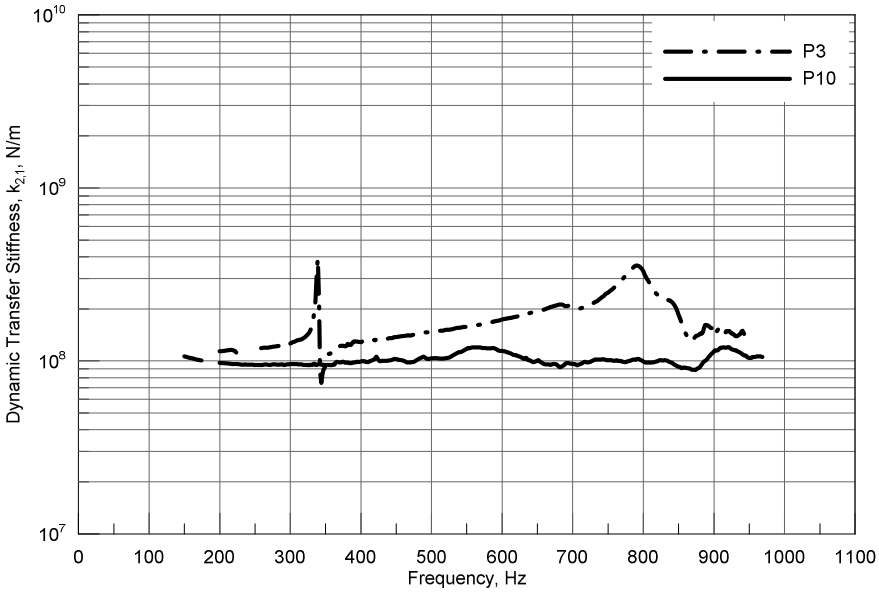

Figure 9.38 - Pillar P3 and P10 at 30 kN preload, dynamic transfer stiffness curves

Validity range for prototype P10 starts from 200 Hz and for P3 from 220 Hz. As seen in the Section 9.8 for the prototype P9, the effect of base plate reduction is clear. Moreover, vibration isolator without viscoelastic layer, P10, shows another small decrease of stiffness values if compared with P3 prototype and an approximately constant stiffness on the measurement range.

The high frequency dynamic characterization test draws the attention to some errors in the design of the prototypes. Most prototypes have been built with a large base, however, the normal modes of the base plate affect consistently the accuracy of the stiffness measure. This design issue repeats systematically on all the prototypes with the same design. With a constant base dimension and similar external shell shape and dimension, also the dynamic behaviour of the prototypes is affected in a similar way by normal modes of the base plate. This is clear considering the shape and the frequency at which the peaks are present in the different prototypes stiffness curves. The measurements were too altered to quantify precisely the effect of such variations. Moreover, the constant inaccuracy due to the base motion allowed to draw general considerations on the behaviour of

the prototypes when parameters like the static preload or the viscoelastic layer thickness had been changed.

In any case, in this development phase the results were enough to identify a layout with lower stiffness than the other tested and therefore, rather than continuing with the measurement of the dynamic characteristics of prototypes with improved design, the development process moves to the next phase assessing the effectiveness of the isolator on the mock-up. After the effectiveness of the isolator has been assessed, the dynamic characterization test can be carried out using an isolator device with a design closer to the final solution, in this way the test can be used to measure its real stiffness.

Despite some inaccuracies in the first part of the experimental tests, the layout without viscoelastic layer is the one with the lower stiffness, moreover, increasing the static preload also the stiffness of the prototypes increases. At last, the stiffness of the prototypes with small base shows a nearly constant stiffness on all the analysis range.

10 Low frequency tests results

The indirect method measurement allows comparing the different prototypes and finding the most promising design among those tested. Despite the approximation due to the motion of the base plate, the different solutions have been compared on a qualitative basis, identifying the effects of the variation introduced in the design. After a small output flange has been adopted, the dynamic transfer stiffness measurement using the indirect method gave accurate results showing an approximately constant value for the dynamic transfer stiffness of the pillar isolator in the all the measurement range analysed. Nonetheless, considering the layout of the test rig and the high stiffness of the pillar isolator, for the "softer" isolator, prototype P10, the available range for the dynamic characterization starts from 200 Hz. A new test rig has been designed and installed at the NVL laboratories at the University of Trieste in order to investigate the dynamic behaviour of the isolator in a lower frequency range.

The prototype P10, with a small base plate and without viscoelastic filling in the containing shell, has been tested on the low frequency rig. Figure 10.1 shows the prototype placed in the test rig between the dynamic force measurement system, rigidly connected to the rig foundation, and the excitation mass. The excitation mass is connected to the hydraulic exciter and suspended with a soft isolator bed. Accelerometers are used to measure the accelerations of the different parts of the structure. One accelerometer is placed near the centre of the excitation mass measuring along the vertical direction, while a triaxial accelerometer is placed at the side of the excitation mass to measure the accelerations on the perpendicular plane. Since the centre of the force distribution plate is not measurable, two accelerometers, measuring along the vertical directions, are positioned on two opposite sides and their signal is averaged to get the acceleration of the plate.

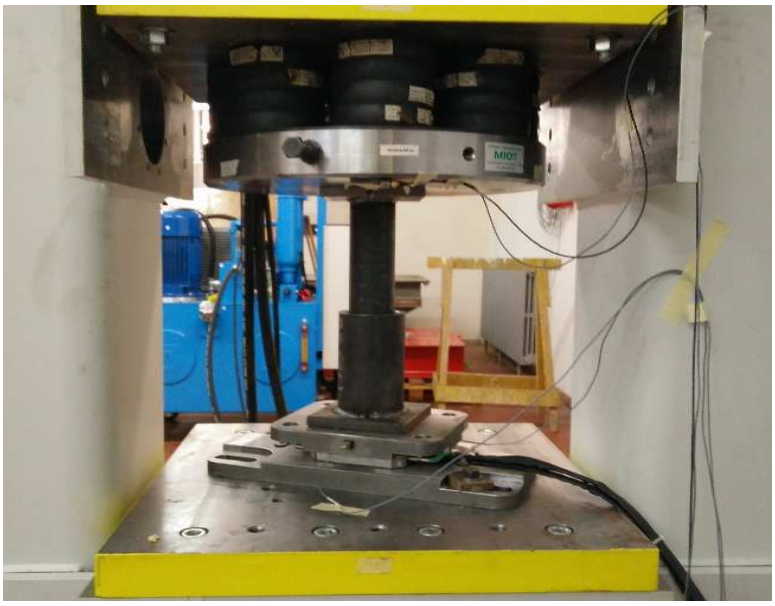

Figure 10.1 - Prototype P10 on the low frequency test rig

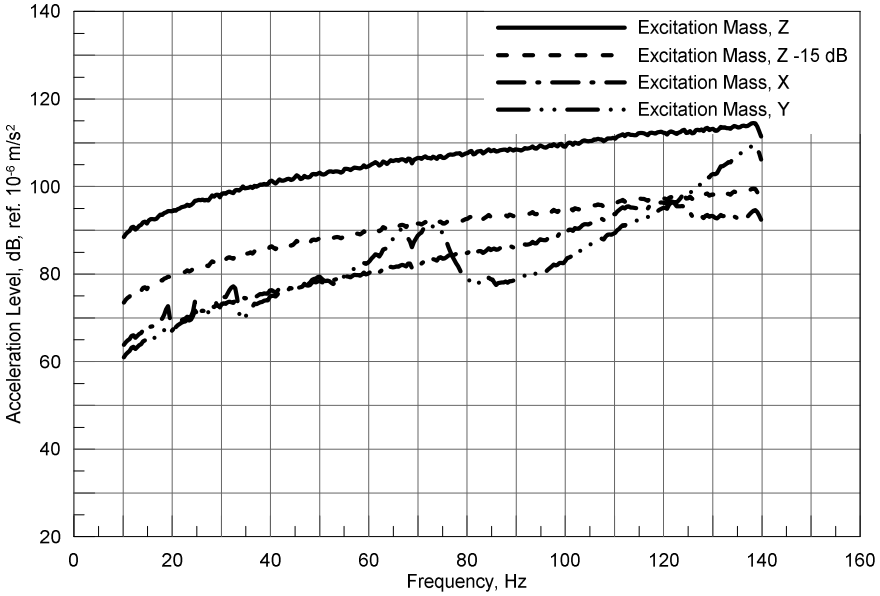

Figure 10.2 - Pillar P10 at 30 kN preload, accelerations levels measured on excitation mass on low frequency test rig

Figure 10.2 shows the excitation spectrum measured on the excitation mass along with the acceleration measured on the perpendicular directions. The accelerations on the lateral directions have to be at least 15 dB below the excitation level to ensure the accuracy of the test, as explained in Section 4.1. At lower frequency, the transversal motion of the excitation mass are well below the limit, while at higher frequency, they tend to increase and exceed the limit at 125 Hz.

Figure 10.3 shows the acceleration level measured on the force distribution plate compared with the acceleration level on the excitation mass and the suggested limit for the accuracy of the test, which is set 20 dB lower than the excitation level. In the whole range of the test the limit is not exceed. Considering the force level, Figure 10.4, the inequality (4.3) is satisfied in all the analysis range being 13 kg the mass of the force distribution plate and more than 100 kg the maximum allowed.

Transversal motions of the excitation mass, exceeding the limit at 125 Hz, set the upper frequency limit for test accuracy.

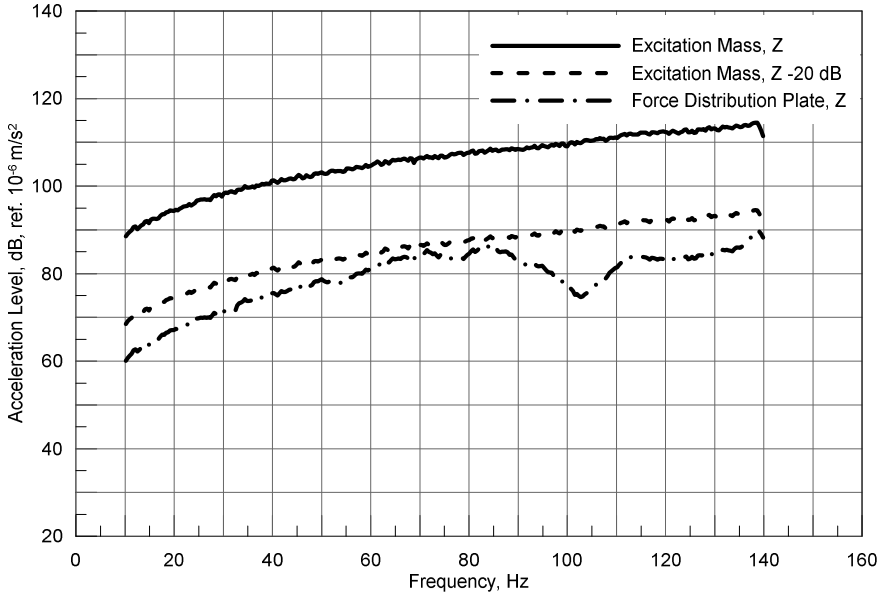

Figure 10.3 - Pillar P10 at 30 kN preload, accelerations levels measured on excitation mass and on force distribution plate on low frequency test rig

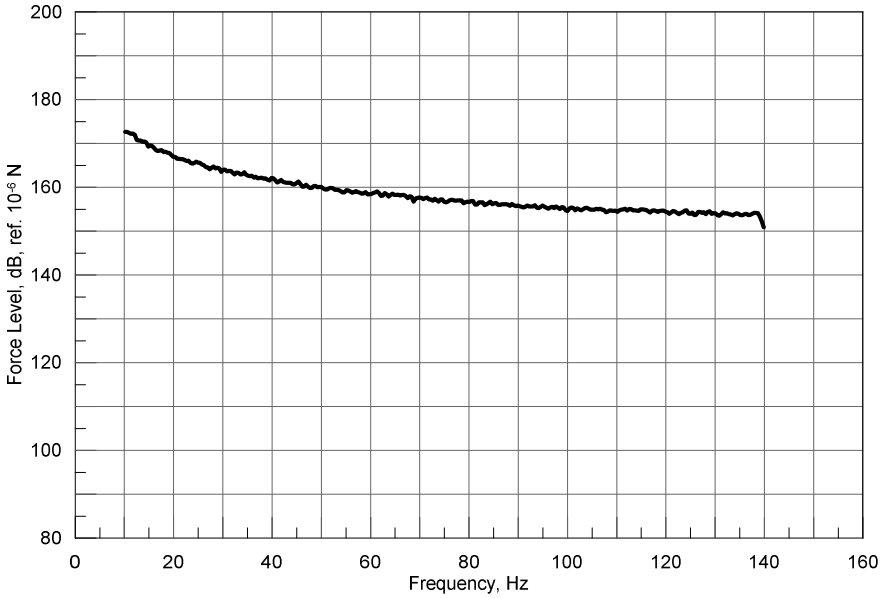

Figure 10.4 - Pillar P10 at 30 kN preload, force measured on low frequency test rig

Linearity test results are reported in Figure 10.5 and in Figure 10.6. The first one shows the acceleration spectra used as input, which are required to differ at least of 10 dB, while the second one shows of the resulting stiffness. The stiffness curves, reported in third octave band, have a difference lower than 1 dB. Therefore, the isolator prototype shows a linear behaviour also at low frequencies.

During the test on the prototype P10, to investigate the behaviour both of the test rig and of the pillar isolator, a comparison between a sine frequency and random excitation has been carried out. In one case, a random spectrum with constant velocity has been used to excite the test element, while in the other case the prototype was excited with a fixed frequency sine. In the last case the sine excitation was performed every 5 Hz from 10 to 125 Hz as showed in Figure 10.7 along with the power spectral density used to define the random signal. The profile has been chosen on the basis of the limitations imposed by the hydraulic actuator. The profile has a constant displacement amplitude of 0.1 mm from 10 to 40 Hz and a constant velocity profile, with 5 mm/s amplitude, from 60 to 125 Hz. In the remaining frequency, from 40 to 60 Hz, it has linear constant decrease of velocity from the values resulting at 40 Hz to the values fixed for the next interval. The dynamic transfer stiffness measured for both the excitation inputs is reported in

Figure 10.8 showing that the values obtained are very close, despite the different methods adopted to excite the prototype.

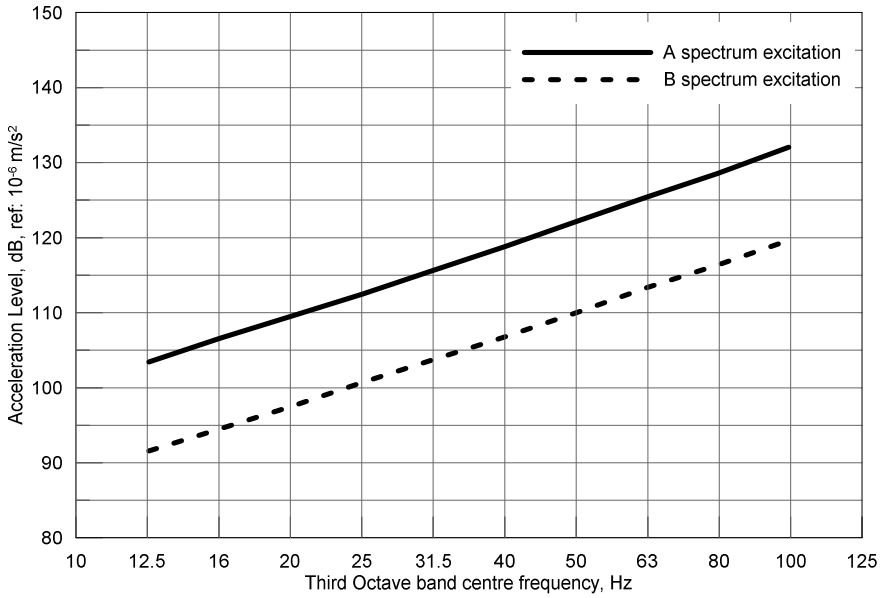

Figure 10.5 - Pillar P10 at 30 kN preload, acceleration levels comparison for linearity test

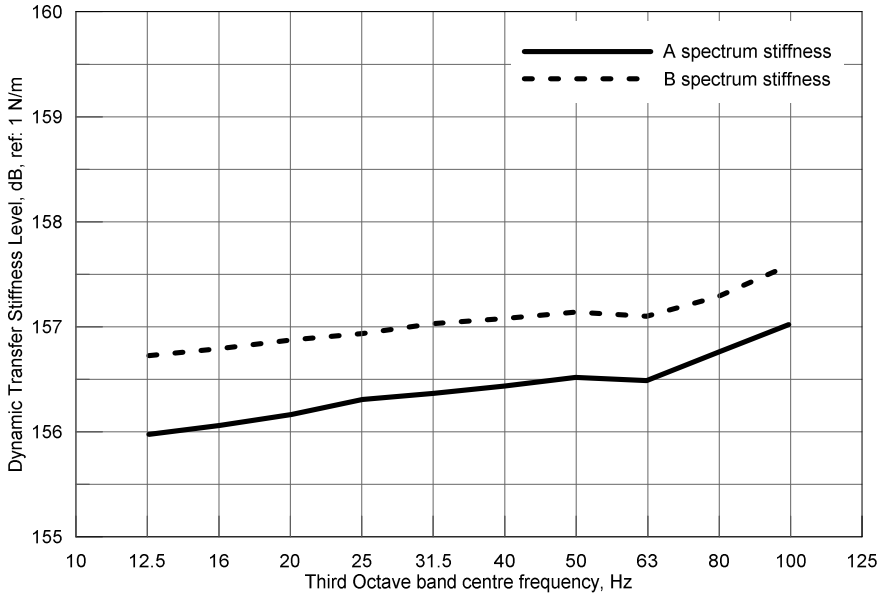

Figure 10.6 - Pillar P10 at 30 kN preload, dynamic transfer stiffness levels comparison for linearity test

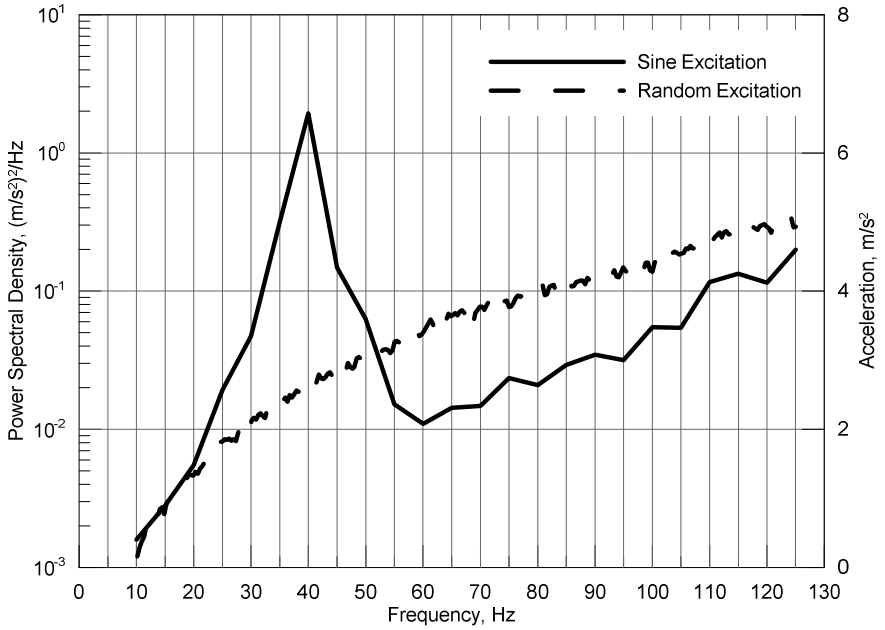

Figure 10.7 - Pillar P10 at 30 kN preload, excitations with random signal and step sine

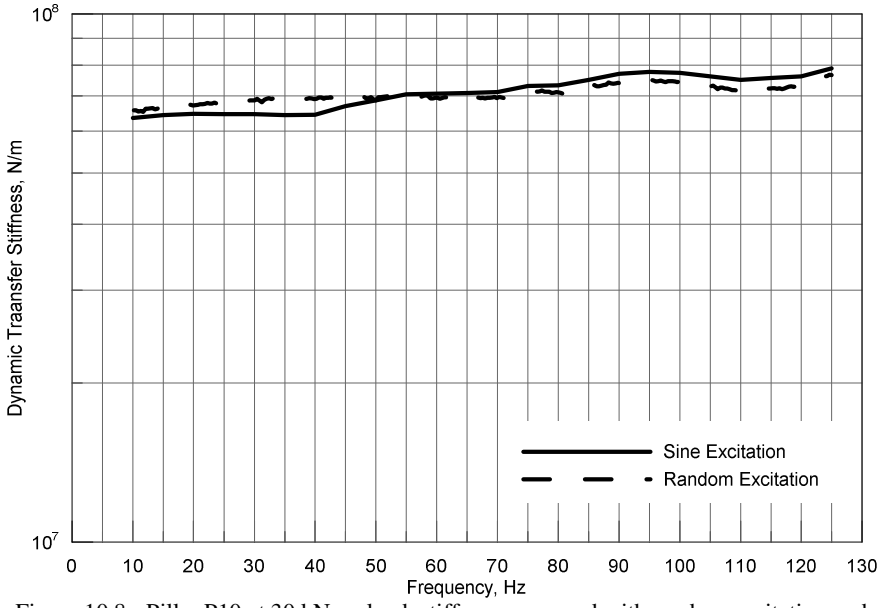

Figure 10.8 - Pillar P10 at 30 kN preload, stiffness measured with random excitation and step sine excitation

The dynamic transfer stiffness measured using the direct method is reported in Figure 10.9 along with the one measured with the indirect method on the high frequency test rig. Both the curves have been measured on the prototype P10 with a static preload of 30 kN and the curves have been drawn to the limit of their accuracy range. At low frequency, the stiffness shows a light increase whereas at high frequency it is almost constant with an approximate value of 100 MN/m. At their ends, the differences of the two stiffness curves are about 20% of the high frequency stiffness, nevertheless, there is still a grey area in the frequency range between 125 Hz and 200 Hz.

The results obtained with the two experiments, although not fully covering the frequency of interest, show rather close stiffness values. The results confirm the effectiveness of the low frequency test rig and the validity of the indirect test method on the high frequency test rig, which is an important result since there was no experience in testing of such kind of isolator. Moreover, this first attempt to use the low frequency test rig has been followed by other experimental trials on a softer marine resilient mount, confirming the reliability of the low frequency test rig [81].

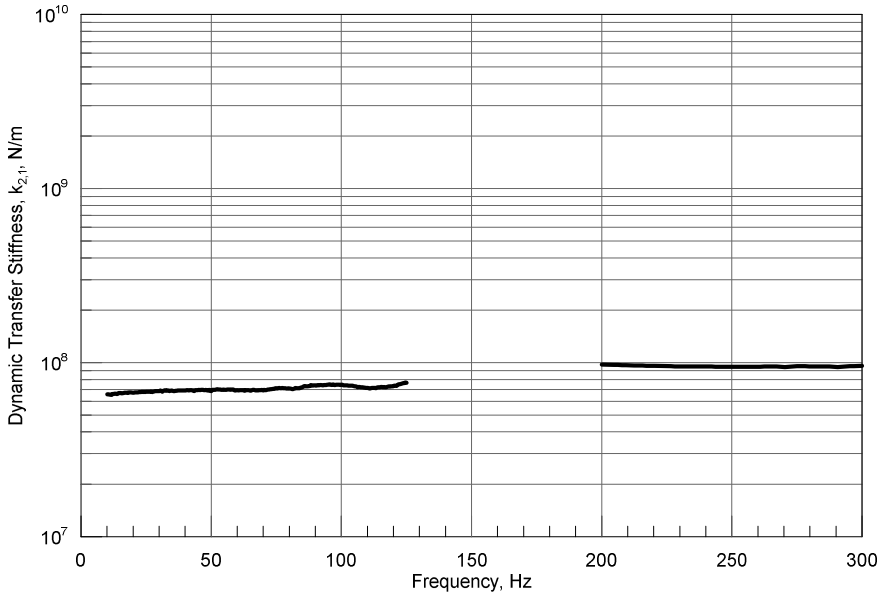

Figure 10.9 - Pillar P10 at 30 kN preload, dynamic transfer stiffness measured on the low frequency test rig (left side) and on the high frequency test rig (right side)

11 Real scale test

After the definition of the most promising prototype layout, the pillar isolator has been tested on the real scale mock-up presented in Section 5. The experimental tests are intended to compare the vibration transmission between two different layouts of the mock-up, one with the standard pillar and one with the isolated pillar. On the mock-up, a square section pillar, having 80 mm edge and 8 mm thickness, has been installed and so a square isolator device, without viscoelastic filling in the containing shell, has been used as isolator. The structure has been excited using an electrodynamic shaker and the resulting accelerations have been measured on several points on the structure, Figure 5.2. The structure has been excited in a frequency range from 10 to 4000 Hz and a measure of the applied force ensured that the excitation was comparable in both the cases. Moreover, since the output power of the shaker was limited, the frequency range of interest was divided into several intervals so to concentrate the vibrational power in smaller bands and guarantee an acceleration level in all the measure points of at least 15 dB higher than the background noise level. Figure 11.2 shows the resulting force level in third octave bands. Each excitation frequency interval has been defined to give a full coverage of the third octave bands comprised in its interval.

Figure 11.1 shows the transmission loss of both the standard pillar and the isolated pillar measured on the mock-up. The transmission loss is defined as the difference between the vibration velocity level measured on a point on the supporting plate at the bottom of the pillar and the vibration velocity level measured on the distribution plate above the pillar. The difference is calculated considering the top and the bottom of the same mock-up layout. Considering the transmission loss curve, the standard pillar behaves like a SDOF system. Indeed, at low frequency, up to 63 Hz, its transmission loss is zero, this means that the all the vibration measured at the base is transmitted to the top of the pillar. After 63 Hz the vibration transmission increases, so reducing the transmission loss, and reaching its peak at resonance corresponding to the 160 Hz third octave band. At higher frequencies, the

transmission is reduced, resulting in an increase of the transmission loss. The isolated pillar shows a small increase in transmission at lower frequency and after 31.5 Hz the transmission reduces radically with values of transmission loss up to

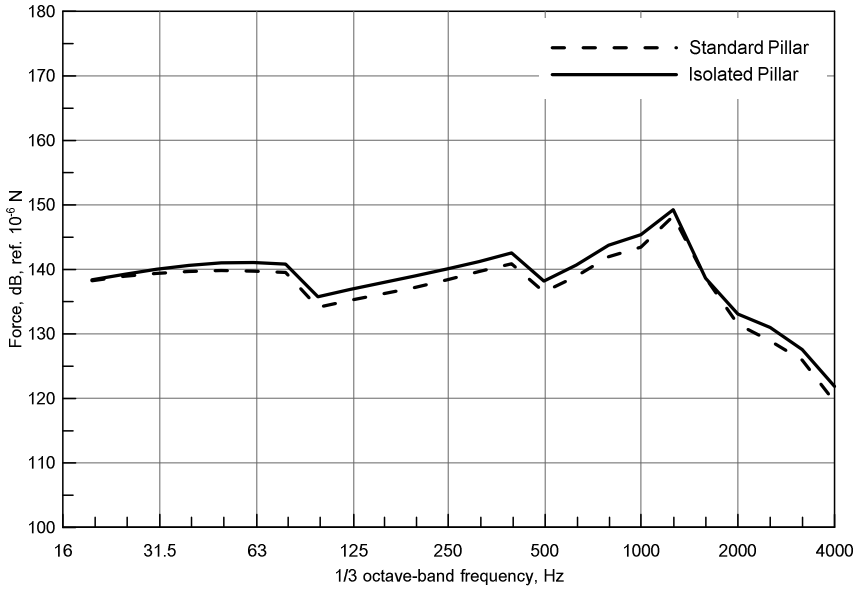

Figure 11.2 - Force excitation spectrum used during the real scale test

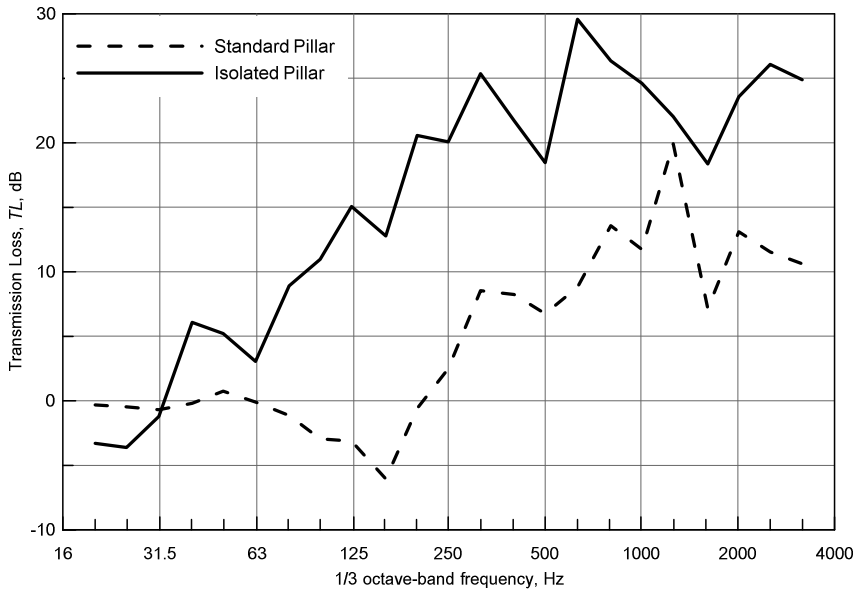

Figure 11.1 - Transmission loss through pillar for standard pillar and isolated pillar

30 dB, that means a reduction of 97% of the vibration velocity measured at the base of the pillar. The comparison of the transmission loss between the two solutions shows the effectiveness of the pillar isolator in the reduction of the vibration transmitted through the pillar. Indeed, the isolated pillar shows an increase of transmission loss of about 15 dB for all the frequencies above 100 Hz comparing to the standard pillar.

The transmission loss shows how the isolated pillar affects the local vibration transmission through the pillars. In order to assess the global behaviour of the isolated pillar, the insertion loss for the complete upper deck has been measured as shown in Figure 11.3. The insertion loss is defined as the difference between the average velocity levels of the points measured on the upper deck with the standard pillar and the average vibration velocity levels of the same points measured when the pillar isolator was installed. The index shows the variation of vibration levels due to the change in the mock-up structure.

The use of the pillar isolator lightly increases the vibration level in the low frequency up to 31.5 Hz. From 40 Hz to 100 Hz the value of insertion loss oscillates with moderately positive values while for frequency higher than 100 Hz the isolator introduces an effective vibration reduction except for the band

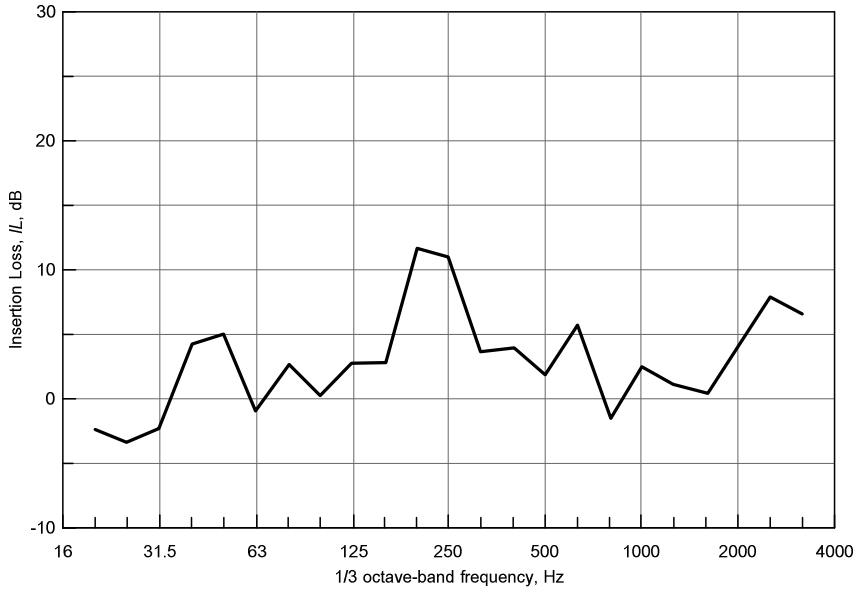

Figure 11.3 - Insertion loss measured on the whole upper deck

corresponding to 800 Hz where the vibration levels measured with the standard pillar and the isolated pillar are comparable. The measure shows the effectiveness of the isolated pillars in the reduction of the vibration transmitted to the upper deck. A reduction of the vibration is particularly clear for frequency higher than 100 HZ where peaks of insertion loss exceed 10 dB.

The insertion loss measured on the complete upper deck shows the effectiveness of the isolator. Furthermore, some local consideration could help to understand how the vibration transmission changes after the introduction of the isolator. Local analyses have been carried out defining local insertion loss index in which the average of the vibration levels was limited only to the points belonging to same portion of the mock-up. Four areas of interest have been defined: the area right above the pillar, the area corresponding to the centre of the mock-up deck, the area corresponding to the main beam supporting the upper deck and the area near the side plating and the bulkhead.

Figure 11.4 shows the insertion loss measured above the pillar. In low frequency range, up to 31.5 Hz, isolated pillar increases a little the vibration velocity level measured above the pillar, while after 100 Hz band it shows a high reduction of the

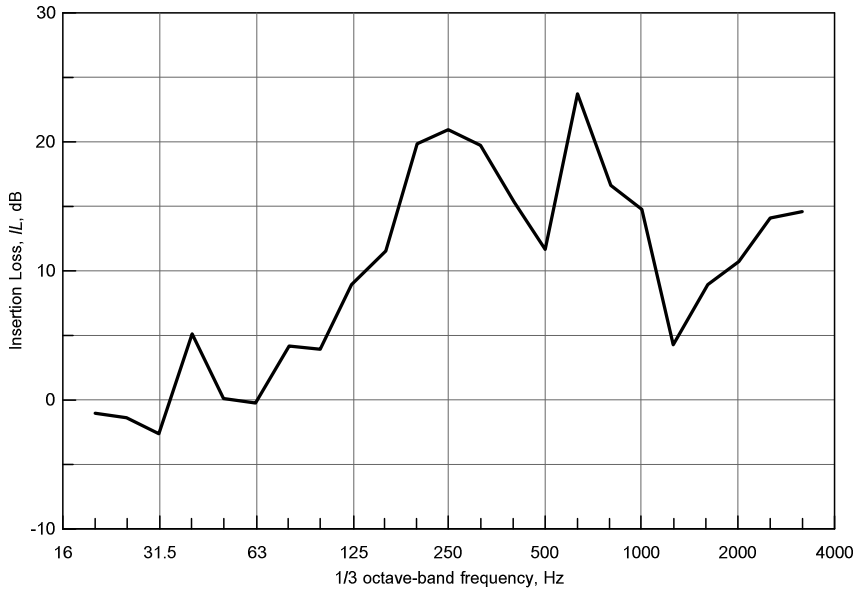

Figure 11.4 - Insertion loss at top of the pillar

vibration levels with peaks value over 20 dB and an average value of nearly 15 dB for frequencies above 125 Hz.

Figure 11.5 shows the insertion loss evaluated on the couple of points on the upper deck. Comparing it to the result obtained directly above the pillar, a reduction of the insertion loss values is appreciable, however, a reduction of the vibration velocities around 10 dB, with respect to those obtained with the standard pillar, still persists for frequency above 100 Hz.

The insertion loss measured along the upper deck beam is shown in Figure 11.6 where positive values have reduced their amplitude and some negative values appear for higher frequency.

Insertion loss measured along the side plate and the bulkhead, Figure 11.7, shows a general decrease with values turning negative on most frequency ranges of analysis, pointing out the change in the transmission path induced by the use of the pillar isolator.

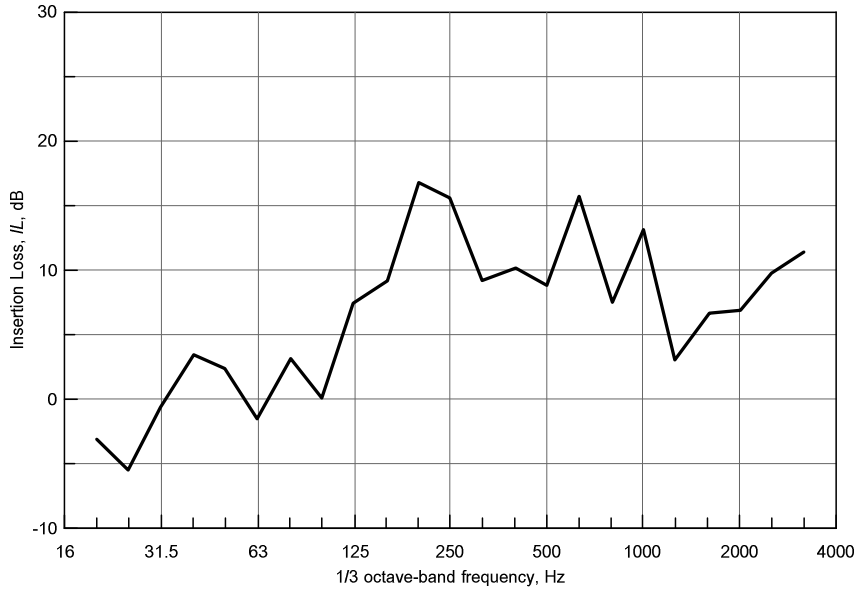

Figure 11.5 - Insertion loss on the upper deck

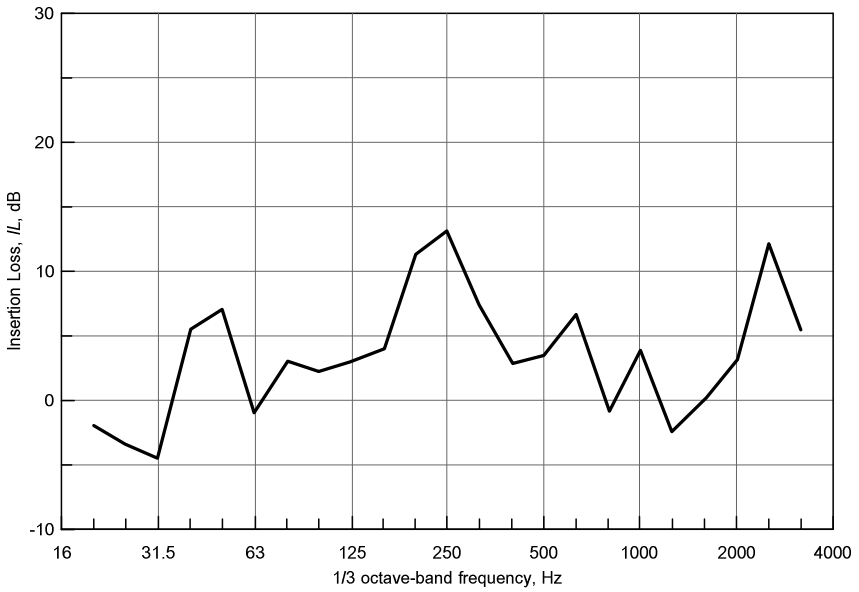

Figure 11.6 - Insertion loss measured near one main beam

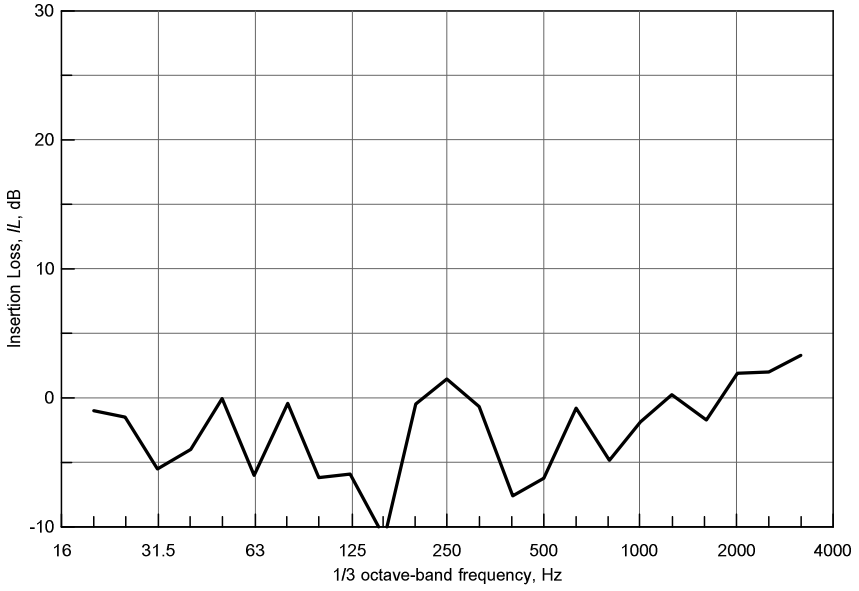

Figure 11.7 - Insertion loss measured near bulkheads

Testing a complex structure is important to evaluate the effectiveness of the isolated pillar in a real condition, where multiple vibration transmission paths are

present. The experiments show high reduction of vibration transmission through the pillar with corresponding vibration reduction measured in the area directly above the pillar. Vibration reduction, though lower than the one measured right above the pillar, has been measured also on the deck area between two deck beams and on a deck beam. Reaching the areas corresponding to the junction with the side plating and the bulkhead, an increase in the vibration level is clear. The main reason of the increment in these areas is the change in the transmission path following the introduction of the isolator, which increases the vibrational energy flow through the other paths. The overall results of the analysis are graphically summarized in Figure 11.8 where the areas of transmission reduction and increase are identified in green and red respectively.

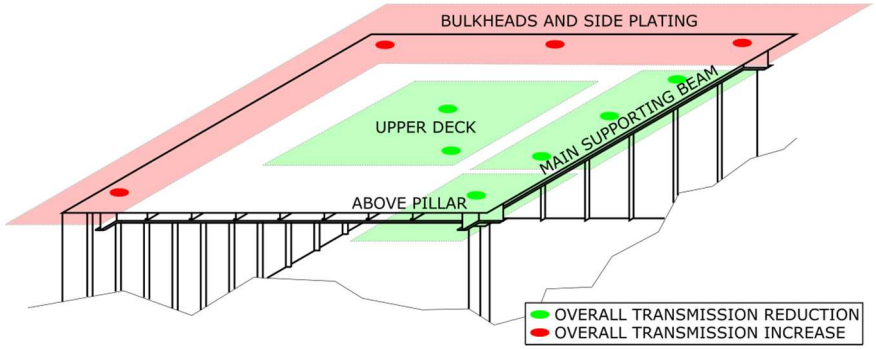

Figure 11.8 – Pillar isolator effect on vibration transmission

The tests performed show both pros and cons of the use of an isolated pillar, though its effectiveness is clear, it has to be kept in mind that its use does not eliminate the vibrations but changes the vibration transmission paths. This real scale test was a first approach to the topic and, despite of the limited number of points measured, it shows the effectiveness in the reduction of the overall vibration levels measured on the upper deck. In order to refine the results, in future experiments it is considered worthwhile to increase the number of measure points, especially in the unsupported upper deck area, and to investigate the behaviour of the structure applying input vibration in other points and directions.

12 Simplified finite element model

The first step in the set-up of the pillar isolator simplified finite element model is the definition of the mock-up model with the standard pillar. As explained in Section 6, the cabins fitted inside the mock-up have been neglected, but their effects have been taken into account distributing their mass on the FE model. Figure 12.1 shows the accelerance, defined as the ratio between the measured acceleration and the applied force [41], measured and predicted by FE model, for the measure point 3, placed on the upper deck right above the pillar. The compliance between the two curves is showed in Figure 12.2 using the Local Amplitude Criterion index as defined in Section 6.1.

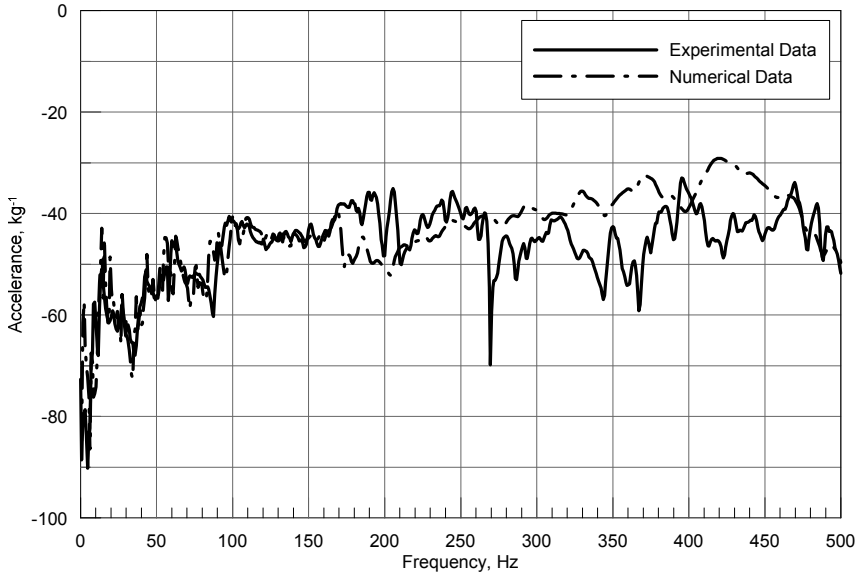

Figure 12.1 - Measure point 3, accelerance comparison between experimental and numerical data

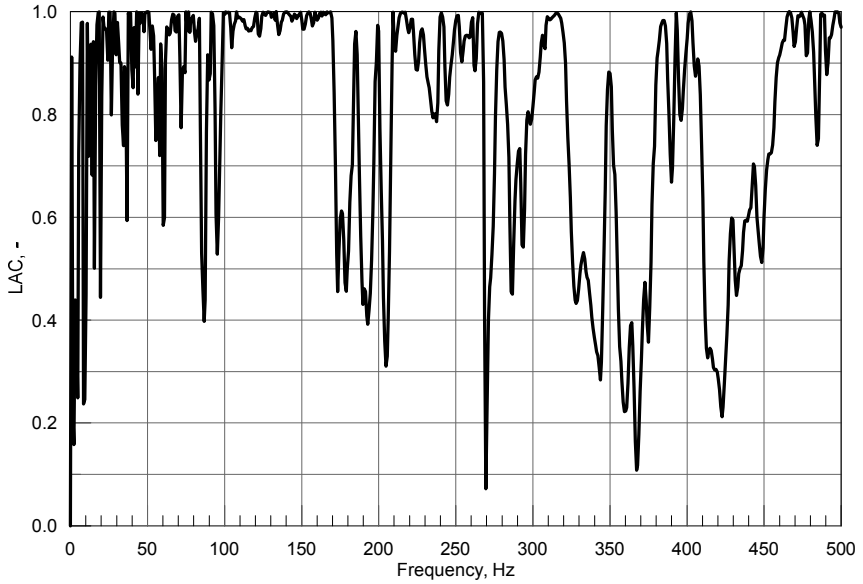

Figure 12.2 - Measure point 3, LAC index

LAC index, evaluated on point 3, shows a general good approximation of the numerical model, while, for the frequencies ranging from 280 to 400 Hz it shows lower values. Considering the simplifications introduced in the FE model definition, such as neglecting the cabins and using beam elements to model the pillar, the numerical model approximates quite well the behaviour of the real mock-up. Furthermore, available data is not enough for a process of model updating and such procedure lies outside the aim of this work.

The pillar isolator simplified model has been defined as a BUSH element with different stiffness for each degree of freedom and has been placed at the bottom of the pillar to simulate the connection between the pillar and its supporting plate. The axial stiffness along x and y axis and the rotational around the z axis have been assumed as infinitely rigid, the simplification adopted makes the dynamic behaviour of the simplified model close to the one of the standard pillar along these three DOF. Indeed, only a small portion of the original pillar has been replaced with the element representing the isolator and the pillar dynamics along these three DOF would not be subject to significant change. Moreover, the resilient pad constituting the isolator is enclosed in the containing shell, there is no gap between

the pad and the containing shell, and its thickness is very low so to justify the former assumption.

During the set-up process of the simplified model, the values of the vertical stiffness and of the rotational stiffness around the *x* and *y* axis have been adjusted to obtain the closest solution to the measured data. The different steps of the analysis are summarized in Table 12.1 and the resulting accelerances for the measure point 3 are showed in Figure 12.4 along with the experimental one.

Table 12.1 - Main characteristics of the isolator simplified numerical model

Simplified model	*z*-longitudinal stiffness	*x* and *y* rotational stiffness
	N/m	Nm/rad
SM00	$1.77 \cdot 10^8$	10^2
SM01	Tabular profile (Figure 12.3)	10^3
SM02	$5.62 \cdot 10^7$	10^3
SM03	$1.77 \cdot 10^7$	10^3
SM04	$1.77 \cdot 10^7$	10^7

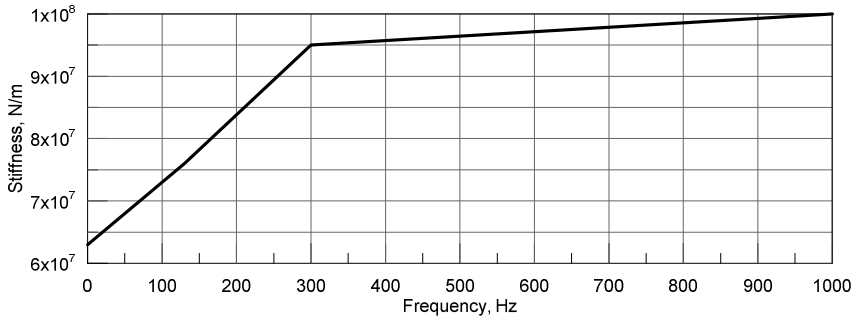

Figure 12.3 - Stiffness curve used in definition of simplified model SM01

For the first model, SM00, the vertical stiffness has been taken as constant and its value is the result of the experimental measure made on prototype P2 fixed to the blocking mass, Figure 9.24, averaged in the range from 200 to 1000 Hz excluding the peak values. The rotational stiffness values about the two horizontal axes cannot be predicted from former experimental test. The corresponding parameters of the simplified element has been first set to low values and later increased in order to assess the response of the FE mock-up model. The comparison of the predicted and measured accelerance shows great difference especially at frequency higher than 100 Hz where the measured accelerance tends to decrease.

Since the isolator tested on the real scale mock-up had no viscoelastic filling, the second attempt, SM01, was carried out to approximate the stiffness of the pillar to the one measured on the prototype P10, Figure 10.9, in this case the nonlinearities of the stiffness against the frequency has been modelled as shown in Figure 12.3. This model also shows to be far from the experimental results.

An estimation of the static preload acting on the pillar on the mock up shows that the compressive force acting on the pillar was about 10 kN while the tests carried out on laboratory's prototypes were done with 30 or 60 kN of static compression. In SM02 the vertical stiffness value was extrapolated from the available data from the two laboratory's test condition. The comparisons with the experimental data shows that the simplified model is stiffer than the reality.

In model SM03 the axial stiffness has been reduced once more to a third of the previous values. This model shows good agreement with the experimental data. In the simplified model SM04 the rotational stiffness has been increased, the result shows no difference between the former model and the two curves of SM03 and SM04 are overlapped in all the frequency range of the analysis. The LAC for SM03 model evaluated on the measure point 3 is reported in Figure 12.5 confirming the

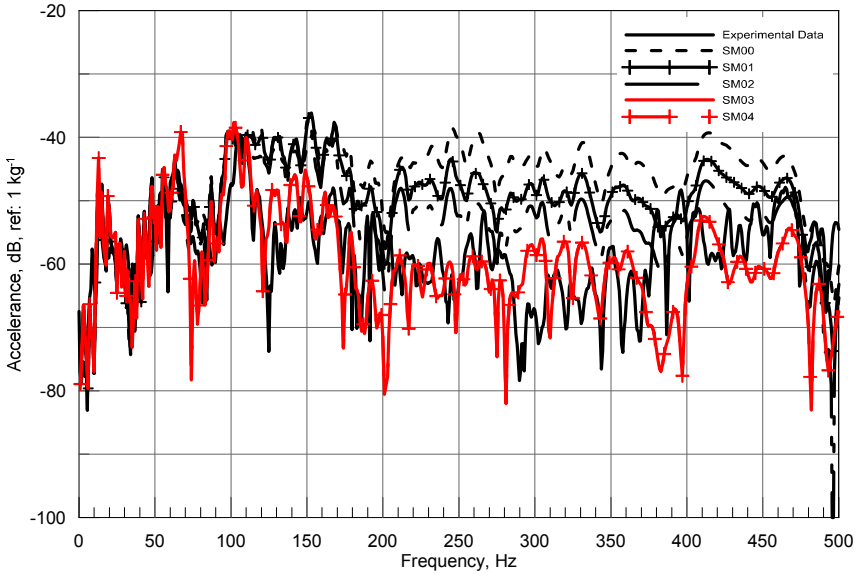

Figure 12.4 - Measure point 3, accelerance comparison of different isolator simplified numerical model

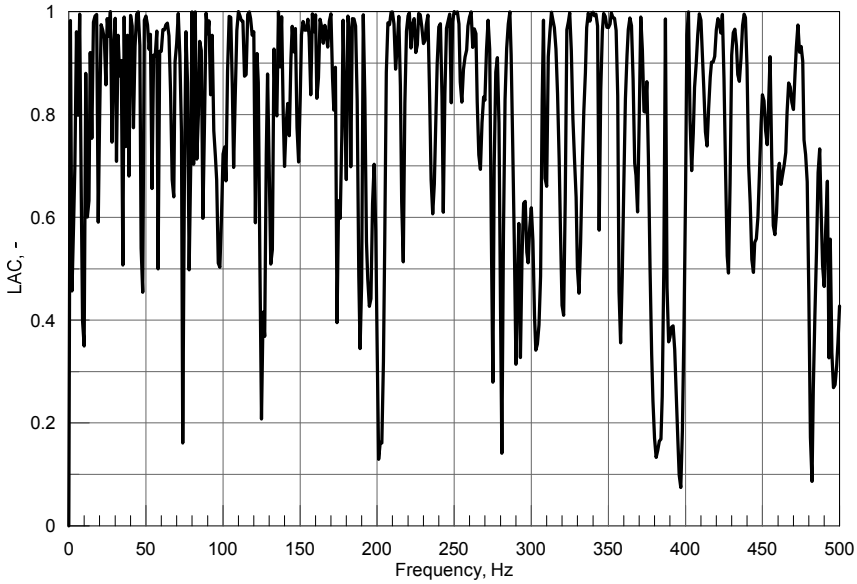

Figure 12.5 - LAC index for isolator simplified model SM03 on measure point 3

agreement of the predicted and experimental accelerance on all the frequency ranges of analysis.

At the end of the set-up process, the stiffness of the simplified model highly differs from the stiffness measured in laboratory test. Approximating the weight of the cabin placed on the upper deck and evaluating from the numerical model the force transmitted to the pillar, it turns out that the compressive force acting on the pillar on the mock-up structure was about 10 kN. The difference of the preload applied during the dynamic characterization test and during the real-scale test could justify the reduction of the stiffness value resulting from the numerical set-up process.

For the specific excitation used in the tests, along vertical direction near the pillar base, the setting of rotational stiffness around the section axis shows to be of minor importance. The results obtained were unresponsive to rotational stiffness variation from very small values, around 100 Nm/rad, to stiffness values of the same order of greatness than the one set for the longitudinal axis. The results suggest that further experiment with different excitation spot and direction need to be carried out in order to improve the definition of the isolator simplified model.

The simplified model with a frequency dependent stiffness, given the increase of the computational costs, did not show a significant improvement of the solution. Moreover, the result of the models with a constant stiffness shows results quite close to the measured data, thus suggesting the use of a simplified element with constant stiffness.

The results obtained underline the importance of the real static preload on the resulting stiffness value. This consideration suggests that different preload values need to be taken into account when dynamic characterization tests are performed in order to completely map the behaviour of the dynamic behaviour of the isolator. Further analysis needs to be done to investigate the rotational stiffness associated to the model, to achieve this result, experimental tests with various excitation spots need to be done. In addition, the test carried out suggests the use of a constant stiffness value instead of a frequency dependent stiffness, considering the high computational cost introduced by such nonlinearity the approximation in the use of a constant stiffness is acceptable.

13 Simulation on a superyacht finite element model

The pillar isolator simplified model as defined in Section 12 has been used to evaluate the improvement in comfort levels on a yacht. A FE model of an existing yacht has been used to compare the acceleration levels obtained with the standard and the isolated pillar. The FE model was already built and used to carry out predictions on normal modes and forced vibration response of local structure [67, 68]. The yacht, showed in Figure 13.1, is 54 m of overall length and 9.5 m breadth with a draft equal to 2.7 m.

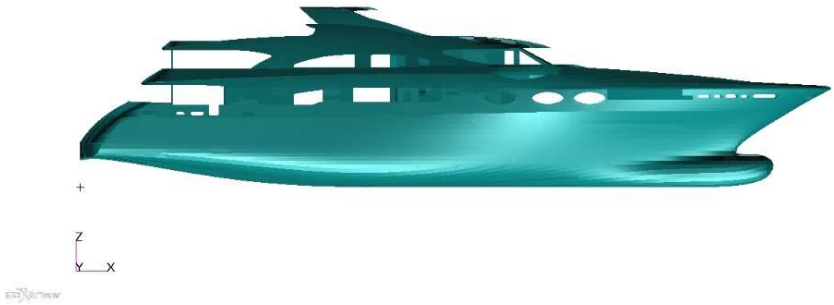

Figure 13.1 - FE model of the superyacht

Figure 13.2 shows a section of the FE model in way of the engine room. The girders have been modelled using plate elements both for the web and for the flange. As for the frame, plate elements have been used only for the webs while the flanges have been modelled as beam elements. The same elements have been used also to model longitudinals, bulkhead stiffeners and pillars. The mesh has an average size of 250 mm.

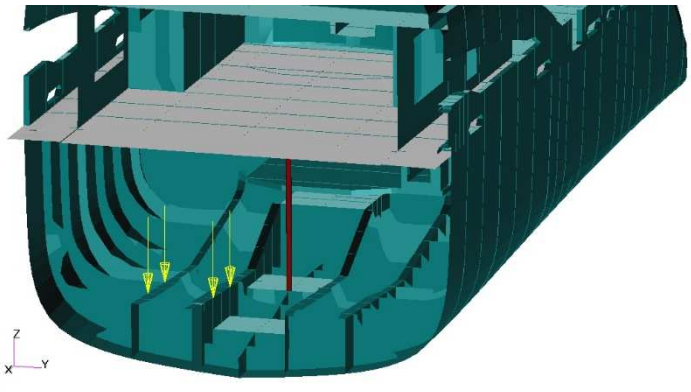

Figure 13.2 - Section of the FE model in way of engine room

In order to estimate the vibration reduction that could be achieved by an isolated pillar, a linear frequency response analysis has been carried out on two models. The model with the standard pillar, being the reference value, and the model with the isolated pillars. The isolator has been applied on the pillar placed in the engine room, the red pillar in Figure 13.2, supporting the main deck, the grey area. Some assumption has been made to simplify the analysis. Firstly, since the analysis is focused on the local action of the pillar isolator, the water surrounding the hull has been neglected. Indeed, the effect of added mass due to the fluid-structure interaction affects mainly the normal-modes of the global structure, while its effect at higher frequency, i.e.: significantly higher than the first global modes, and on local structure is negligible. Moreover, aim of the study is to investigate the effect of the isolated pillar and therefore, the hypothesis of dry hull would lead to similar approximation on both the FE model, thus allowing to compare their results. Secondly, only the vertical excitation of one main diesel engine has been taken into account and its contribution has been approximated as four forces acting on the engine foundation considering the engine moving as a rigid body [82]. The excitation used in the analysis is a sinusoidal unitary force in the frequency range of analysis going from 1 to 200 Hz, the yellow arrows in Figure 13.2 show the points of application of the forces. The analysis herein carried out is only partial, indeed to perform a complete analysis, all vibration sources should to be taken into account.

The axial stiffness of the isolator has been chosen on the basis of the evaluation of the static preload acting in still water condition considering the distribution of the outfitting as distributed non-structural mass. The static analysis shows that the pillar is subject to a compressive load of $3.6 \cdot 10^4$ N. Considering the acting preload, the solution tested in prototype P10 can withstand the load giving the lower stiffness of the isolator. The axial stiffness of the isolator has been approximated as constant in frequency with 100 MN value, stiffness along transversals direction, as long as the torsional stiffness around the vertical axis, has been set to a very high value to simulate a very stiff behaviour along this DOFs. The remaining rotational stiffness, along the transversals axis, has been set to a low value.

The resulting accelerance is used to compare the standard and the isolated solution. Use of a transfer function is convenient when addressing vibration prediction because, once the actual force spectrum is known, the actual acceleration values can be easily computed. The accelerance has been compared on several points on the deck above the engine room and the results are showed for a point above the pillar, Figure 13.3, and for a point away from the pillar, Figure 13.4.

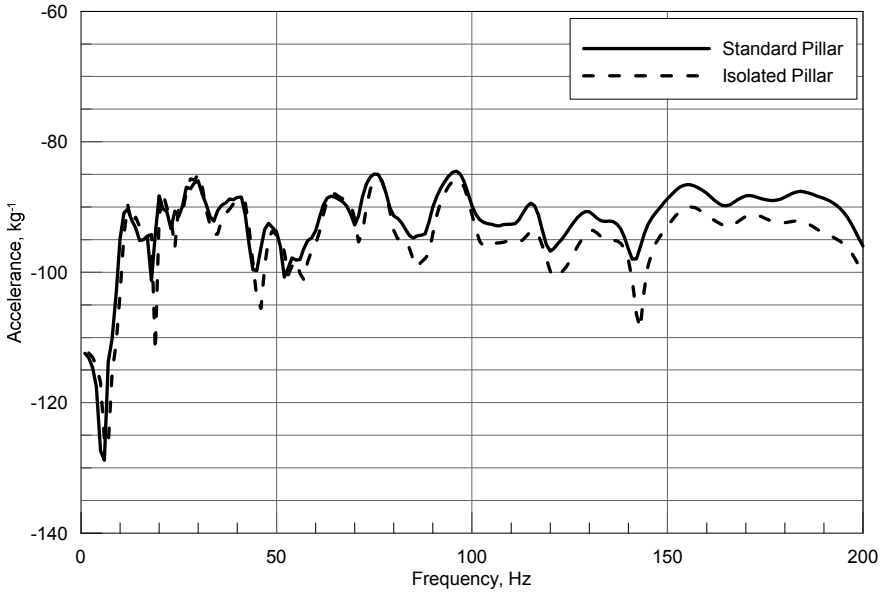

Figure 13.3 - Accelerance predicted on main deck above the pillar

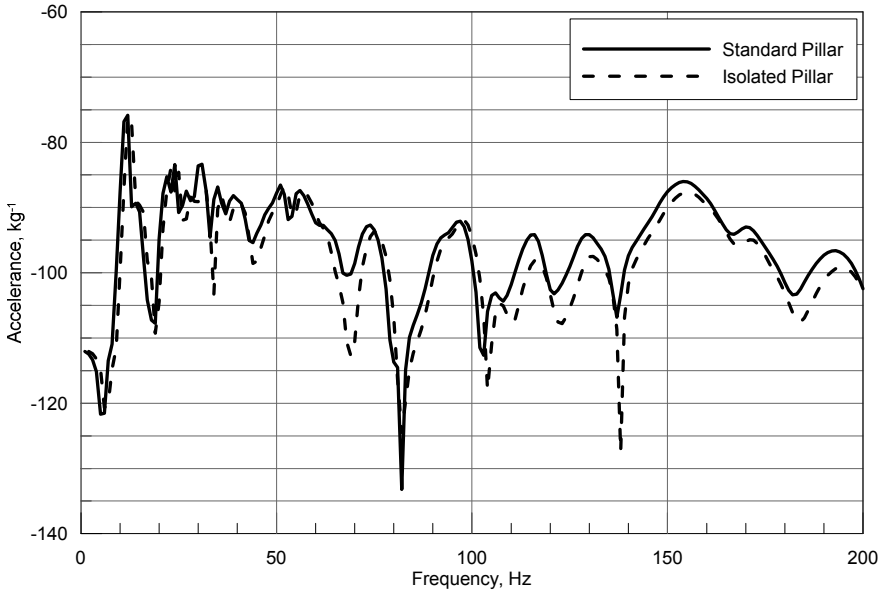

Figure 13.4 - Accelerance predicted on main deck on a point 1.5 m away from the pillar

The influence of the isolator, as highlighted in the real scale test, is higher right above the pillar, while at a point far from the pillar, its influence diminishes. The accelerance reduction is clear above 100 Hz and it increases as the frequency increases. Figures from Figure 13.5 to Figure 13.12 show the change in accelerations predicted on deck using the standard and the isolated pillar for some relevant frequencies. The figures shows the acceleration, expressed in mm/s^2, resulting from the engine vertical unitary excitation.

Recalling Figure 13.2, the side portions of the main deck are interrupted from the side plating supporting the upper deck. In addition, two other technical spaces limit the free span of the deck. Comparing two plots corresponding to the same frequency, the reduction due to the isolator is clear at deck centre. Moving to the side of the bulkhead and to the side of the hull, the effect of the isolator disappear. At the centre of the deck, where the influence of the isolator is higher, the acceleration predicted in the standard pillar case is reduced by more than a third.

The FE model of the yacht structure is a complete model in which all the transmission paths are modelled, which makes it different from the mock-up structure where only a quarter of the side plating was present. The analysis shows

a good capability to mitigate the vibration transmission also on a complete structure demonstrating the effectiveness of the pillar isolator. Moreover, the element dimensions on the yacht FE model allow the investigation up to 200 Hz but as the experiment on the real scale mock-up points out, the reduction in vibration transmission increases with the frequency.

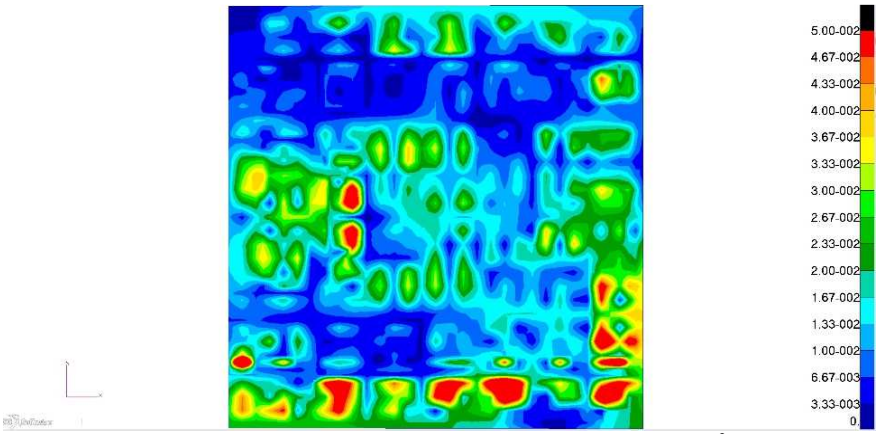

Figure 13.5 - Accelerations on yacht deck with standard pillar, mm/s^2, at 86 Hz

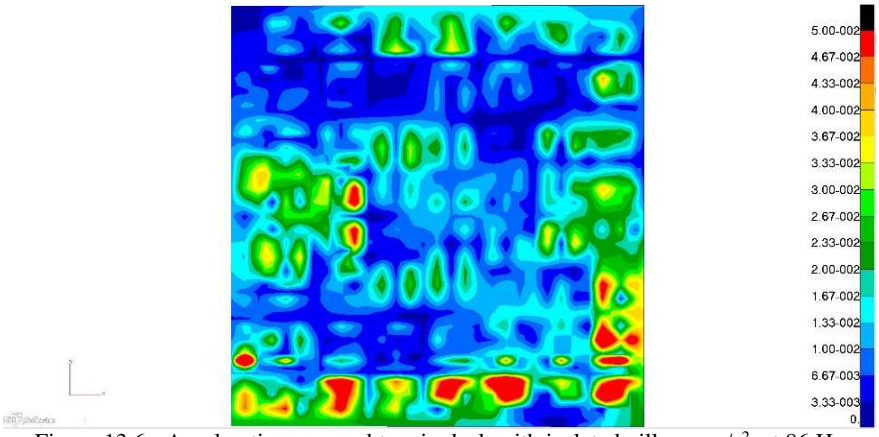

Figure 13.6 - Accelerations on yacht main deck with isolated pillar, mm/s^2, at 86 Hz

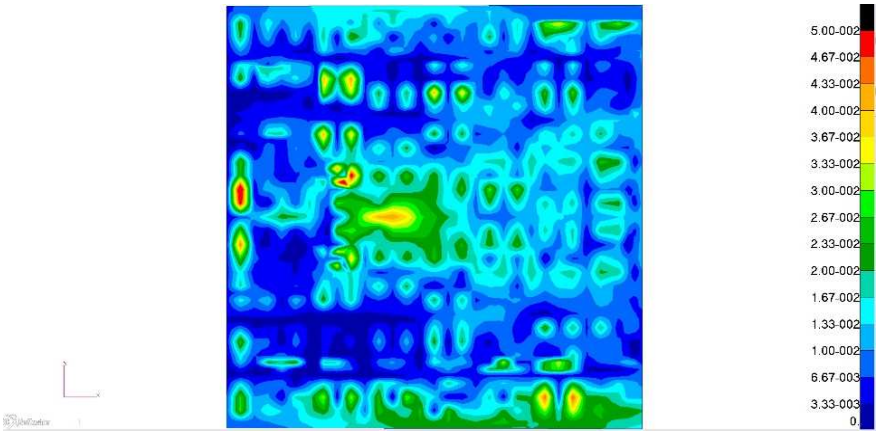

Figure 13.7 - Accelerations on yacht deck with standard pillar, mm/s^2, at 116 Hz

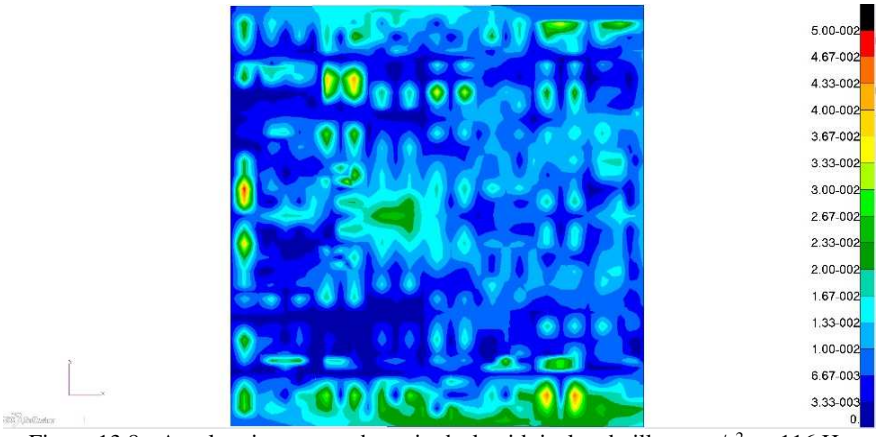

Figure 13.8 - Accelerations on yacht main deck with isolated pillar, mm/s^2, at 116 Hz

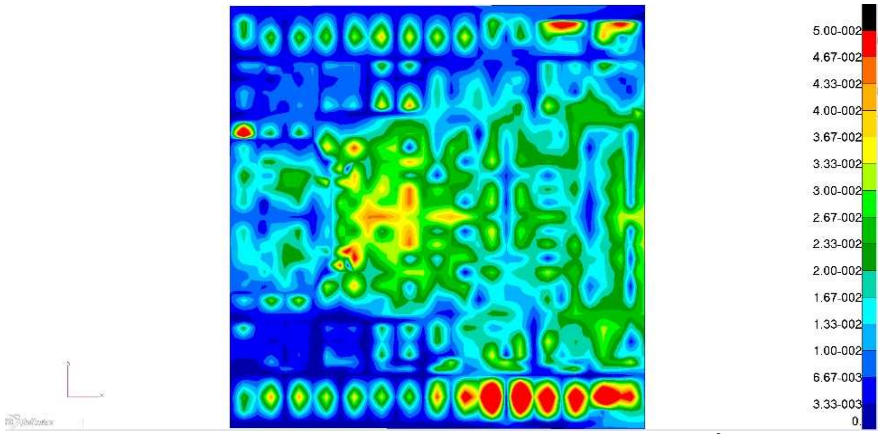

Figure 13.9 - Accelerations on yacht deck with standard pillar, mm/s^2, at 130 Hz

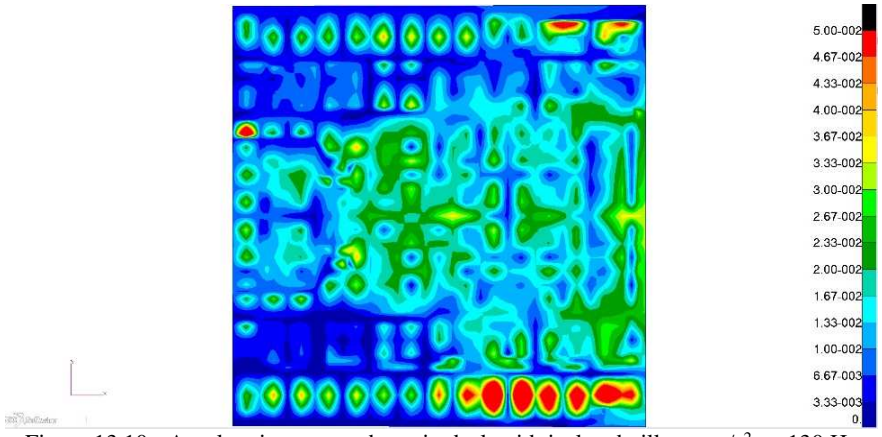

Figure 13.10 - Accelerations on yacht main deck with isolated pillar, mm/s^2, at 130 Hz

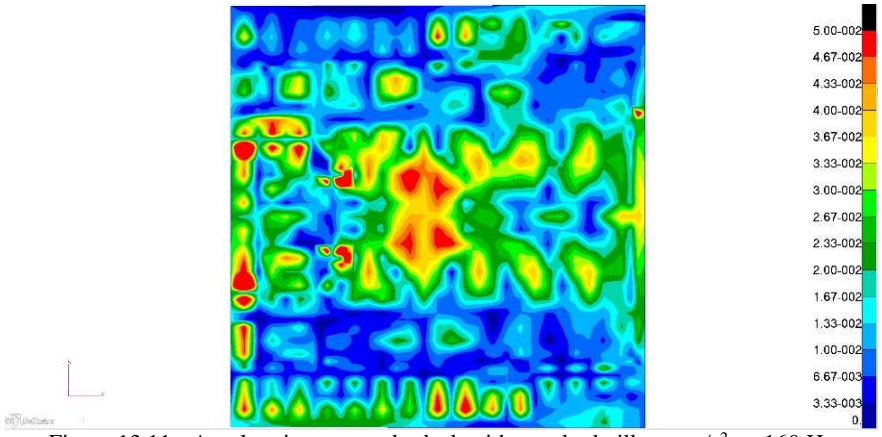

Figure 13.11 - Accelerations on yacht deck with standard pillar, mm/s^2, at 160 Hz

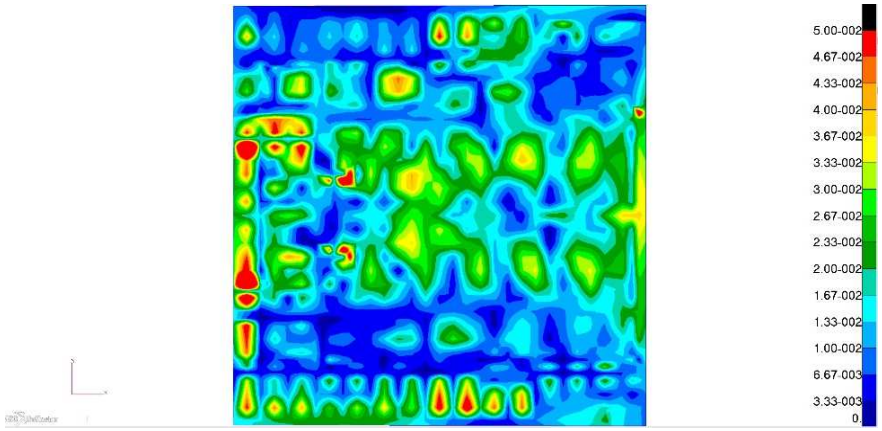

Figure 13.12 - Accelerations on yacht main deck with isolated pillar, mm/s^2, at 160 Hz

Conclusions and future development

Noise and vibrations are major problems in the shipbuilding industries. While many studies and researchers were involved in developing the prediction methods or reducing the vibrations transmitted from the source to the ship, much lower was the number of studies aiming at investigating the phenomenon of vibration transmission through the ship structure. During the years, few studies addressed the pillar as one of the weakest points in vibration transmission through the ship structure and, even though some solutions have already been adopted in the pleasure yacht field, no trace of studies on pillar isolator device appears in literature.

This work is a first trial to assess the effectiveness of a pillar isolator to reduce the vibration transmissions through pillars to the whole ship structure. The initial phase identified the maximum working loads of the pillars generally supporting decks in cruise ships and on superyachts. These data led to the definition of resilient element materials to be used in the isolator. Different prototypes were built based on a simplified layout of the isolator supposed to work only on compressive loads. The prototypes differ as for shape, dimensions and thickness of the lateral viscoelastic layer.

The experimental tests for the high frequency characterization of the prototypes dynamic behaviour show some errors in the design of the base for the experimental prototypes leading to inaccuracy in the stiffness measurement of the element under test. However, the systematic occurrence of the same problem on all prototypes tested was relevant to understand the effects of changing preload or viscoelastic thickness on isolator stiffness. With the improvement of the prototype design, the result of the high frequency dynamic characterization showed a constant stiffness of the isolator in the range of analysis. The prototype without viscoelastic filling showed to be the most promising solution.

The high frequency tests were carried out using the indirect method for the measure of dynamic transfer stiffness. Because of the high stiffness of the prototypes, the

lower frequency limit for the stiffness measure was about 200 Hz at its minimum. A new experimental rig, compliant with the "direct method" was designed in order to investigate the low frequency dynamic behaviour of the pillar isolator. The best solution was tested and the isolator showed a linear increase of the stiffness from 10 to 120 Hz. The difference between the stiffness values measured on the low and high frequency test rig is about 20% with respect to the high frequency stiffness value. The stiffness value ranging from 120 Hz to 200 Hz is still unknown nonetheless, the results, on one hand confirm the stiffness evaluation methods on the high frequency rig and, on the other hand assess the capability of the new low frequency test rig.

The pillar isolator prototype was tested on a real scale mock-up built with the typical structure of a cruise ship. Real scale experiments of such device are non-standard measure and no such tests were available in literature. The indexes used to evaluate the effectiveness of the isolator were inspired from the test procedure adopted in the experimental evaluation of structure-borne transmission reduction of marine deck insulations and floors carried out on a real scale deck panel. The test done on the real scale mock-up shows the effectiveness of the isolator in the reduction of the transmitted vibration through the pillars. Vibration levels were found to be significantly lower near the pillar, at the upper deck centre and above one of the girders supporting the upper deck while an increase of vibration levels was measured near the bulkhead and near the side plating. These findings show a variation in the vibration transmission path, which needs to be investigated more accurately in further studies increasing both the number of measure points and the excitation points and direction.

A simplified numerical model of the isolator has been defined using the experimental measure of dynamic transfer stiffness. The simplified model has been set-up on the experimental data from the real scale test. A FE model of the mock-up structure was created and validated with the experimental data using a local correlation index. The same index was used in the isolator simplified model set-up process in which the element stiffness was gradually modified until the FE model results were close to the experimental measure. The set-up result shows the importance of the real static force acting on the pillar. The set-up process of the simplified model leads indeed to stiffness values significantly lower than those

measured during the test on the experimental rig. This difference is mainly due to the different working conditions between the real scale test and the laboratory tests. A factor to take into account in order to improve the quality of the experimental results is the actual working load of the pillar. A further improvement could be the development of a system to control the actual load on the pillars without altering the dynamic behaviour of the upper deck. In the future, the simulations could be improved by developing a process of model updating requiring a large amount of data points to be measured.

The simplified numerical model was used to assess the increase of comfort level on a large yacht. The stiffness values associated to the simplified model were drawn from the experimental measure, since on the yacht the compressive load acting on the pillars was close to the one used in the experiments. In the simulation, the effects of the water surrounding the hull has been neglected being the analysis focused on local vibration instead of global behaviour of the hull girder. Other simplifications were considering only one propulsion engine as excitation source, considering its force only in vertical direction of excitation and neglecting the phasing between each engine feet. Nonetheless, the predictions showed a remarkable vibration transmission reduction also in a real case where all transmission paths were modelled.

The results obtained show the effectiveness of the isolator in the reduction of vibration transmission from a deck to the next through the pillars. The positive results obtained, both on real scale experiment on a between deck mock-up and by numerical simulations, led to the development of a new experimental prototype. This new device, shown in Figure 14.1, can withstand both compression and traction and allows easily changing and precompressing the resilient pad.

Figure 14.1 - New experimental prototype for the dynamic characterization of the pillar isolator

Bibliography

[1] Y. Tamura, T. Kawada and Y. Sasazawa, “Effect of ship noise on sleep,” *Journal of Sound and Vibration,* vol. 205, no. 4, pp. 417-425, 1997.

[2] International Maritime Organization, “MSC/Circ. 1014: Guidance on fatigue mitigation and management,” International Maritime Organization, London, 2001.

[3] B. Goujard, A. Sakout and V. Valeau, “Acoustic comfort on board ships: an evaluation based on a questionnaire,” *Applied Acoustics,* vol. 66, pp. 1063-1073, 2005.

[4] Lloyd's Register, “Rules and regulations for the classification of ships,” Lloyd's Register Group, London, UK, 2016.

[5] Germanischer Lloyd, “Harmony class - Rules on rating noise and vibration for comfort, cargo ships,” in *Rules for classification and construction*, Hambueg, Germany, Germanischer Lloyd Aktiengesellschaft, 2009.

[6] Det Norske Veritas, “Rules for classification of ships, Part 6 Chapter 33, Newbuildings: special equipment and systems - Additional class, Comfort class,” Det Norske Veritas AS, 2014.

[7] American Bureau of Shipping, “Guide for passenger comfort on ships,” American Bureau of Shipping, Houston, TX, 2001.

[8] A. Blanchet, “Comfort class and passenger ships,” in *The 29th International congress and exhibition on noise control engineering, inter.noise 2000*, Nice, France, 2000.

[9] M. Biot and F. De Lorenzo, “Criteria for designing noise and vibration comfort of passengers on board of ships,” in *21st Congreso Panamericano de Ingegneria Naval*, Montevideo, Paraguay, 2009.

[10] International Maritime Organization, “Resolution MSC.337(91): code on noise levels on board ships,” International Maritime Organization, 2012.

[11] R. W. Fischer, C. B. Burroughs and D. L. Nelson, “Technical and research bulletin no. 3-37: design guide for shipboard airborne noise control,” The Society of Naval Archirtects and Marine Engineers, New York, 1983.

[12] I. Asmussen, W. Menzel and H. Mumm, GL Technology: Ship Vibration, Hamburg, Germany: Germanisher Lloyd , 2001.

[13] Lloyd's Register, “Guidance notes: general overview of ship structural viobration problem,” Lloyd's Register, London, UK, 2015.

[14] J. W. Verheij, Multui-path sound transfer from resiliently mounted shipboard machinery, Delft: Institute of applied physics tno-th, 1982.

[15] L. Cremer, M. Heckl and E. E. Ungar, Structure-borne sound: structural vibrations and sound radiation at audio frequencies, Heidelberg, Germany: Springer-Verlag Berlin, 1988.

[16] F. Fahy, “Foundations of engineering acoustics,” Accademic Press, San Diego, CA, 2005.

[17] C. A. J. Beijers, *A modelling approach to hybrid isolation of structure-borne sound,* Enschede: University of Twente, 2005.

[18] L. He, Y. Li and C.-g. Shuai, “Active-passive vibration isolation forr ship machinery using electromagnetic actuator and air spring,” in *22nd International Congress on Sound and Vibration (ICSV 22)*, Florence, Italy, 2015.

[19] S. Daley, A. F. Johnson, B. J. Pearson and R. Dixon, "Active vibration control for marine applications," *Control engineering practice,* vol. 12, pp. 465-474, 2004.

[20] J. Orivuori, I. Zazas and S. Daley, "Active control of frequency varying disturbances in a diesel engine," *Control engineering practice,* vol. 20, pp. 1206-1219, 2012.

[21] T. Bsten and A. Berkhoff, "Active vibration control for underwater signature reduction of navy ship," in *The 17th International Congress on Sound nad Vibration (ICSV17)*, Cairo, Egipt, 2010.

[22] T. Yang, Y. Sun, Z. Liubin, M. J. Brennan and L. Zhigang, "Practical demonstration of a large-scale active vibration isolation system," *Case studies in mechanical systems and sugnal processing,* vol. 1, pp. 32-37, 2015.

[23] J. D. Dickens, Investigation of asymmetrical vibration isolators for maritime machinery applications, Melbourne: DSTO Aeronautical and Maritime Research Laboratory, 1999.

[24] D. J. Thompson, W. J. van Vliet and J. W. Verheij, "Developments of the indirect method for measuring the high frequency dynamic stiffness of resilient element," *Journal of sound and vibration,* vol. 213, no. 1, pp. 169-188, 1998.

[25] M. Biot and L. Moro, "Experimental study of resilient mounting," in *11th International Marine Design Conference, IMDC 2012*, Glasgow, UK, 2012.

[26] L. Moro and M. Biot, "Laboratory test pave the way for the knowledge of dynamic response of resilient mounting on board ships," in *12th International Symposium on Practical Design of Ships and Other Floating Structures, PRADS 2013*, Changwon, South Korea, 2013.

[27] C. J. Norwood and J. D. Dickens, "The effect of vibration isolator properties and structural stiffness on isolator performance," *Journal of Vibration and Control,* vol. 4, pp. 253-275, 1998.

[28] M. Biot, L. Moro and P. N. Mendoza Vassallo, "Prediction of the structure-borne noise due to marine diesel engines," in *The 21st Internetional Congress on Sound and Vibration, (ICSV 21)*, Beijing, China, 2014.

[29] P. Dylejko, I. Macgillivray and A. Skvortsov, "Isolator internal resonance and radieted noise from ships," in *Internoise 2014*, Melbourne, Australia, 2014.

[30] J. S. Tao, G. Liu and K. Y. Lam, "Design optimization of marine engine-mount system," *Journal of Sound and Vibration,* vol. 253, no. 3, p. 477.494, 2000.

[31] L. Moro, E. Brocco, A. Badino, P. N. Mendoza Vassallo, A. Clericuzio and M. Biot, "Design procedure for the development of new floating floors to improve," in *Proceedings of PRADS2016*, Copenhagen, 2016.

[32] Japan Ship Technology Research Association, "Experimental Study Report on Noise Reduction in Ship Accomodation Spaces," Japan Ship Technology Research Association, Tokyo, 2012.

[33] J. H. Song, S. Y. Hong and W. H. Joo, "Analysis of structure-borne noise in ship cabins using a floating floor with an inserted viscoelastic layer," *Journal of Marine Science and Technology,* vol. 14, no. 1, pp. 127-135, 2009.

[34] S. Cha and H. Chun, "Insertion loss prediction of floating floors used in ship cabins," *Applied Acoustics,* vol. 69, pp. 913-917, 2008.

[35] A. Ferrari and E. Rizzuto, "Modal behaviour of a full-scale deck panel with anti-noise treatments," in *Proceedings of the 11th International Congress of the International Maritime Association of the Mediterranean*, Lisbon, 2005.

[36] A. Ferrari and E. Rizzuto, "Measuring damping properties of viscoelastic materials for marine applications," in *Advancements in Marine Structures*, Glasgow, 2007.

[37] D. J. Eyres, Ship construction, Oxford, UK: Butterworth-Heinemann, 2001.

[38] S. Curletto and C. Tarditi, "Key factors of a ship internal noise prediction procedure," in *23rd International Congress on Sound and Vibration*, Athens, 2016.

[39] American Bureau of Shipping, Guidance notes on noise and vibration control for inhabited spaces, Houston, Texas: American Bureau of Shipping, 2014.

[40] R. W. Fischer, W. Snider and W. L. Hurley, Jr., "Noise control program for a large tractor tug," *Marine Technology,* vol. 36, no. 1, January 1998.

[41] C. W. de Silva, Vibration, foundamental and practice, Boca Raton, FL: CRC Press, 2007.

[42] F. Fahy and D. Thompson, Fundamentals of sound and vibration, Boca Raton, FL: CRC Press, 2015.

[43] L. Kari, "On the dynamic stiffness of preloaded vibration isolators in the audible frequency range: Modeling and experiments," *The Journal of the Acoustical Society of America,* vol. 113, no. 4, pp. 1909-1921, 2003.

[44] C. J. Snowdon, "Occurence of wave effects in rubber antivibration mountings," *The journal of the Acoustical Society of America ,* vol. 37, no. 6, pp. 1027-1032, 1965.

[45] International Organization for Standardization, *ISO 10846-1:2008 Acoustics and vibration -- Laboratory measurement of vibro-acoustic transfer properties of resilient elements -- Part 1: Principles and guidelines,* Geneve: International Organization for Standardization, 2008.

[46] International Organization for Standardization, *ISO 10846-2:2008 Acoustics and vibration -- Laboratory measurement of vibro-acoustic transfer properties of resilient elements -- Part 2: Direct method for determination of the dynamic stiffness of resilient supports for translatory motion,* Geneve: International Organization for Standardization, 2008.

[47] International Organization for Standardization, *ISO 10846-3:2002 Acoustics and vibration -- Laboratory measurement of vibro-acoustic transfer properties of resilient elements -- Part 3: Indirect method for determination of the dynamic stiffness of resilient supports for translatory motion,* Geneve: International Organization for Standardization, 2002.

[48] International Organization for Standardization, *ISO 10846-4:2003 Acoustics and vibration -- Laboratory measurement of vibro-acoustic transfer properties of resilient elements -- Part 4: Dynamic stiffness of elements other than resilient supports for translatory motion,* Geneve: International Organization for Standardization, 2003.

[49] International Organization for Standardization, *ISO 10846-5:2008 Acoustics and vibration -- Laboratory measurement of vibro-acoustic transfer properties of resilient elements -- Part 5: Driving point method for determination of the low-frequency transfer stiffness of resilient supports for translatory,* Geneve: International Organization for Standardization, 2008.

[50] J. C. Snowdon, "Vibration isolation: use and characterization," *Journal of Acoustical Society of America,* vol. 66, no. 5, pp. 1245-1274, 1979.

[51] J. C. Snowdon, "Mechanical four-pole parameters and their application," *Journal of Sound and Vibration,* vol. 15, no. 3, pp. 307-323, 1971.

[52] J. C. Snowdon, "Mechanical four-pole parameters: transmission matrices," The Pennsylvania State University, Institute for Science and Engineering Applied Research Laboratory, State College, 1976.

[53] T. Ten Wolde, Reciprocity experiment on transmission of sound in ships, Delft: Technical University of Delft, 1973.

[54] J. H. Lee and R. Singh, "Critical analysis of analogous mechanical models used to describe hydraulic engine mounts," *Journal of Sound and Vibration,* vol. 311, pp. 1457-1464, 2008.

[55] W. Xu and H. Lin, "Performance evaluation of mounting system for high-frequency vibration isolation of electric motor," in *23rd International Congress on Sound and Vibration*, Athens, 2016.

[56] B. R. Mohta, *Evaluation of methods for analysis of multi-degree-of-freedom system with damping,* vol. Paper 5272, Rolla, Missouri: The University of Missouri at Rolla, 1968.

[57] C. T. Molloy, "Use of four-pole parametrs in vibration calculation," *The Jounrnal of the Acoustical Society of America,* vol. 29, no. 7, pp. 842-853, 1957.

[58] M. Harrison, A. O. Sykes and M. M., "Wave effect in isolation mount," *The journal of the acoustical society of america,* vol. 24, no. 1, pp. 62-71, 1952.

[59] R. J. Diehl, U. J. Kurze and P. Hofmann, "Laboratory testing of elastic layers for raylway application," in *Proceedings of the eleventh International Congress on Sound and Vibrations*, St. Petersburg, Russia, 2004.

[60] E. Brocco, A. Hecquet, B. de' Vidovich and M. Biot, "Design of a test rig for the dynamic characterization of isolator in low frequency range," Università di Trieste, Internal Report, Trieste, 2015.

[61] C. B. Borrughs, R. W. Fishcer and F. L. Shiflet, "Structure-borne noise transmission through ship stanchions," *The Journal of the Acoustical Society of America,* vol. 66, no. S5, 1979.

[62] S. Sun, Determination of isolator transfer matrix and insertion loss with application to spring mounts, vol. Paper 71, Theses and Dissertation - Mechanical Engineering, 2015.

[63] A. Badino and E. Rizzuto, "Innovative de-coupling materials for the isolation of ship cabins," in *Maritime technology and engineering*, Lisbon, 2014.

[64] L. Ødegaard, "Sound insulation properties of marine flooring construction manufactured by Sika Cufaden A/S," Fredensborg, 2004.

[65] A. Ferrari and E. Rizzuto, "Characterisation of anti-noise treatments for cabin floor," in *ICMRT 2005, International Conference on Marine Research and Transportation*, Naples, 2005.

[66] L. Moro, M. Biot, E. Brocco, F. De Lorenzo and P. N. Mendoza Vassallo, "Hull vibration analysis of river boat," in *Safety and Energy Efficiency in River Transportation for a Sustainable Development of the Peruvian Amazon Region*, Iquitos, Perù, 2013.

[67] D. Boote, T. Pais and S. McCartan, "Vibration analysis of large yacht structures," *Bulletin de l'Association Technique Maritime et Aéronautique,* vol. 113, 2014.

[68] M. Biot, D. Boote, E. Brocco, L. Moro, T. Pais and S. Delle Piane, "Numerical and experimental analysis of the dynamic behaviour of main engine foundation," in *Proceedings of the Twenty-fifth (2015) International Ocean and Polar Engineering Conference*, Kona., Big Island, Hawaii, 2015.

[69] MSC Software, MSC Nastran 2014: quick reference guide, Newport Beach (CA): MSC Software, 2014.

[70] J. Parunov, C. Pestelli, S. Rudan, N. Hadžić and I. Senjanović, "Review of methods for structure borne noise prediction on ships," *Brodogradnja,* vol. 63, no. 2, pp. 134-139, 2012.

[71] S. Sehgal and H. Kumar, “Structural dynamic model updating techniques: a state of the art review,” *Archives of computational methods in engineering,* vol. 23, pp. 515-533, 2016.

[72] D. J. Ewins, “Model validation: correlation for updating,” *Sādhanā,* vol. 25, no. 3, pp. 221-234, 2000.

[73] C. Zang, H. Grafe and M. Imregun, “Frequency-domain criteria for correlating and updating dynamic finite element models,” *Mechanical Systems and Signal Processing,* vol. 15, no. 1, pp. 139-155, 2001.

[74] R. Moreira and J. D. Rodrigues, “The modelisation of constrained damping layer treatments using the finite element method: spatial model and viscoelastic behaviour,” in *International Conference on Structural Dynamics Modelling, Test, Analysis, Correlation and Validation*, Funchal, Madeira, Portugal, 2002.

[75] Lloyd's Registeer, “Structural design assessment: primary structure of passenger ships,” Lloyd's Registeer, London, UK, 2004.

[76] Lloyd's Register, “Structural design assessment: primary structure of Ro-Ro ships,” LLoyd's Registeer, London, UK, 2012.

[77] E. Brocco and M. Biot, “Progettazione numerico-sperimentale del sistema di riduzione del rumore strutturale trasmesso dalle linee di puntellatura - Report A1d2,” Trieste, Italy, 2016.

[78] A. Brandt, Noise and vibration: signal analysis and experimental procedures, Chichester, UK: John Wiley & Sons, 2010.

[79] P. P. Hujare and A. D. Sahasrabudhe, “Effect of thickness of damping material on vibration control of structural vibration in constrained layer damping treatment,” *Applied Mechanics and Materials,* Vols. 592-594, pp. 2031-2034, 2014.

[80] R. U. H. Syed, M. I. Sabir, J. Wei and D. Y. Shi, "Effect of viscoelastic material thickness of damping treatment," *Research Journal of Applied Sciences, Engineering and Technology,* vol. 4, no. 17, pp. 3130-3136, 2012.

[81] A. Hecquet, B. de'Vidovich, E. Brocco, M. Biot, F. Liciulli, G. Fabro, C. Pestelli, H. Le Sourne and L. Moro, "On the experimental characterization of resilient mounting elements," in *6th International Conference on Marine Structures, MARSTRUCT 2017*, Lisboa, Portugal, 2017.

[82] T. R. Lin, J. Pan, P. J. O'Shea and C. K. Mechefske, "A study of vibration and vibration control of ship structures," *Marine Structures,* no. 22, pp. 730-743, 2009.

[83] L. Moro, Structure borne noise due to marine diesel engines: experimental study and numerical symulation for the prediction of the dynamic behaviour of resilient mounts, Trieste: Ph. D. Thesis, 2014.